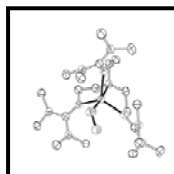
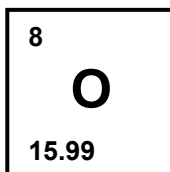
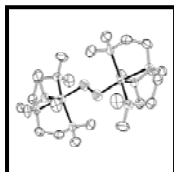
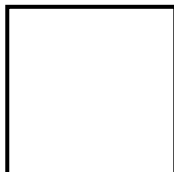
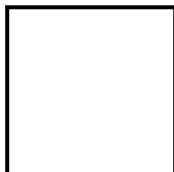
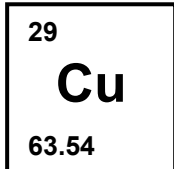


2008

JUSTUS-LIEBIG-UNIVERSITÄT GIESSEN
INSTITUT FÜR ANORGANISCHE
UND ANALYTISCHE CHEMIE



End-On “Copper Dioxygen Adduct Complexes”

Inaugural-Dissertation zur Erlangung des
Doktorgrades der Naturwissenschaften im
Fachbereich Biologie und Chemie
der Justus-Liebig-Universität Gießen

vorgelegt von Christian Würtele aus Hanau

Die vorliegende Arbeit wurde in der Zeit von Februar 2005 bis August 2008 am Institut für Anorganische und Analytische Chemie der Justus-Liebig-Universität Gießen unter der Anleitung von Prof. Dr. Siegfried Schindler durchgeführt.

Kernstück dieser Arbeit sind in englischer Sprache abgefasste wissenschaftliche Publikationen, welche bereits in Fachzeitschriften veröffentlicht oder zur Einreichung fertiggestellt sind. Diese Publikationen sind in Kooperation mit den Arbeitsgruppen von Prof. Dr. Jörg Sundermeyer (Philipps-Universität Marburg), Prof. Dr. Felix Tuczek (Christian Albrechts Universität Kiel), Prof. Dr. Max C. Holthausen (Johann Wolfgang Goethe-Universität Frankfurt), Prof. Dr. Kenneth D. Karlin (The Johns Hopkins University, Baltimore, USA) und Dr. Patrick K. Wick (ETH Hönggerberg Zürich, Schweiz) entstanden. Aus diesem Grund ist der wissenschaftliche Teil meiner Dissertation in englischer Sprache verfasst.

Danksagung

Mein aufrichtiger Dank gilt Prof. Dr. Siegfried Schindler, für die interessante Themenstellung, die vielseitige wissenschaftliche Anregung und die stets gewährte Unterstützung meiner Arbeit, auch in finanzieller Hinsicht.

Ich bedanke mich auch bei meinen Kollegen und ehemaligen Kollegen Dipl.-Chem. Alexander Beitat, Jennifer Friebe, Dipl.-Chem. Anja Henß, Dipl.-Chem. Tobias Hoppe, Dipl.-Chem. Sandra Kisslinger, Dipl.-Chem. Frank Mehlich, Dipl.-Chem. Jörg Müller, Dipl.-Chem. Thomas Nebe, Jonathan Becker, Sabine Löw, Janine Cappell, Dr. Ildikó Kerecsi, Dipl.-Chem. Lars Kohler, Vanessa Mook, Sabrina Schäfer, Janine Will, Dr. Sabrina Turba, Dipl.-Chem. Tatjana Neuwert, Prof. Dr. Jing-Yuan Xu und Dr. Jörg Astner sowie der Sekretärin Ursula Gorr für die freundliche Zusammenarbeit, die vielfältigen wissenschaftlichen Diskussionen und das tolle Arbeitsklima.

Dr. Olaf Walter und Dr. Michael Serafin danke ich für die Einführung in die Geheimnisse der Kristallographie. Günter Koch danke ich für seine Geduld, die er bei der Durchführung meiner Messungen aufbringen musste.

Thomas Waitz, Dipl.-Chem. Volker Lutz, Dr. Jörg Glatthaar und Dr. Erwin Röcker danke ich für die Hilfe bei den TG-, IR- und GC-Messungen.

Stefanie Haffer und Dipl.-Chem. Andreas Lotz danke ich für die gnadenlose Jagd nach Rechtschreibfehlern.

Darüber hinaus bedanke ich mich bei unseren Kooperationspartnern sowie deren Mitarbeitern: Dr. Ekaterina Gaoutchenova, Prof. Dr. Jörg Sundermeyer, Prof. Dr. Max C. Holthausen, Debabrata Maiti, Prof. Dr. Dong-Heon Lee, Dr. Amy A. Narducci Sarjeant, Prof. Dr. Kenneth D. Karlin, Dipl.-Chem. Ole Sander, Prof. Dr. Felix Tuczek und Dr. Patrick K. Wick.

Und natürlich danke ich allen Mitarbeiterinnen und Mitarbeitern der Chemie im Fachbereich 08, die ich hier leider nicht alle namentlich aufzählen kann.

Dem DAAD und der DFG danke ich für die finanzielle Unterstützung.

*Für meine Eltern,
ohne die diese Arbeit nicht möglich gewesen wäre, da sie immer an mich glaubten
und mir moralisch als auch finanziell immer eine Stütze waren.*

*Für Sandra,
die den ganzen Leidensweg der Erstellung dieser Arbeit mit ertragen musste und mir
immer wieder zu neuem Mut verhalf.*

Table of Contents

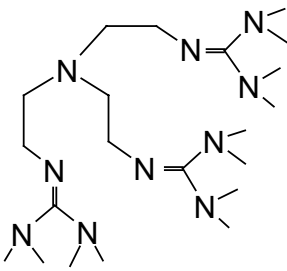

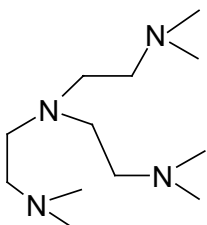

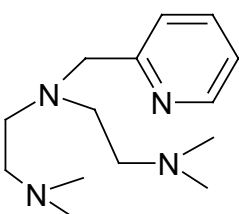

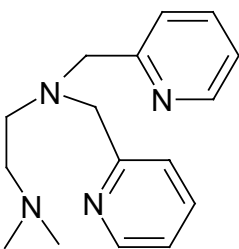

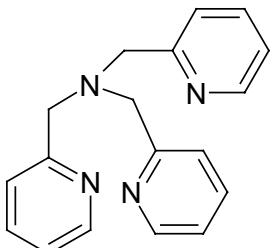

Table of Contents	1
Ligands used	5
Chapter 1 – Introduction	7
1.1 Motivation	7
1.2 Copper proteins	7
1.3 “Dioxygen complexes”	9
1.4 Model compounds for copper proteins	10
1.5 Tripodal ligands	12
1.6 Projects	16
1.6.1 Superoxo complexes	16
1.6.2 Peroxo complexes	17
Chapter 2 – Superoxo Complexes	19
2.1 Crystallographic Characterization of a Synthetic 1:1 End-On Copper Dioxygen Adduct Complex	21
2.1.1 Experimental Section	25
2.2 Selected parts of supporting information and unpublished results for chapter 2.1	27
2.2.1 Synthesis of [Cu(TMG ₃ tren)]PF ₆ .	28
2.2.2 Synthesis of [Cu(TMG ₃ tren)]BPh ₄ .	28
2.2.3 Low temperature stopped-flow studies	30
2.3 Reaction of a Copper(II) Superoxo Complex Lead to C-H and O-H Substrate Oxygenations: Modeling Copper-Monooxygenase C-H Hydroxylation	31
2.4 Selected parts of supporting information for chapter 2.3	39
2.4.1 Synthesis of [Cu ^I (TMG ₃ tren)]B(C ₆ F ₅) ₄	39
2.4.2 Generation of [Cu ^{II} (TMG ₃ tren)(O ₂)]B(C ₆ F ₅) ₄	39
2.4.3 Reaction of [Cu ^{II} (TMG ₃ tren)(O ₂)]B(C ₆ F ₅) ₄ with <i>p</i> -MeO-2,6- ^t Bu ₂ -phenol	40
2.4.4 Reaction of [Cu ^{II} (TMG ₃ tren)(O ₂)]B(C ₆ F ₅) ₄ with 2,4,6- ^t Bu ₃ -phenol	44
2.4.5 Reaction of [Cu ^{II} (TMG ₃ tren)(O ₂ ⁻)]B(C ₆ F ₅) ₄ (1) with 2,6- ^t Bu ₂ -phenol	44
2.4.6 Reaction of 2,4- ^t Bu ₂ -phenol with [Cu ^{II} (TMG ₃ tren)(O ₂)]B(C ₆ F ₅) ₄	45

2.4.7	Reaction of $[\text{Cu}^{\text{II}}(\text{TMG}_3\text{tren})(\text{O}_2^-)]\text{B}(\text{C}_6\text{F}_5)_4$ with 3,5- $^t\text{Bu}_2$ -Catechol	46
2.4.8	Synthesis of $[\text{Cu}^{\text{II}}(\text{TMG}_3\text{tren})]^{2+}$	46
2.4.9	Reaction of $[\text{Cu}^{\text{II}}(\text{TMG}_3\text{tren})](\text{ClO}_4)_2$ with $\text{H}_2\text{O}_2/\text{Et}_3\text{N}$	46
2.4.10	Reaction of $[\text{Cu}^{\text{I}}(\text{TMG}_3\text{tren})]\text{B}(\text{C}_6\text{F}_5)_4$ with PhIO	47
2.4.11	Reaction of $[\text{Cu}^{\text{II}}(\text{TMG}_3\text{tren})(\text{O}_2^-)]\text{B}(\text{C}_6\text{F}_5)_4$ with TEMPO-H	47
Chapter 3 – Peroxo Complexes		49
3.1	Reversible Binding of Dioxygen by Copper(I) Complexes with Tripodal Tetraamine Ligands	51
3.1.1	Abstract	51
3.1.2	Keywords	51
3.1.3	Introduction	51
3.1.4	Experimental Section	54
3.1.4.1	Materials and Methods	54
3.1.4.2	Stopped-Flow Experiments	55
3.1.4.3	Electrochemistry	56
3.1.4.4	X-ray crystallography	56
3.1.5	Results and Discussion	57
3.1.5.1	Synthesis and characterization	57
3.1.5.2	Electrochemistry	62
3.1.5.3	Kinetic Measurements	65
3.1.5.4	Kinetic and Thermodynamic Parameters	68
3.1.5.5	Formation and Dissociation of the Cu-O ₂ 1:1 adducts	69
3.1.5.6	Formation and Dissociation of the Cu-O ₂ 2:1 Adducts	70
3.1.6	Conclusion	70
3.2	Selected parts of supporting information and unpublished results for chapter 3.1	73
3.2.1	Synthesis of Me ₆ tren (tris(2-dimethylaminoethyl)amine)	73
3.2.2	Synthesis of Me ₄ apme (bis(2-dimethyl-aminoethyl) (2-pyridylmethyl)-amine)	73
3.2.3	Synthesis of Me ₂ uns-penp (2-dimethyl-aminoethyl)bis (2-pyridylmethyl)-amine)	74
3.2.4	Synthesis of tmpa (tris(2-pyridylmethyl)amine)	75
3.2.5	Synthesis of $[\text{Cu}(\text{Me}_6\text{tren})]\text{BPh}_4$	76

3.2.6	Synthesis of $[\text{Cu}(\text{Me}_4\text{apme})]\text{BPh}_4$	76
3.2.7	Synthesis of $[\text{Cu}(\text{Me}_2\text{uns-penp})]\text{BPh}_4$	76
3.2.8	Synthesis of $[\text{Cu}(\text{tmpa})]\text{BPh}_4$	77
3.2.9	Synthesis of $[\text{Cu}(\text{Me}_6\text{tren})\text{Cl}]\text{BPh}_4$	77
3.2.10	Synthesis of $[\text{Cu}(\text{Me}_4\text{apme})\text{Cl}]\text{BPh}_4$	77
3.2.11	Synthesis of $[\text{Cu}(\text{Me}_2\text{uns-penp})\text{Cl}]\text{BPh}_4$	78
3.2.12	Synthesis of $[\text{Cu}(\text{tmpa})\text{Cl}]\text{BPh}_4$	78
3.3	Extreme Stabilization of Copper Peroxo Complexes in the Solid State by Anion Encapsulation	83
3.3.1	Experimental Section	89
3.4	Supporting information for chapter 3.3 and continuing research for the peroxo complexes described	91
3.4.1	Synthesis of $[\text{Cu}_2(\text{L})_2(\text{O}_2)](\text{BPh}_4)_2$ (L = Me_6tren , Me_4apme , $\text{Me}_2\text{uns-penp}$ and tmpa)	92
3.4.2	Synthesis of $[\text{Cu}_2(\text{L})_2(\text{O}_2)](\text{BPh}_4)_2$ in the solid state (L = Me_6tren , Me_4apme , $\text{Me}_2\text{uns-penp}$ and tmpa)	92
3.4.3	Synthesis of $[\text{Cu}_2(\text{Me}_6\text{tren})_2(\text{O}_2)](\text{BPh}_4)_2 \cdot 3 (\text{CH}_3)_2\text{CO}$ as single crystals	92
3.4.4	Thermal analysis of $[\text{Cu}_2(\text{L})_2(\text{O}_2)](\text{BPh}_4)_2$ in the solid state (L = Me_6tren , Me_4apme , $\text{Me}_2\text{uns-penp}$ and tmpa)	93
3.4.5	Oxidation of toluene by using solid state copper peroxo complexes	94
3.4.6	Reaction of $[\text{Cu}_2(\text{Me}_6\text{tren})_2(\text{O}_2)](\text{B}(\text{C}_6\text{H}_5)_4)_2$ with toluene	95
3.4.7	Reaction of $[\text{Cu}_2(\text{Me}_4\text{apme})_2(\text{O}_2)](\text{B}(\text{C}_6\text{H}_5)_4)_2$ with toluene	95
3.4.8	Reaction of $[\text{Cu}_2(\text{Me}_2\text{uns-penp})_2(\text{O}_2)](\text{B}(\text{C}_6\text{H}_5)_4)_2$ with toluene	96
3.4.9	Reaction of $[\text{Cu}_2(\text{tmpa})_2(\text{O}_2)](\text{B}(\text{C}_6\text{H}_5)_4)_2$ with toluene	97
Chapter 4 – Materials, Methods and Crystallography		99
4.1	Materials and Methods	99
4.1.1	Chemicals and solvents	99
4.1.2	Air sensitive compounds	99
4.1.3	Electrochemistry	99
4.1.4	Elemental analysis	99
4.1.5	EPR-spectroscopy	100
4.1.6	ESI-MS-spectrometry	100
4.1.7	GC and GC-MS-spectrometry	100

4.1.8	Low temperature IR-spectroscopy	101
4.1.9	Low temperature Stopped-Flow studies	101
4.1.10	NMR-spectroscopy	101
4.1.11	Resonance Raman spectroscopy	101
4.1.12	Thermal analysis	102
4.1.13	UV-vis spectroscopy	102
4.2	Crystallography	103
Chapter 5 – Summary / Zusammenfassung		119
5.1	Summary	119
5.1.1	Superoxo complexes	120
5.1.2	Peroxo-complexes	121
5.2	Zusammenfassung	125
5.2.1	Superoxokomplexe	125
5.2.2	Peroxokomplexe	127
Publications		131
Curriculum Vitae		135
References		137

Ligands used

<p>TMG₃tren</p> 		<p>Tris(tetramethylguanidino)tren</p> <p>C₂₁H₄₈N₁₀ 440.68 g/mol</p> <p>¹H NMR (CDCl₃): δ 3.23 (6H, m), 2.84-2.59 (42H, m)</p>
<p>Me₆tren</p> 		<p>Tris(2-dimethylaminoethyl)amine</p> <p>C₁₂H₃₀N₄ 230.40 g/mol</p> <p>¹H-NMR (CDCl₃): δ 2.55 (6H, t), 2.32 (6H, t), 2.16 (16H, s)</p>
<p>Me₄apme</p> 		<p>Bis(2-dimethyl-aminoethyl)(2-pyridylmethyl)amine</p> <p>C₁₄H₂₆N₄ 250.39 g/mol</p> <p>¹H-NMR (CDCl₃): δ 8.47 (1H, d), 7.59 (1H, t), 7.43 (1H, d), 7.09 (1H, t), 3.75 (2H, s), 2.62 (4H, t), 2.38 (4H, t), 2.15 (12H, s)</p>
<p>Me₂uns-penp</p> 		<p>2-Dimethyl-aminoethyl)bis(2-pyridylmethyl)-amine</p> <p>C₁₆H₂₂N₄ 270.38 g/mol</p> <p>¹H-NMR (CDCl₃): δ 8.52 (2H, d), 7.65 (2H, t), 7.53 (2H, d), 7.14 (2H, m), 3.86 (4H, s), 2.71 (2H, t), 2.48 (2H, t), 2.17 (6H, s)</p>
<p>tmpa</p> 		<p>Tris(2-pyridylmethyl)amine</p> <p>C₁₈H₁₈N₄ 290.37 g/mol</p> <p>¹H-NMR (CDCl₃): δ 8.55 (3H, d), 7.84 (3H, t), 7.79 (3H, d), 7.24 (3H, m), 3.87 (6H, s)</p>

Chapter 1 – Introduction

1.1 Motivation

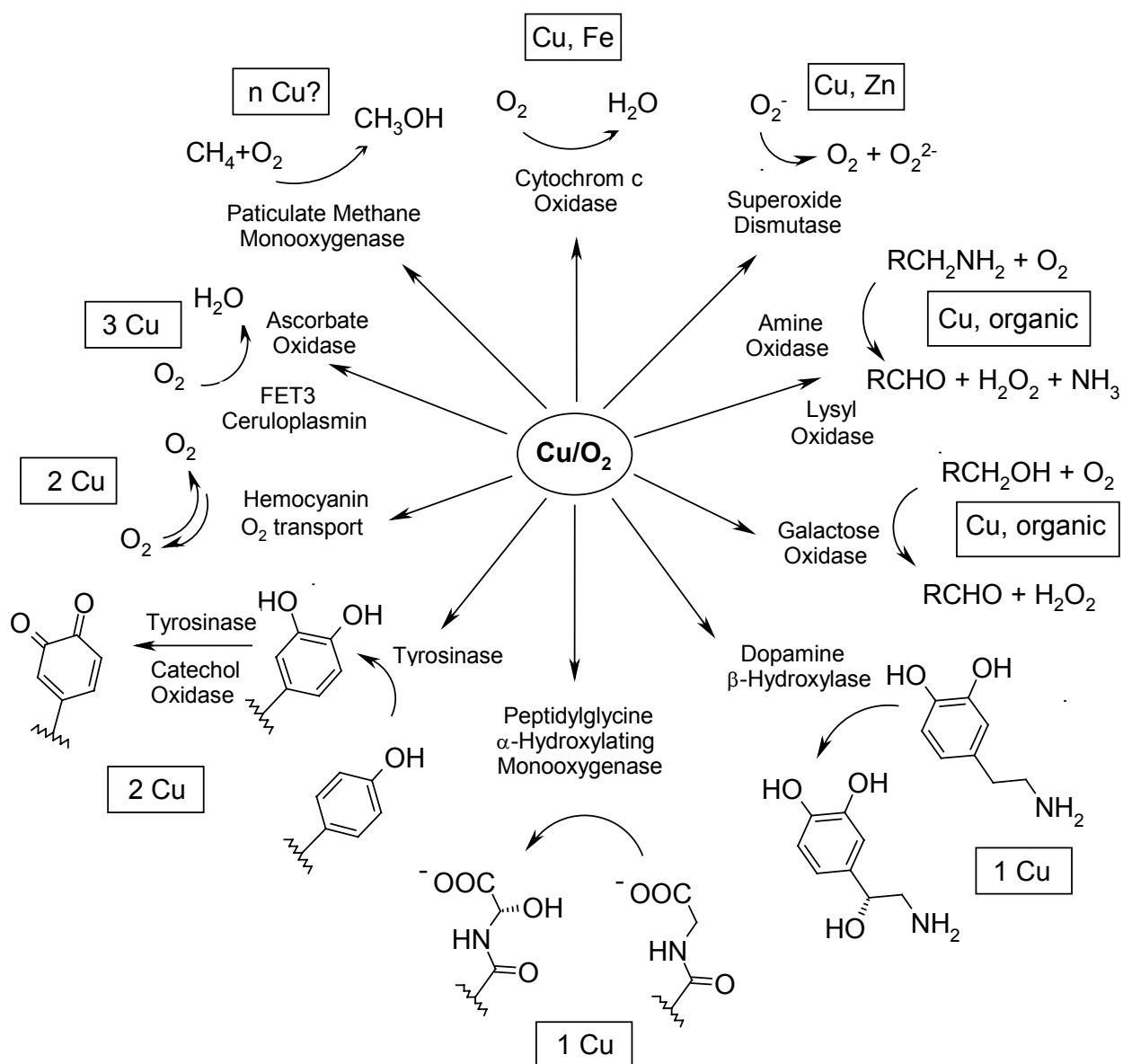
Copper with its 0.005 % (in weight) in the earth's crust has always been an important element for mankind and is essential for a large number of biological functions in plants and animals (including humans). Besides the occurrence of the element in the lithosphere as oxides, sulfides and carbonates it is therefore observed in the active site of several redox active metalloproteins.^[1-8]

For example copper proteins are responsible for the blue colored blood (hemocyanin) of molluscs (e. g. snails) and arthropods (e. g. lobster) or for the browning reaction of vegetables and fruit (tyrosinase). Phenomena like this fascinate scientists as well as science fiction authors and a copper protein based blood for example was described for Mr. Spock in the movie series Star Trek.^[2, 9, 10]

Detailed investigations of copper proteins during the past three decades led to important results about their structure, function and reactivity. This research was always accompanied by studies on low molecular weight complexes that can be regarded as model compounds for these proteins. Because of the ability of many of the known copper enzymes to catalyze selective oxidations with air, one of the goals in bioinorganic chemistry currently is to model this functionality and to use such small molecular synthetic copper complexes as catalysts for selective oxidation reactions in the laboratory and in industry.^[3, 6, 7]

1.2 Copper proteins

So far the known copper proteins are categorized into three types according to their biological function and characteristic properties. However, more recently it was realized that these three types are not sufficient and further differentiations were made. The new types are sometimes described as non classical copper proteins.^[2, 9] In scheme 1.2.1 important copper proteins and their biological function in dioxygen activation are shown.^[6]



Scheme 1.2.1: Selected copper enzymes and their function in nature.^[6]

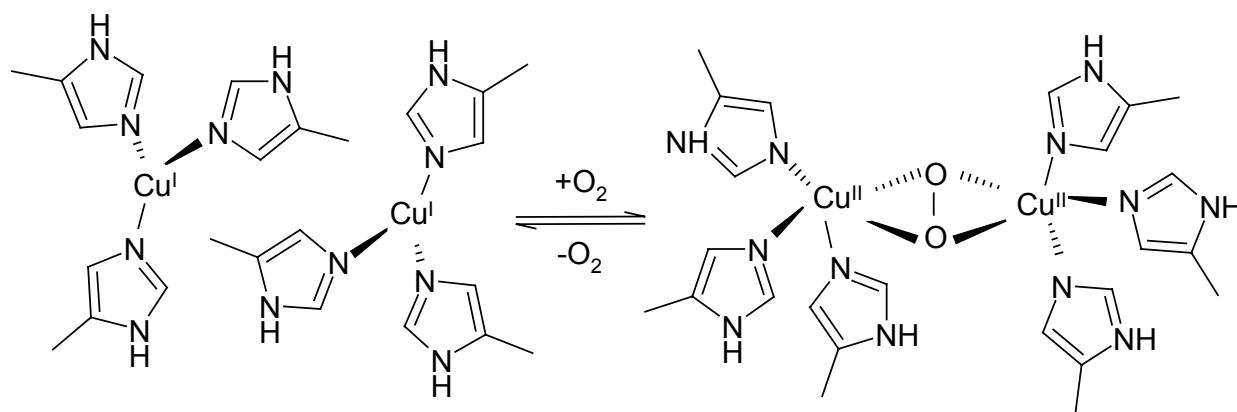
Type 1 copper proteins, for example plastocyanin or azurin, are classified as “blue” copper proteins due to their intensive blue color. They are responsible for electron transfer reactions in plants and bacteria.^[2, 9]

Type 2 copper proteins include amine oxidase and dopamine β-monooxygenase. They are responsible for either amine oxidations in plants and mammals or for the oxidation of dopamine in the kidney of mammals.^[2, 9]

Type 3 copper proteins, for example tyrosinase, are responsible for the browning reaction of vegetables and fruit as well as for the pigment melanine production in our skin. The protein hemocyanin is responsible for the dioxygen transport in the blue blood of animals such as spiders, snails and crabs.^[2, 9]

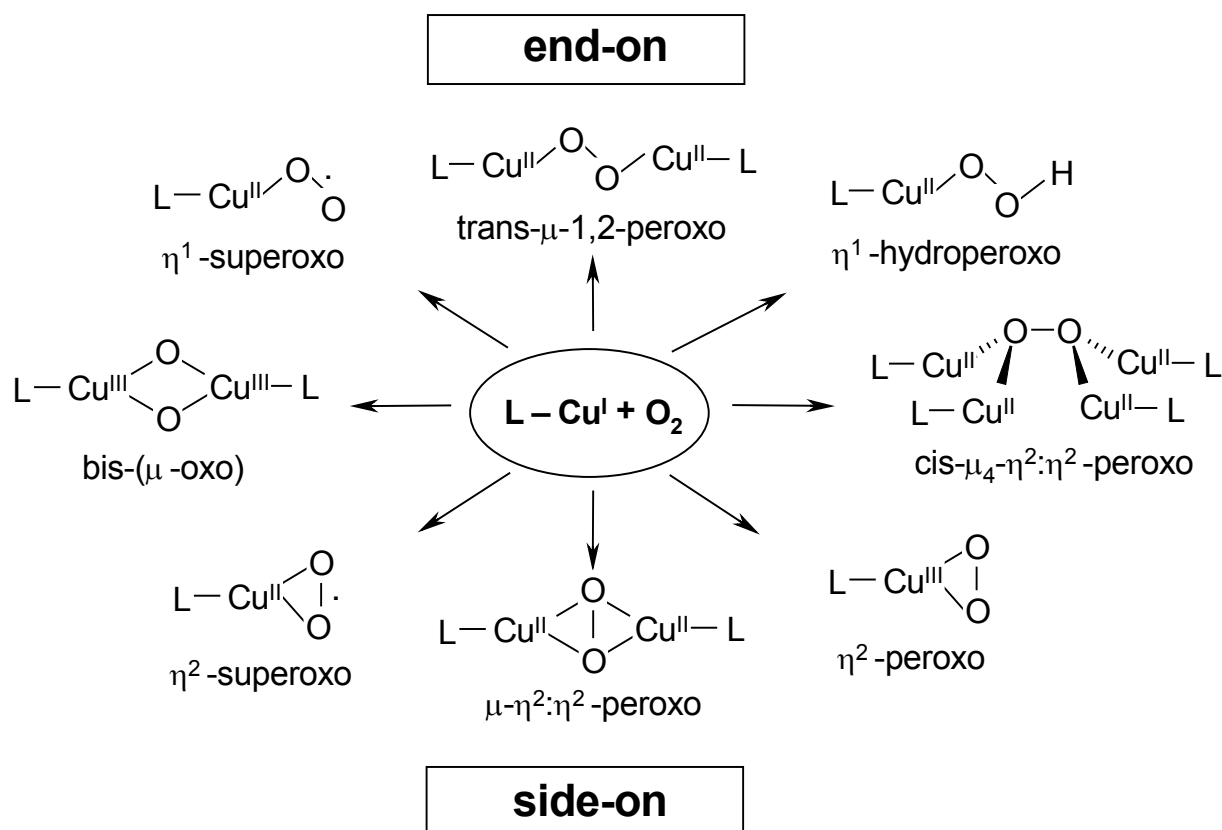
1.3 “Dioxygen complexes”

As described above hemocyanin, a type 3 copper protein, is responsible for the dioxygen transport in the blood of molluscs and arthropods similar to the iron protein hemoglobin in the blood of mammals. The active site of hemocyanin consists of a dinuclear copper complex, with the ability to bind and release dioxygen reversibly.^[4]



Scheme 1.3.1: Reversible binding of dioxygen in hemocyanin.

The $\mu\text{-}\eta^2\text{:}\eta^2$ -coordination of the peroxo ligand in hemocyanin is just one of the many possibilities how oxygen can coordinate to metal ions. The geometry and electronic properties of the protein or the synthetic analogue are responsible for the different coordination behavior. In scheme 1.3.2 some of these different coordination modes for possible “dioxygen adduct complexes” are shown. All of these complexes have been characterized in detail previously.^[11-18] Quite important is the distinction in the different binding modes between end-on and side-on coordinated complexes.^[3, 7]



Scheme 1.3.2: Selective copper dioxygen species in different coordination environments.

1.4 Model compounds for copper proteins

In 1989 Kitajima and co-workers described the first synthetic copper peroxo complex with a side-on coordination of the dioxygen ligand (Figure 1.4.1a) as a perfect model complex for hemocyanin. As a ligand they had used the tridentate $\text{HB}(3,5\text{-iPr}_2\text{pz})_3$, a hydrotris(pyrazolyl)borate.^[13] Five years later, a minor modification of this ligand allowed Kitajima and co-workers to synthesize the first copper superoxo complex with a side-on coordination (Figure 1.4.1b). The ligand used, $\text{HB}(3\text{-tBu-5-iPrpz})_3$, is sterically much more demanding than $\text{HB}(3,5\text{-iPr}_2\text{pz})_3$ because of the substitution of the three iso-propyl groups with tert-butyl groups.^[14]

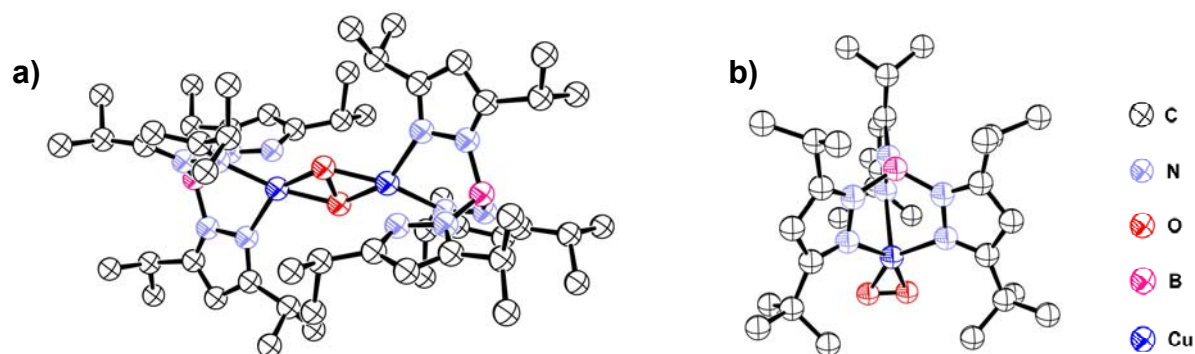


Figure 1.4.1: a) Molecular structure of the side-on coordinated copper peroxo complex $[(\text{HB}(3\text{-tBu-5-iPrpz})_3)_2(\text{O}_2)]$. b) Molecular structure of the side-on coordinated copper superoxo complex $[\text{HB}(3,5\text{-iPr}_2\text{pz})_3(\text{O}_2)]$.

However, the first crystal structure of a synthetic copper peroxo complex was described even earlier by Karlin and co-workers in 1988.^[12] This complex displayed an end-on coordination of the peroxo ligand. Karlin and co-workers used the tripodal ligand tris(2-pyridylmethyl)amine (tmpa), a tetradentate ligand, with one aliphatic and three aromatic N-donor atoms (Figure 2.1.2). It turned out, that this type of a tripodal ligand in general is perfectly suited for end-on coordination of dioxygen. Spectroscopic and kinetic studies showed that prior to the formation of the peroxo complex a superoxo complex is formed.^[19, 20] However, all attempts to isolate and to characterize this highly reactive superoxo intermediate were unsuccessful.

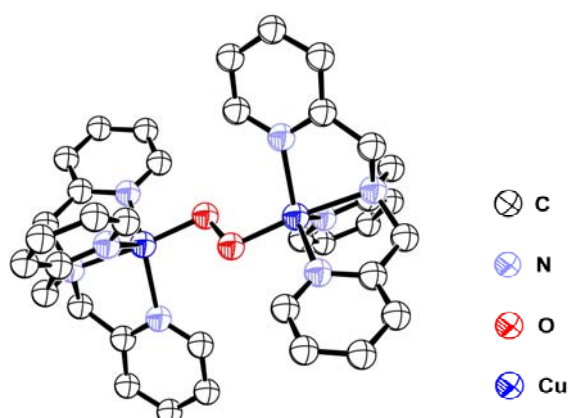


Figure 1.4.2: First molecular structure of a synthetic copper peroxo complex. The peroxo ligand is end-on coordinated between two $[\text{Cu}(\text{tmpa})]^{2+}$ units.

In 2004 Suzuki and co-workers described another example of a copper peroxo complex with an end-on coordination of the dioxygen ligand (only the second crystal structure of this type of complexes).^[21] Based on the results of the Schindler group they used tris(N-benzyl-N-methylaminoethyl)amine (Bz₃tren), another tripodal ligand from the tren family (with benzyl groups at the three terminal aliphatic N-donor atoms).^[22] Low temperature UV-vis measurements showed that similar to the copper/tmpa system a superoxo complex prior to the peroxo complex was formed. Here as well all efforts to isolate and characterize this species were unsuccessful.

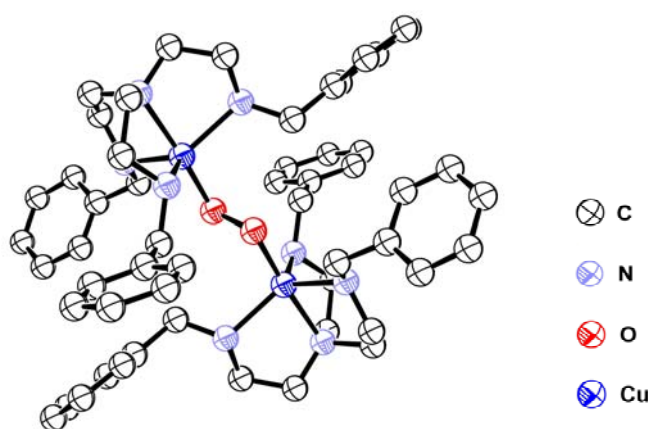


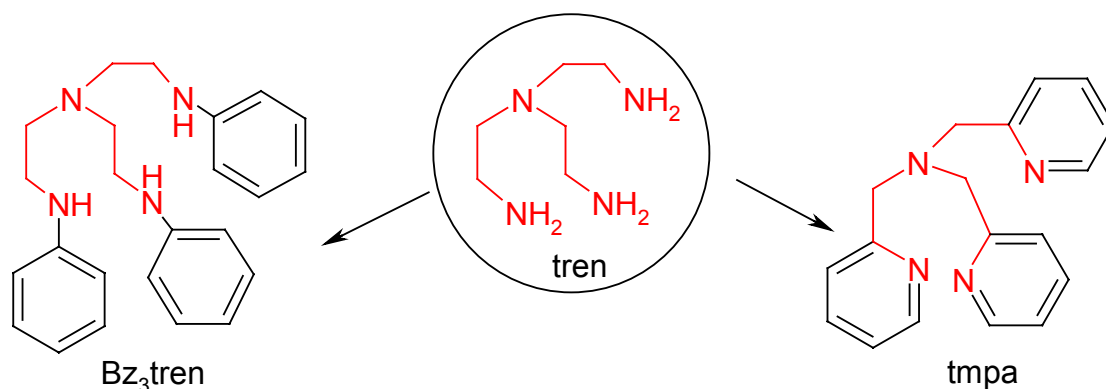
Figure 1.4.3: Molecular structure of a synthetic copper peroxo complex with Bz₃tren as ligand. The peroxo ligand is end-on coordinated between two [Cu(Bz₃tren)]²⁺ units.

1.5 Tripodal ligands

Ligands like tmpa or Bz₃tren are tetradentate ligands based on the parental amine tren (tris(2-aminoethyl)amine) as a tripodal unit. Tren is a chelate ligand with four aliphatic N-donor atoms, perfectly suited for the coordination of copper ions. A copper ion will be coordinated by the four nitrogen atoms, thus allowing to coordinate to an additional fifth ligand (e. g. peroxide) such that a trigonal bipyramidal geometry is adopted.^[23, 24]

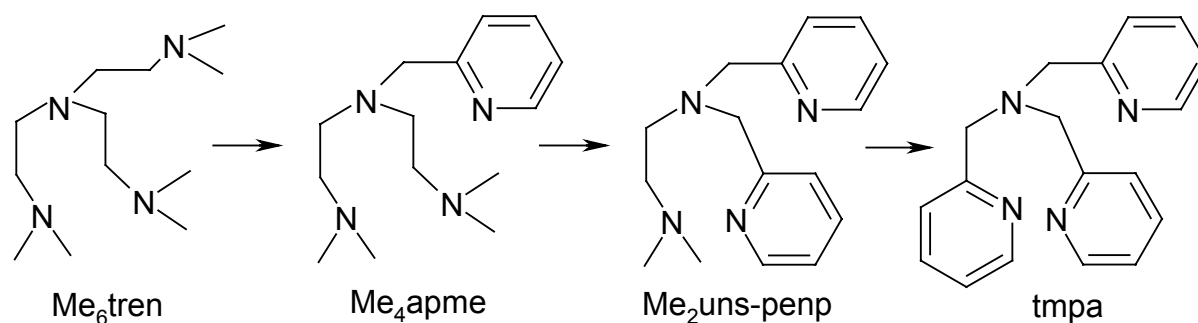
Therefore, tren should be an excellent ligand for the formation of end-on copper superoxo or peroxo complexes. However, due to the primary amine groups protonation of the “dioxygen adduct” complexes occurs and a fast irreversible decay

of the formed intermediates is observed. Still, in a dilute solution at low temperatures, a superoxo copper tren species could be observed spectroscopically for a very short time.^[3, 25]



Scheme 1.5.1: Tripodal ligands based on the parental amine tren.

Substitution of the hydrogen atoms through methyl groups solved this problem. Me_6tren , the fully methylated form of tren supported the formation of copper superoxo and peroxo complexes.^[25]



Scheme 1.5.2: Variation of ligands with tripodal tren skeleton.

If the harder aliphatic arms in Me_6tren (tris(2-dimethylaminoethyl)amine) are substituted in a systematic way by introducing the softer pyridine N-donor atoms the ligands Me_4apme (bis(2-dimethyl-aminoethyl)(2-pyridylmethyl)amine), $\text{Me}_2\text{uns-penp}$ (2-dimethyl-aminoethylbis(2-pyridylmethyl)-amine) and tmpa (tris(2-pyridyl-methyl)amine) are obtained. Systematic low temperature stopped-flow studies of the oxidation of the copper(I) complexes with these tripodal ligands showed a slight

stabilization of superoxo complexes when aliphatic N-donor atoms are present. Aromatic N-donor atoms in contrast seem to support formation of peroxy complexes.^[25, 26] Figure 1.5.1 shows the low temperature time resolved UV-vis spectra of the reaction of $[\text{Cu}(\text{Me}_6\text{tren})]^+$ and $[\text{Cu}(\text{tmpa})]^+$ with dioxygen under the same conditions in acetone. From the results of these measurements it is obvious that for the copper Me_6tren complex the superoxo complex (absorbance band at 410 nm) is still in equilibrium with the peroxy complex (absorbance band at 530 nm) while for the copper tmpa complex the superoxo complex is completely transformed to the according peroxy complex during the same reaction time.^[27]

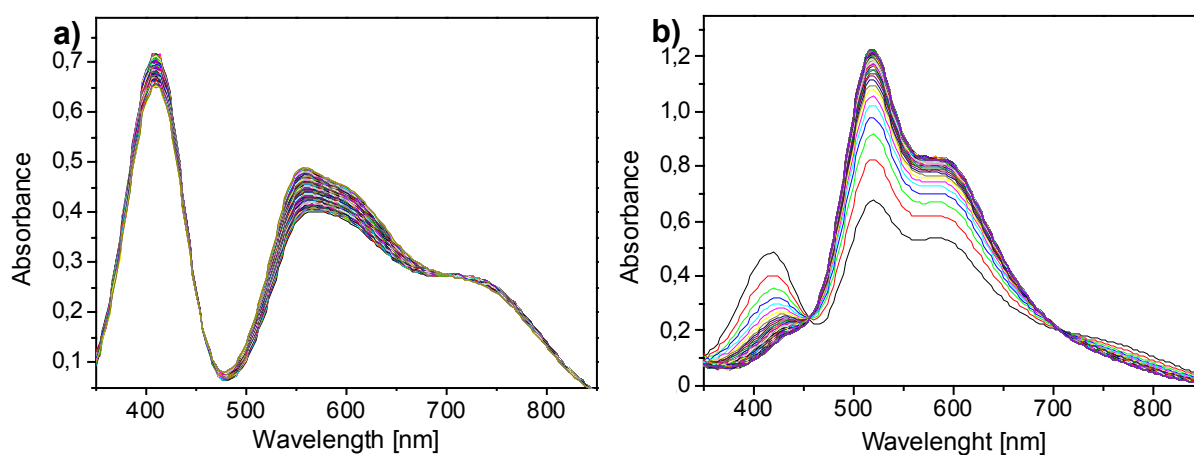
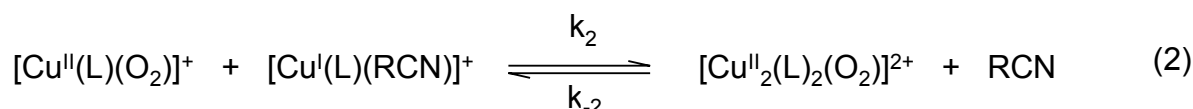
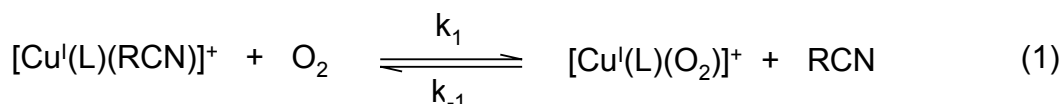


Figure 1.5.1: Time resolved spectra of a) the reaction of $[\text{Cu}(\text{Me}_6\text{tren})]\text{BPh}_4$ with dioxygen b) the reaction of $[\text{Cu}(\text{tmpa})]\text{BPh}_4$ with dioxygen by using low temperature stopped-flow techniques.

An important result of the systematic low temperature stopped-flow studies was, that the research groups of Karlin and Zuberbühler could elucidate the mechanism for this type of reaction.^[19, 20]

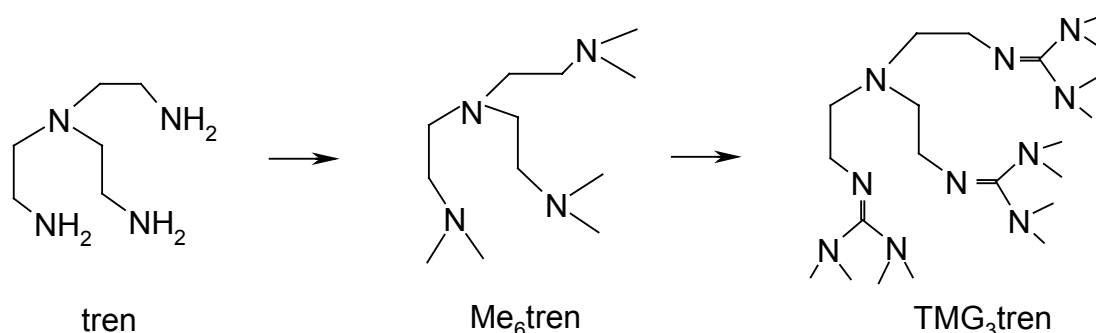
In the first step (equation 1) the copper(I) complex reacts reversibly with dioxygen to form a mononuclear superoxo intermediate that can be detected by the absorbance maximum at approximate 410 nm in the UV-vis spectrum. The second reversible reaction step (equation 2) is the formation of the dinuclear peroxy complex as a quite stable intermediate. This intensive blue colored complex, detectable with an absorbance maximum at around 530 nm, is formed through the reaction of the

superoxo complex with the copper(I) complex (available due to the equilibrium shown in equation 1). The final reaction step (equation 3) is the irreversible decay of the peroxo species.^[19, 20]



Scheme 1.5.3: Postulated mechanism for the reaction of copper(I) complexes with dioxygen.

Due to the fact that a copper end-on superoxo complex at that time has not been isolated and characterized, it was tried to improve the stability of this very reactive intermediate using an optimized ligand system. With the aliphatic tren system it was demonstrated that there would be a chance if the ligand could be modified accordingly. Based on the results on the tren chemistry a tren derivative tris(tetramethylguanidino)tren (TMG₃tren) developed by the Sundermeyer group was applied (Scheme 1.5.4).^[28]



Scheme 1.5.4: Ligands based on the tren unit.

DFT calculations and low temperature Resonance Raman measurements demonstrated that the copper(I) complex with TMG₃tren as ligand indeed led exclusively to the formation of a quite stable copper end-on superoxo complex.^[29]

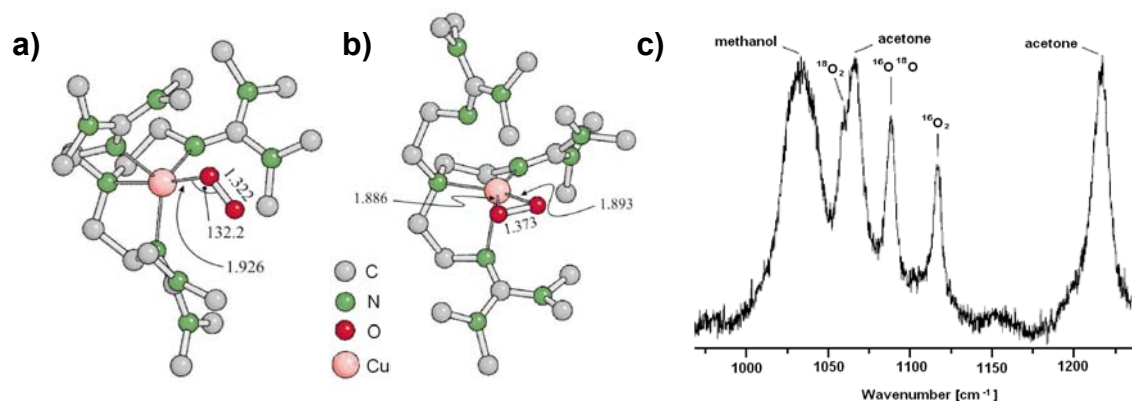


Figure 1.5.2: a) DFT calculated molecular structure of $[\text{Cu}(\text{TMG}_3\text{tren})\text{O}_2]^+$ with the preferred end-on coordination of the superoxo ligand. b) DFT calculated molecular structure of $[\text{Cu}(\text{TMG}_3\text{tren})\text{O}_2]^+$ with a side-on coordinated superoxo ligand. c) Resonance Raman spectrum of $[\text{Cu}(\text{TMG}_3\text{tren})\text{O}_2]^+$ in acetone by using a mixture of $^{16}\text{O}-^{16}\text{O}$, $^{16}\text{O}-^{18}\text{O}$ and $^{18}\text{O}-^{18}\text{O}$ at -70°C .

1.6 Projects

As described in the introduction it was observed many times that the reaction of dioxygen with copper(I) complexes with tripodal ligands can lead to the formation of two highly reactive intermediates: superoxo complexes as a 1:1 product in the first step and peroxo complexes as a 2:1 product in a consecutive step. Modification of the ligands applied allowed to isolate, characterize and investigate these species separately. For this reason the results of the research projects described herein are presented in two parts.

1.6.1 Superoxo complexes

Chapter 2 describes the results of investigations in regard to the end-on superoxo complex obtained with the ligand TMG₃tren. In detail the following results are discussed:

- After a large number of experiments, it was finally possible to obtain and to structurally characterize $[\text{Cu}(\text{TMG}_3\text{tren})\text{O}_2]\text{SbF}_6$ as the first synthetic copper superoxo complex with an end-on coordination (Chapter 2.1 and 2.2).

- The reactivity of $[\text{Cu}(\text{TMG}_3\text{tren})\text{O}_2]\text{SbF}_6$ towards C-H and O-H substrate oxygenations as a model for the copper monooxygenase C-H hydroxylation has been investigated (Chapter 2.3 and 2.4).

1.6.2 Peroxo complexes

Chapter 3 describes the copper peroxo complexes with the ligands Me_6tren , $\text{Me}_2\text{uns-penp}$, Me_4apme and tmpa . The results in detail are presented in the following way:

- Systematic synthetic and kinetic studies on the reversible binding of dioxygen of the copper complexes with the ligands $\text{Me}_2\text{uns-penp}$ and Me_4apme have been performed. Furthermore, in comparison with these systems a large number of crystallographic studies on the copper(I)/(II) complexes of the ligands Me_6tren , $\text{Me}_2\text{uns-penp}$, Me_4apme and tmpa have been performed. The major goal of this work was to identify copper peroxo complexes that can persist at room temperature (Chapter 3.1 and 3.2).
- The synthesis of extremely stabilized solid copper peroxo complexes of Me_6tren , $\text{Me}_2\text{uns-penp}$, Me_4apme and tmpa as ligands is described. The possible use of these complexes for selective oxidations with dioxygen in organic synthesis has been tested. This study includes the crystal structure of $[\text{Cu}_2(\text{Me}_6\text{tren})_2(\text{O}_2)](\text{BPh}_4)_2$ (Chapter 3.3 and 3.4).

Chapter 2 – Superoxo Complexes

This chapter includes two publications that were published in the journal “Angewandte Chemie” previously. These two publications have been obtained in cooperation with the following research groups and their individual participation in these projects is highly acknowledged:

- Prof. Dr. Jörg Sundermeyer, Dr. Ekaterina Gaoutchenova and Dr. Klaus Harms at the Philipps-Universität Marburg.
- Prof. Dr. Max C. Holthausen at the Johann Wolfgang Goethe-Universität Frankfurt.
- Prof. Dr. Kenneth D. Karlin, Debabrata Maiti, Prof. Dr. Dong-Heon Lee and Dr. Amy A. Narducci Sarjeant at the Johns Hopkins University Baltimore, USA.

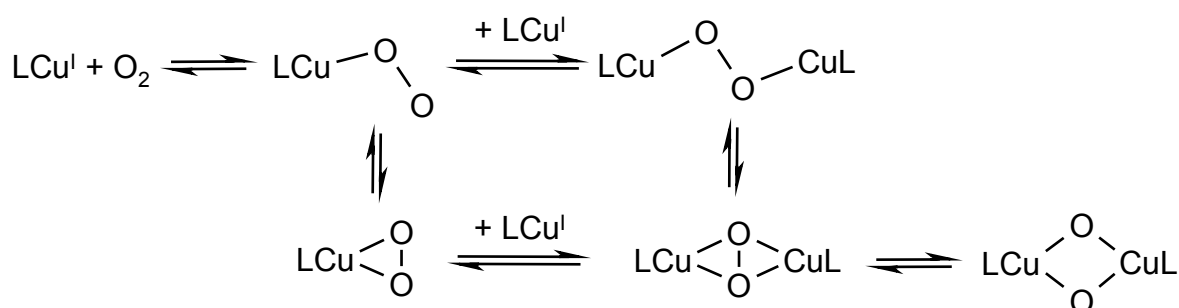
2.1 Crystallographic Characterization of a Synthetic 1:1 End-On Copper Dioxygen Adduct Complex

This work has been published previously in *Angewandte Chemie*.

Christian Würtele, Ekaterina Gaoutchenova, Klaus Harms, Max C. Holthausen, Jörg Sundermeyer and Siegfried Schindler

Angew. Chem., **2006**, 118, 3951 [*Angew. Chem. Int. Ed.*, **2006**, 45, 3867]

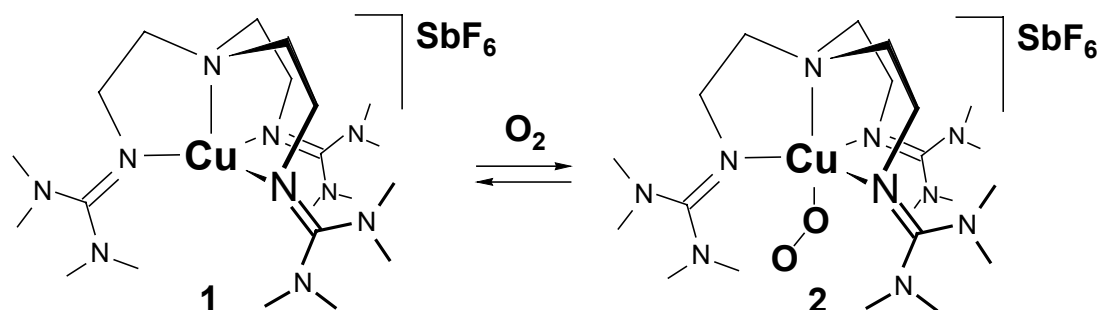
Synthetic bioinorganic copper dioxygen complexes have attracted great interest in the past decades because of their prominent role as oxidants in biochemistry and catalysis. Recent advances in this field form a basis to correlate the pronounced structural diversity of known complexes with the resulting differences in reactivity as oxidants.^[6, 7, 30] Many of these studies have been concerned with the fine tuning of ligand properties to stabilize the various copper oxygen compounds that occur as intermediates in the formation of reactive species and which are largely responsible for the oxidation activity.^[6, 7] The collective picture arising from these studies can be discussed within a general mechanistic framework of oxygen binding to copper complexes (Scheme 2.1.1, charges are omitted)^[3, 6, 7, 30] analogous to a scheme recently proposed for iron complexes.^[31]



Scheme 2.1.1: Possible reaction pathways for the reaction of mononuclear copper (I) complexes with dioxygen (charges are omitted).

While ample literature exists on the coordination chemistry and reactivity of 2:1 Cu/O₂ species,^[6, 7, 32, 33] the characterization of 1:1 Cu/O₂ complexes is complicated by the intrinsic tendency of these species to dimerize in solution or to decompose after irreversible ligand oxidation. Accordingly, to date only three crystallographically characterized examples for 1:1 Cu/O₂ complexes exist, all exhibiting a side-on (η^2) coordination mode.^[14, 34-37] End-on copper dioxygen adduct complexes have been proposed as reactive intermediates in the catalytic cycle of mononuclear copper enzymes such as peptidylglycine α -hydroxylating monooxygenase (PHM) or dopamine β -monooxygenase (D β H).^[6, 7] And indeed, very recently the existence of such a species could be demonstrated by X-ray crystallography for a precatalytic PHM complex.^[38] Yet, in the bioinorganic regime all attempts to isolate and characterize a synthetic analogue of the first step in Scheme 2.1.1, that is, the formation of an end-on 1:1 Cu/O₂ complex, failed to date.

With tripodal tetradentate tren (tris(2-aminoethyl)amine) or tmpa (tris(2-pyridylmethyl)amine) ligands, such complexes are short-lived and could only be detected as transient species at low temperatures using stopped-flow UV-vis spectroscopy.^[6, 7, 26, 30, 39, 40] In related studies we showed, however, that the high reactivity of the transient species can be moderated by use of sterically more demanding ligands with stronger N-donor character, such as Me₆tren.^[39] This success led us to employ the sterically congested superbasic^[41] tren derivative tris(tetramethylguanidino)tren (TMG₃tren)^[28] as a ligand and in a recent study we were eventually able to obtain a stable 1:1 Cu/O₂ adduct at low temperatures (Scheme 2.1.2).^[29]



Scheme 2.1.2: Reversible binding of dioxygen to [TMG₃trenCu]⁺.

Most remarkably – and in striking contrast to former experiments with other tren derivatives, for which only irreversible oxidation reactions were observed upon warming – we found that the formation of the Cu-O₂ adduct is reversible: warming of the intensively green solution of the adduct complex to room temperature caused release of dioxygen (colorless solution), while cooling of the sample led to back formation of the Cu-O₂ adduct (see Supporting Information). Warming/cooling cycles can be repeated many times without any evidence of major decomposition reactions. The progress of this reaction can readily be monitored by UV-vis, NMR or resonance Raman spectroscopy.^[29]

Different from other amine or imine tren derivatives the TMG₃tren ligand easily forms stable complexes with copper(I) and with copper(II) ions as shown by crystallographic studies.^[28] This stability is supported by the results of additional electrochemical investigations we performed with the [CuTMG₃tren]⁺ complex: using cyclic voltammetry we observed reversible redox behavior in acetone (-0.024/+0.140 V against Ag/AgCl). Of note is that in crystals of [Cu(TMg₃tren)]⁺ obtained from an acetonitrile solution, no solvent molecule is coordinated as an additional ligand. Even more remarkable is that in [Cu(TMg₃tren)]Cl the chloride anion only functions as counterion and does not coordinate to the copper(I) ion as one would expect.^[28] However, to investigate the general possibility of adding additional ligands we treated the copper(I) complex with CO in acetone at low temperatures. While it was not possible to isolate the corresponding carbonyl complex as a solid to date, we could detect its formation by IR spectroscopy (IR band at 2057 cm⁻¹, acetone solution, -80 °C).

For the present species we were also able to monitor the formation of the superoxo complex using low-temperature IR-spectroscopy ($\tilde{\nu}_{\text{O-O}} = 1122 \text{ cm}^{-1}$, acetone solution, -80 °C). This finding confirms the results of our previous resonance Raman measurements ($\tilde{\nu}_{\text{O-O}} = 1117 \text{ cm}^{-1}$). Based on the almost perfect match between experiment and quantum chemical results for the O-O stretching frequencies we excluded the presence of a side-on coordination mode and we felt safe to assign a stable 1:1 end-on Cu-O₂ adduct, which is best described as an end-on superoxo-copper(II) species.^[29] Yet, erroneous characterizations of 1:1 Cu-O₂ adduct complexes and recent discussions on the assignment of end-on superoxo-copper(II) complexes in the literature^[21, 29, 42] made it clear that only a crystal structure of this

complex would allow for the unambiguous characterization of such a 1:1 end-on Cu-O₂ adduct.^[6, 7, 30] In spite of the observed stability of the Cu-O₂ adduct formed, numerous attempts to obtain crystals of this compound failed. However, after systematic modifications of the crystallization atmosphere we are now able to present the missing link, a high-quality crystal structure of [Cu(TMGe₃tren)O₂][SbF₆] (Figure 2.1.1).

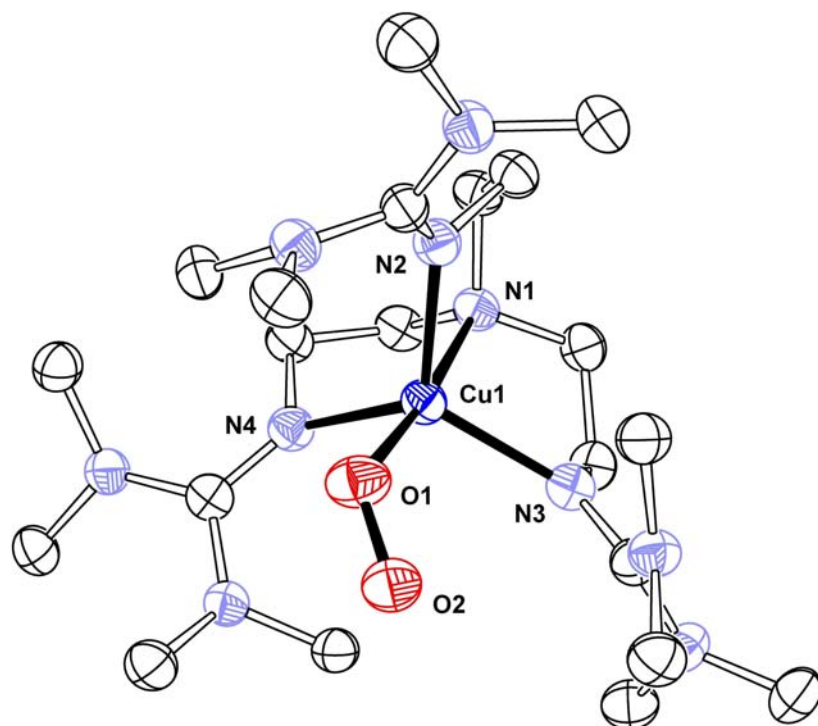


Figure 2.1.1: Molecular structure of [TMG₃trenCu(O₂)]⁺. ORTEP plot with ellipsoids of 50 % probability (hydrogen atoms, acetone solvent molecules present in the crystal lattice, and the 6 % disorder position of O2A are not shown). Selected bond lengths [Å] and angles [°]: O1-O2 1.280(3), O1-Cu1 1.927(2), O2-Cu1 2.842(7), O2-O1-Cu1 123.53(2).

Perfectly in line with our previous quantum chemical characterization^[43] the dioxygen in [Cu(TMGe₃tren)O₂][SbF₆] is coordinated to Cu1 in an end-on fashion as an axial ligand in the trigonal-bipyramidal complex. The O1-O2 bond is 1.280(3) Å and the O2-O1-Cu1 angle is 123.53(18)°. This geometry is consistent with the recent X-ray results on the copper dioxygen complex in PHM^[38] in which the crystal structure, determined to 1.85 Å resolution, showed an end-on coordination mode to a

mononuclear copper ion in the precatalytic enzyme complex with an O-O bond of 1.23 Å and an Cu-O-O angle of 110°.

Our present results clearly demonstrate that end-on coordination of O₂ to copper ions can lead to quite stable intermediates, which lends support to their assumed role as important intermediates in catalytic oxidation reactions. The end-on copper superoxide species most likely represents the primary adduct formed in the interaction of Cu(I) ions with dioxygen molecules preceding the formation of other key copper dioxygen species shown in Scheme 2.1.1. The resolution of the crystal structure of [Cu(TMG₃tren)(O₂)]SbF₆ reported herein is excellent, and of far superior to that of other end-on superoxo transition-metal complexes presented to date. Hence this complex represents a key intermediate with which to correlate spectroscopic and structural features of mononuclear end-on superoxo copper complexes in the future.

2.1.1 Experimental Section

Cyclic voltammetry experiments were performed with a Princeton BAS Model 263 instrumentation, using a 1 mM solution of the copper(I) complex (tetraphenylborate as anion) in acetone. Electrodes employed were glassy carbon (working electrode), Ag/AgCl (reference electrode) and a platinum wire (auxiliary electrode). Ferrocene was used as an internal reference (0.450/0.580 V). IR-spectroscopy in solution was performed using a Nicolet 510 P FT-IR Spectrometer equipped with a low-temperature cell (RIEC) and CaF₂ windows (0.1 mm).

1: Under the inert atmosphere of a glove box TMG₃tren (0.6 g, 1.4 mmol) was dissolved in acetonitrile (4 mL) to which of a solution of [Cu(CH₃CN)₄]SbF₆ (0.6 g, 1.3 mmol in acetonitrile (6 mL) was added. The complex [Cu(TMG₃tren)]SbF₆ was precipitated by addition of diethyl ether (approximately 40 mL). The light yellow solid was filtered and washed with diethyl ether. Yield: 0.637 g (70.34 %).

2: Under inert atmosphere [Cu(TMG₃tren)]SbF₆ was dissolved in a very small amount of acetone, cooled to -55 °C and then oxidized with pure, dry dioxygen for 5 minutes. The green solution obtained was then kept at -80 °C for one week leading to intensively green crystals of the end-on superoxo complex, [Cu(TMG₃tren)O₂]SbF₆, suitable for X-ray structural characterization: Some material was taken under inert atmosphere from the crystallization flask kept at -80 °C and put into precooled

perfluoropolyether oil. A suitable crystal was selected under the microscope using a cryostated loop, it was shock frozen using liquid nitrogen and mounted on the diffractometer which was equipped with a cooling device. For the measurement conditions see the Supporting Information.

A refinement using a first data set collected at 173 K showed a threefold 75:15:10 disorder of the end-on coordinated superoxide ligand and a very short O-O bond length of approximately 1.1 Å (unpublished results). In contrast, refinement on the data set obtained at 100 K showed only a minor disorder of 94:0:6 (see Supporting Information). The O-O bond length converges now to 1.280(2) Å. Because of the small occupation factor, the geometric parameters involving the second position of disorder are not reliable. The highest residual electron density remained in the region of the SbF_6^- -anion.

CCDC 287898 (1) contains the supplementary crystallographic data for this paper. These data can be obtained free of charge from The Cambridge Crystallographic Database Centre via www.ccdc.cam.ac.uk/data_request/cif.

2.2 Selected parts of supporting information and unpublished results for chapter 2.1

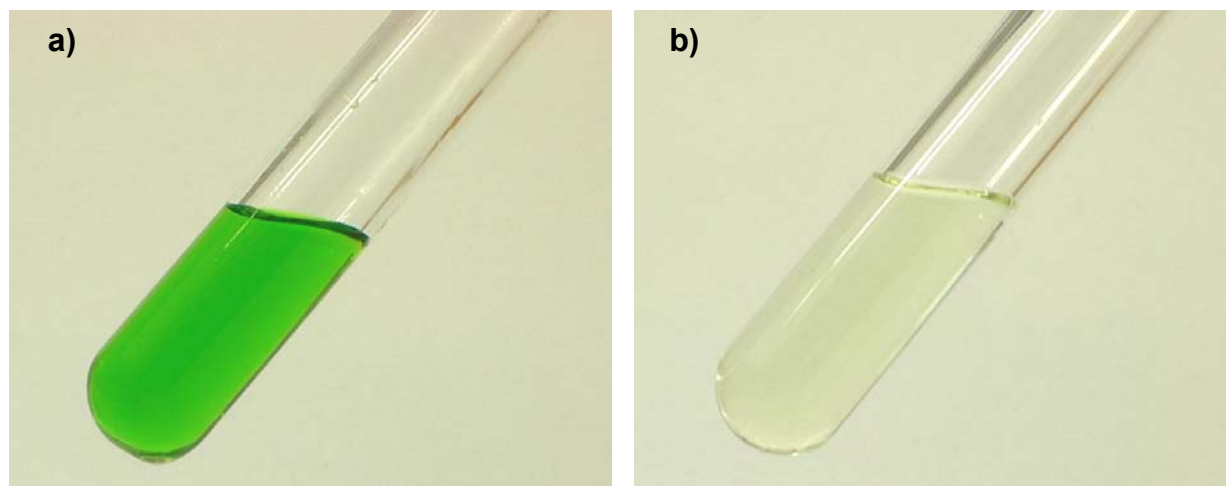


Figure 2.2.1: The photographs show the warming/cooling cycles of the superoxo complex. a) Green solution of $[\text{Cu}(\text{TMG}_3\text{tren})\text{O}_2]\text{SbF}_6$ (5 mmol) in acetone at $-80\text{ }^\circ\text{C}$. b) After warming to room temperature, the solution turned to a slightly yellow color. This cycle could be repeated for many times without any evidence of major decomposition reactions.

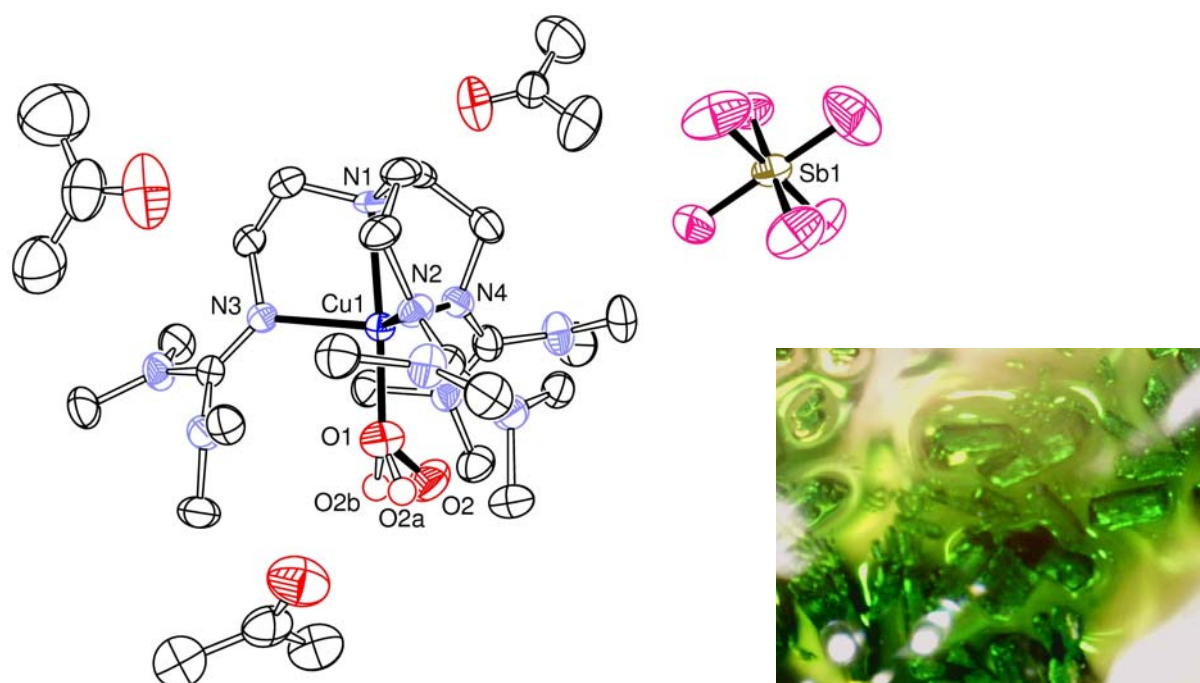


Figure 2.2.2: First molecular structure of $[\text{TMG}_3\text{trenCu}(\text{O}_2)]\text{SbF}_6 \cdot 3 (\text{CH}_3)_2\text{CO}$, data collected at 173 K. ORTEP plot with ellipsoids of 50 % probability show the independent unit of the elementary cell, the threefold 75:15:10 disorder of the end-on

coordinated superoxide ligand and the very short O-O bond length. Selected bond lengths [Å] and angles [°]: O1-O2 1.184(5), O1-Cu1 1.926(3); O2-O1-Cu1 128.3(3). The photograph shows the crystals in acetone at -80 °C.

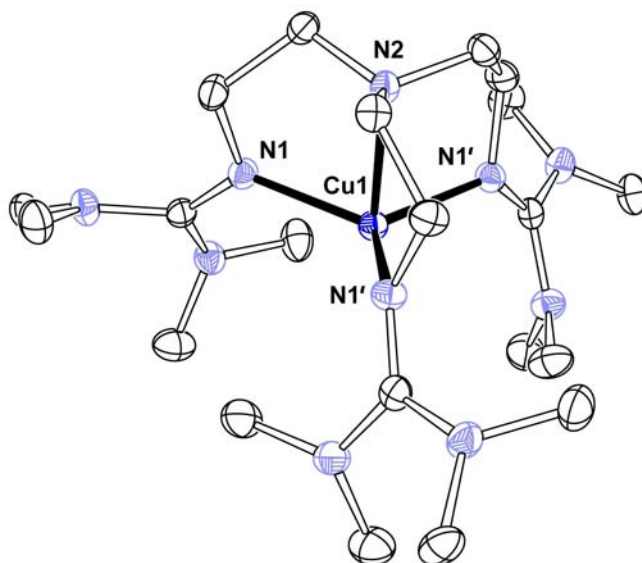


Figure 2.2.3: Molecular structure of $[\text{Cu}(\text{TMG}_3\text{tren})]^+$. ORTEP plot with ellipsoids of 50 % probability (hydrogen atoms and SbF_6^- anion are not shown). Selected bond lengths [Å] and angles [°]: Cu1-N2 2.175(4), Cu1-N1 2.048(2); N1-Cu1-N2 84.20(6), N1-Cu1-N1' 118.99(2).

2.2.1 Synthesis of $[\text{Cu}(\text{TMG}_3\text{tren})]\text{PF}_6$.

Under the inert atmosphere of a glove box TMG_3tren (0.18 g, 0.4 mmol) was dissolved in acetone (10 mL) to which of a solution of $[\text{Cu}(\text{CH}_3\text{CN})_4]\text{PF}_6$ (0.15 g, 0.4 mmol in acetone (10 mL) was added. The formed complex solution of $[\text{Cu}(\text{TMG}_3\text{tren})]\text{PF}_6$ in acetone was directly used for low temperature IR measurements.

2.2.2 Synthesis of $[\text{Cu}(\text{TMG}_3\text{tren})]\text{BPh}_4$.

Under the inert atmosphere of a glove box TMG_3tren (0.5 g, 1.13 mmol) was dissolved in acetone (4 mL) to which of a solution of $[\text{Cu}(\text{CH}_3\text{CN})_4]\text{PF}_6$ (0.37 g, 1.0 mmol in acetone (5 mL) was added. To the formed complex of $[\text{Cu}(\text{TMG}_3\text{tren})]\text{PF}_6$ was added a solution of NaBPh_4 (0.34 g, 1.0 mmol in acetone (5 mL). The complex $[\text{Cu}(\text{TMG}_3\text{tren})]\text{BPh}_4$ was precipitated by addition of diethyl ether (approximately 50 mL). The white solid was filtered and washed with diethyl ether. Yield: 0.71 g (86 %).

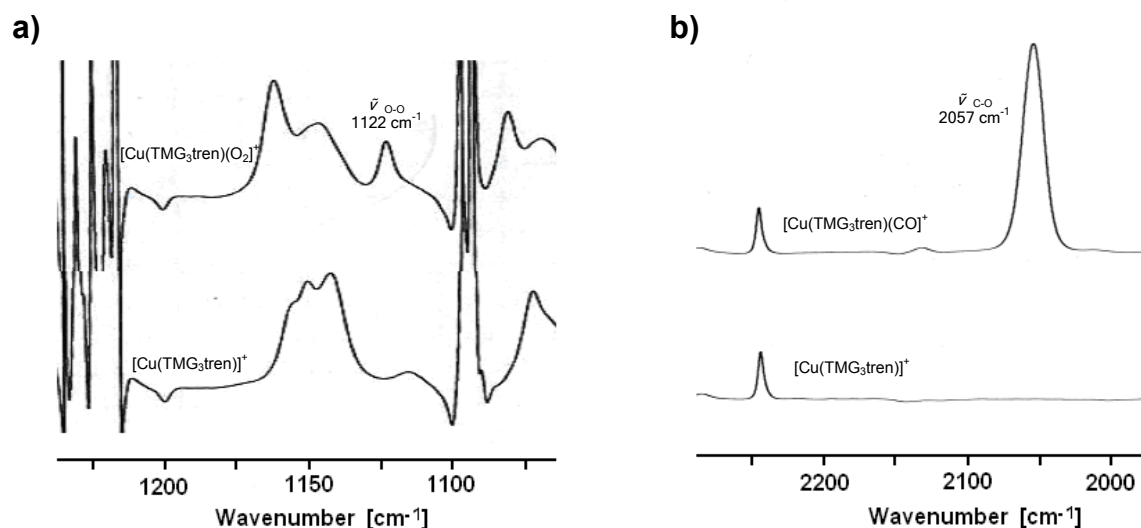


Figure 2.2.4: Low temperature IR-spectra of [Cu(TMG₃tren)]PF₆ (20 mmol) in acetone at -80 °C. a) Observation of the O-O stretch vibration at 1122 cm⁻¹ by adding dioxygen. b) Observation of the C-O stretch vibration at 2057 cm⁻¹ by adding carbon monoxide.

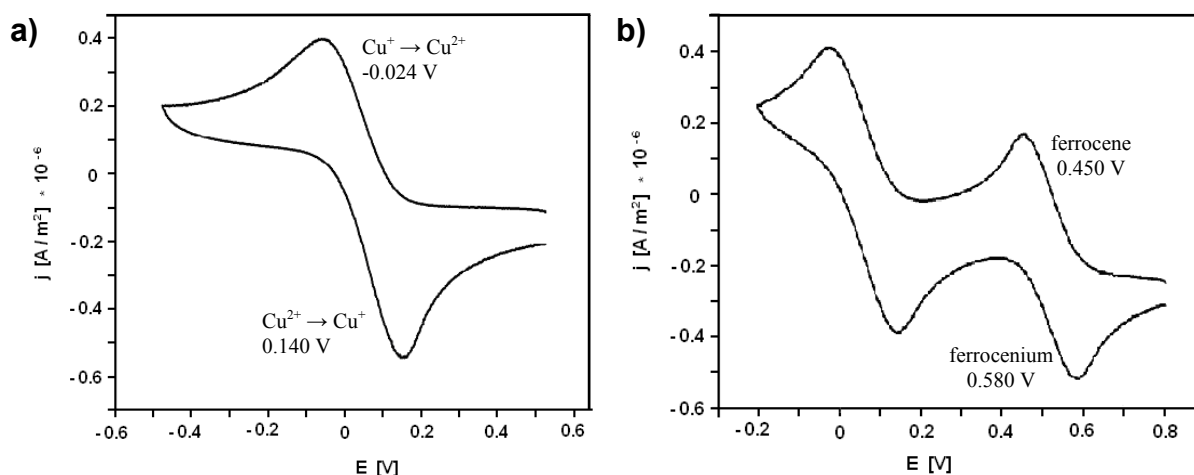


Figure 2.2.5: Cyclic voltammetry of [Cu(TMG₃tren)]BPh₄ (1 mmol/L) in acetone, under argon, at room temperature. Supporting electrolyte [NBu₄]BF₄ = 0.1 mol/L. a) Reversible redox behavior against Ag/AgCl of the pure complex. b) Ferrocene was added as an internal reference.

Table 2.2.1. Cyclic voltammetry for [Cu(TMG₃tren)]BPh₄ in acetone ^[a]

Compound	E_p^{red} [V]	E_p^{ox} [V]	$E_{1/2}$ [V]	ΔE [mV]
[Cu(TMG ₃ tren)]BPh ₄	-0.024	0.140	0.058	164
Ferrocene	0.450	0.580	0.515	130

^[a] All potentials measured with a glassy carbon electrode vs. Ag/AgCl using [NBu₄]BF₄ (0.1 mol/L) as electrolyte. $[E_{1/2} = (E_p^{\text{red}} + E_p^{\text{ox}})/2; \Delta E = E_p^{\text{ox}} - E_p^{\text{red}}]$.

2.2.3 Low temperature stopped-flow studies

Under inert atmosphere a solution of $[\text{Cu}(\text{TMG}_3\text{tren})]\text{SbF}_6$ (0.4 mmol/L) in acetone was mixed with dioxygen saturated acetone, at $-85\text{ }^\circ\text{C}$. The reaction was observed by using low temperature stopped flow measurements (256 UV-vis spectra in a total time of 256 ms). The formation of the superoxo complex $[\text{Cu}(\text{TMG}_3\text{tren})\text{O}_2]^+$ at this temperature is still extremely fast and a detailed kinetic study of this formation reaction is not possible.

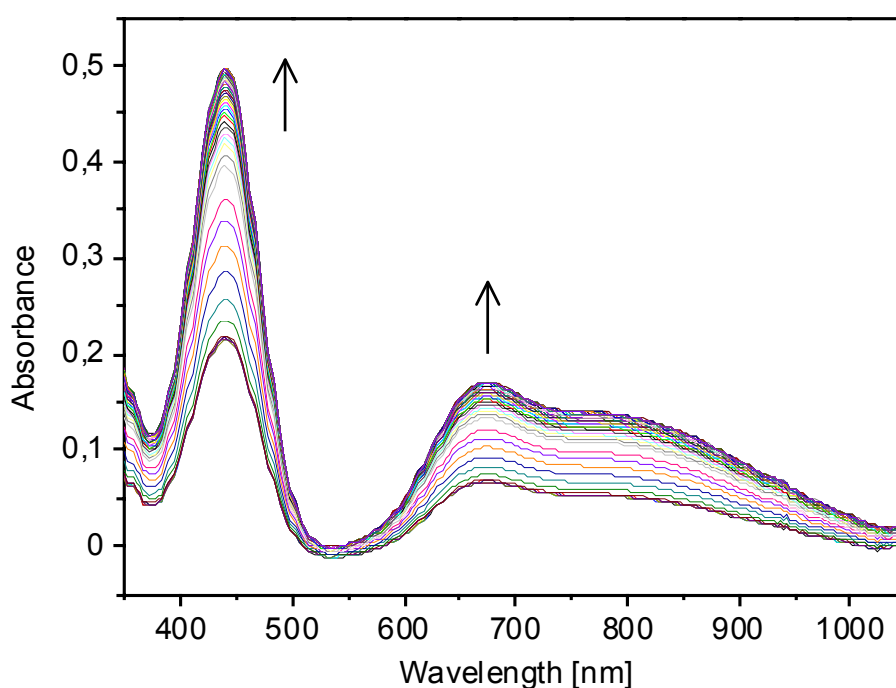


Figure 2.2.6: Time resolved spectra of the reaction of $[\text{Cu}(\text{TMG}_3\text{tren})]\text{SbF}_6$ with dioxygen by using low temperature stopped-flow technique. The spectra show the formation of the absorption bands at 442 and 690 nm.

2.3 Reaction of a Copper(II) Superoxo Complex Lead to C-H and O-H Substrate Oxygenations: Modeling Copper-Monooxygenase C-H Hydroxylation

This work has been published previously in *Angewandte Chemie*.

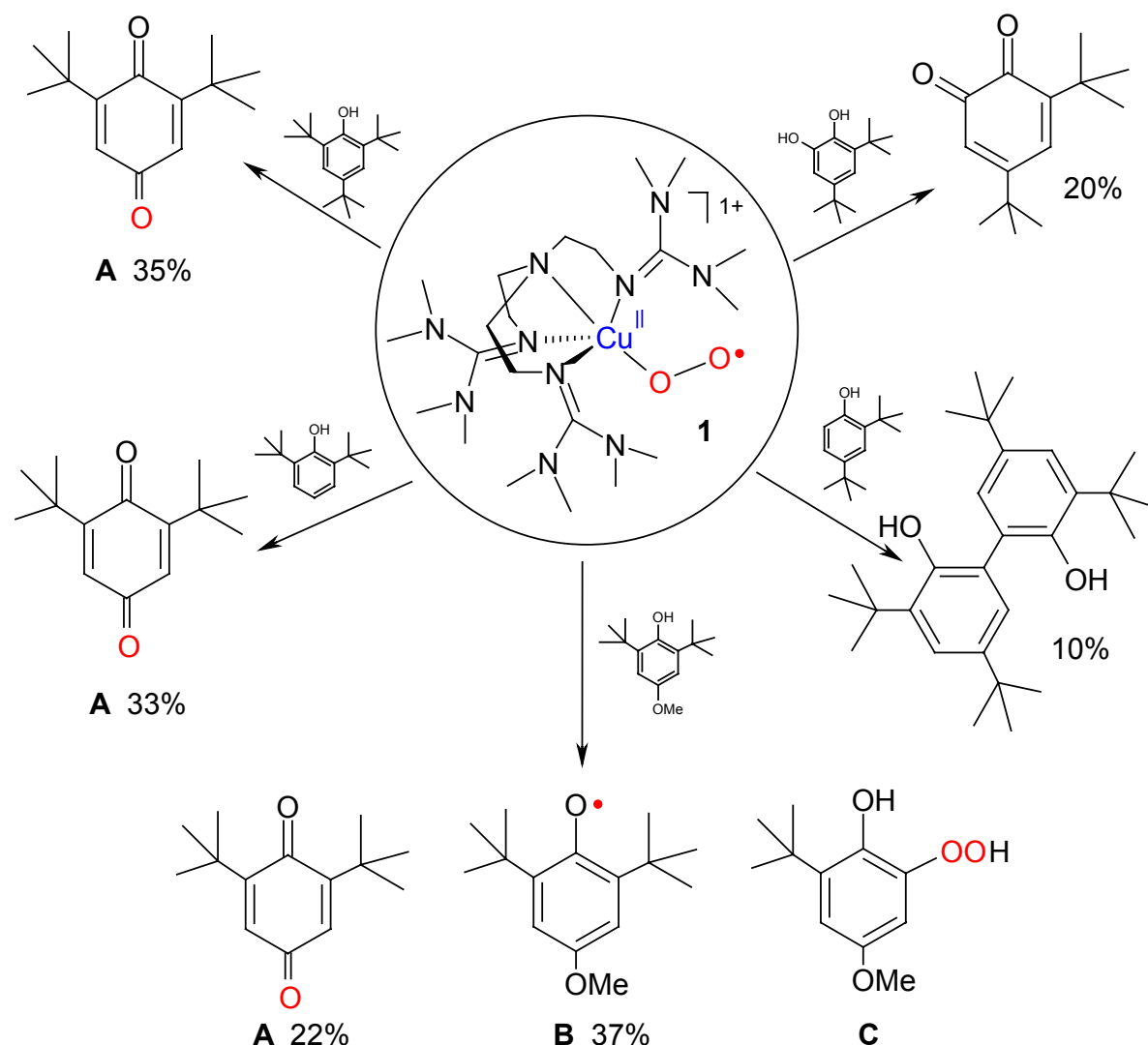
Debabrata Maiti, Dong-Heon Lee, Katya Gaoutchenova, Christian Würtele, Max C. Holthausen, Amy A. Narducci Sarjeant, Jörg Sundermeyer, Siegfried Schindler and
Kenneth D. Karlin

Angew. Chem., **2007**, 120, 88 [*Angew. Chem. Int. Ed.*, **2007**, 47, 82]

Mononuclear species derived from copper(I) and dioxygen such as a cupric superoxide $\text{Cu}^{\text{II}}(\text{O}_2^{\bullet-})$, cupric hydroperoxide $\text{Cu}^{\text{II}}(\text{OOH}^-)$, or even high-valent copper oxo species have all been considered as possible active-site reactive intermediates in the copper monooxygenases dopamine β -monooxygenase (D β M) and peptidylglycine α -hydroxylating monooxygenase (PHM).^[44-50] These enzymes effect neurohormone and neurotransmitter biosyntheses through active-site substrate C-H hydroxylation, which involve H-atom abstraction. However, synthetic investigations have to date revealed only very limited substrate reactivity with $\text{Cu}^{\text{II}}(\text{O}_2^{\bullet-})$ or $\text{Cu}^{\text{II}}(\text{OOH}^-)$ complexes,^[51-57] especially with C-H-containing substrates. There are as yet no discrete examples of, nor evidence for, high-valent copper oxo species $\text{Cu}^{\text{II}}\text{O}^{\bullet-}$ ($\leftrightarrow \text{Cu}^{\text{III}}=\text{O}$)^[58-60] or $\text{Cu}^{\text{III}}-\text{O}^{\bullet-}$ (i.e. $\{\text{CuO}\}^{2+}$).^[48] On the basis of a recent X-ray structure of PHM,^[38] an entity with an η^1 -coordination (end-on) of a superoxo ligand to copper(II) is formulated and suggested to also apply to D β M. Such a cupric superoxo complex capable of effecting an enzymatic substrate hydroxylation by H-atom abstraction has drawn experimental^[61, 62] and theoretical^[47, 63, 64] support, although as mentioned, higher-valent CuO species are predicted to be the hydroxylating agent by some researchers.^[49, 50]

Synthetically derived 1:1 dioxygen-copper(I) adducts are best described as superoxo copper(II) or peroxo copper(III) complexes, with the O_2 moiety bound either in an η^1 (end-on) or η^2 (side-on) metal coordination mode.^[48, 65] Recent efforts employing nitrogenous N_4 tripodal tetradentate ligands have led to the crystallographic

characterization of the mononuclear $\text{Cu}^{\text{II}}(\text{O}_2^{\bullet-})$ complex with an end-on superoxo ligand $[\text{Cu}^{\text{II}}(\text{TMG}_3\text{tren})(\eta^1\text{O}_2^{\bullet-})]^+$ (**1**, TMG_3tren = tris(2-(N-tetra-methylguanidyl)-ethyl)amine; $\angle (\text{Cu}-\text{O}-\text{O}) = 123.5^\circ$, $d(\text{Cu}-\text{O}) = 1.927 \text{ \AA}$, $d(\text{O}-\text{O}) = 1.280 \text{ \AA}$ and $\tilde{\nu}_{\text{O}-\text{O}} = 1118 \text{ cm}^{-1}$ (resonance Raman spectroscopy)), which is formed reversibly from the corresponding cuprous analogue.^[11, 29] Spectroscopic analysis showed that a related dioxygen-copper adduct, $[\text{Cu}^{\text{II}}(\text{NMe}_2\text{-TMPA})(\eta^1\text{-O}_2^{\bullet-})]^+$ (**2**, $\text{NMe}_2\text{-TMPA}$ = tris(4-dimethylaminopyrid-2-ylmethyl)amine), also possesses an end-on superoxo ligand; the chemistry of **2** provided the first clear demonstration of $\text{Cu}^{\text{II}}(\text{O}_2^{\bullet-})$ oxidative reactivity with exogenous substrates (substituted phenols), resulting in their oxidation, oxygenation or hydroperoxylation.^[51]



Scheme 2.3.1: Reactivity of **1** with exogenous phenolic substrates. Red oxygen represent ^{18}O .

Herein, we report our initial findings concerning the reactivity of **1**. It also oxygenates or oxidizes phenols in a manner similar to that found for **2**. Of greater interest and importance is our present demonstration that starting with the cupric superoxide complex **1**, addition of a H-atom (H^\bullet) donor leads to a C-H activation, O-atom insertion into a *N*-methyl group on the TMG_3tren ligand, and formation of a copper(II) alkoxide product.

When 4-MeO-2,6-*t*Bu₂-phenol was added to a solution of a newly synthesized tetraarylborate salt $[\text{Cu}^{\text{II}}(\text{TMG}_3\text{tren})(\text{O}_2^{\bullet-})]\text{B}(\text{C}_6\text{F}_5)_4$ (**1**, excess O_2 removed)^[66] at -80°C in 2-methyltetrahydrofuran (MeTHF) and the mixture kept cold for 48 h, the color changed from the initial light to bright green. A sharp strong peak was observed at 407 nm in the absorption spectrum of the reaction solution, and EPR spectroscopy revealed a $g \approx 2$ signal, both of which indicate the formation of the corresponding stabilized phenoxyl radical (**B**, Scheme 2.3.1) formed in approximately 37 % yield. Other products identified in this reaction of **1** and 4-MeO-2,6-*t*Bu₂-phenol are the 2,6-*t*Bu₂-benzoquinone (**A**, ca. 22 % yield) and the aryl hydroperoxide (**C**). More importantly, a crystalline, green copper complex was also isolated in approximately 80 % yield; the product is the alkoxide complex $[\text{Cu}^{\text{II}}(\text{TMG}_3\text{trenO}^-)]\text{B}(\text{C}_6\text{F}_5)_4$ (**3**, ESI-MS: m/z 518.19; $[\text{Cu}^{\text{II}}(\text{TMG}_3\text{trenO}^-)]^+$).

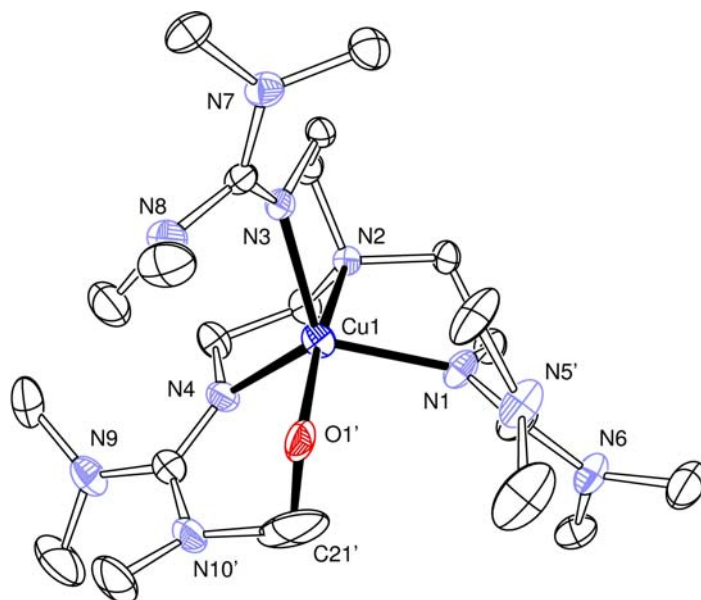


Figure 2.3.1: X-ray structure of $[\text{Cu}^{\text{II}}(\text{TMG}_3\text{trenO}^-)]\text{B}(\text{C}_6\text{F}_5)_4$ (**3**) with near trigonal-bipyramidal copper-ion coordination. Selected bond lengths [Å] and angles [°]: Cu1-O1' 1.972(5), Cu1-N2 2.091(2), Cu1-(N1,N3,N4) 2.053–2.117; O1'-Cu1-N2 170.01(16).

Its X-ray structure^[67] reveals that hydroxylation of a ligand methyl group has occurred, with the result that the cupric ion is now coordinated by the inserted O atom of the alkoxide (Figure 2.3.1).^[68, 69] With an $^{18}\text{O}_2$ source used in the generation of **1** and subsequent addition of 4-MeO-2,6-*t*Bu₂-phenol, GC-MS reveals ^{18}O incorporation into **A** and **C** (68 % and 85 %, respectively). For product cupric complex **3**, the ESI-MS positive ion parent peak (which shows the expected $^{63,65}\text{Cu}$ isotope pattern) shifts to m/z 520.27 (99 % incorporation), thus indicating that $[\text{Cu}^{\text{II}}(\text{TMG}_3\text{tren}^{18}\text{O}^-)]^+$ has formed; the alkoxide O atom is derived from dioxygen.^[66]

The observed oxidative reactivity of $\text{Cu}^{\text{II}}[(\text{TMG}_3\text{tren})(\text{O}_2^{\bullet-})]^+$ (**1**) is similar to the Cu_M -centered action at the PHM active site (Cu_M has His₂Met coordination), in which oxygenation of a prohormone peptide substrate C-H group adjacent to an amide nitrogen atom occurs.^[46] Furthermore, our cupric alkoxide complex **3** mimics the “product complex” discussed for both PHM and D β M,^[46] which is formed in the enzyme in the step just prior to product release. When **1** is warmed from -80 °C to room temperature, O_2 is released giving the cuprous compound $[\text{Cu}^{\text{I}}(\text{TMG}_3\text{tren})]^+$.^[28] Thus, the cupric superoxo complex itself is not capable of the observed hydroxylation reaction. As described above, reaction of **1** with a phenol is required.

Superoxo complex **1** also reacts with other phenols to give oxidation products similar to those seen for **2** (Scheme 2.3.1).^[51] As determined by low-temperature reactions subsequent warming and workup, 2,6-*t*Bu₂-phenol and 2,4,6-*t*Bu₃-phenol produce benzoquinone **A** (Scheme 2.3.1, 33 and 35 % respectively). With $^{18}\text{O}_2$ -labeled **1**, approximately 65 % ^{18}O -atom incorporation into **A** occurs for the reaction of **1** and 2,4,6-*t*Bu₃-phenol. With 2,4-*t*Bu₂-phenol, the typical^[30] oxidative coupling product 4,4',6,6'-*t*Bu₄-2,2'-biphenol (10 %) is observed. Reaction of 3,5-*t*Bu₂-catechol with **1** leads to the corresponding benzoquinone (20 %, Scheme 2.3.1).^[66]

In fact, all of the reactions of **1** with these other phenols also lead to substantial yields (65 % or more)^[66] of ligandhydroxylated copper(II) alkoxide $[\text{Cu}^{\text{II}}(\text{TMG}_3\text{trenO}^-)]^+$ (**3**), as determined by comparison of authentic **3** (see above) ESI-MS and EPR spectroscopic signatures of the dark green crystalline solids obtained. As we concluded for the chemistry of **2** with phenols,^[51] the products observed with **1** (Scheme 2.3.1) can be explained by initial phenol-substrate H-atom abstraction and subsequent addition of the superoxo complex to the ArO^\bullet species. We suggest that alkoxide complex **3** arises from the course of reaction $\{\text{Cu}^{\text{II}}(\text{O}_2^{\bullet-})\} + \text{ArOH} \rightarrow \{\text{Cu}^{\text{II}}-$

(OOH⁻) + ArO•, wherein a highly reactive cupric hydroperoxo species is produced in close proximity to the TMG₃tren *N*-methyl group.

To further test this hypothesis we use a H-atom donor that might not itself react further. Reaction of **1** with TEMPO-H (Scheme 2.3.2) at -80 °C or below (i.e. to -120 °C) in MeTHF over one hour produces a dark green solution. This process leads to disappearance of the characteristic bands ascribed to **1** (447, 680, 780 nm; Figure 2.3.2a),^[29] while a new absorption at approximately 350 nm (sh) appears.

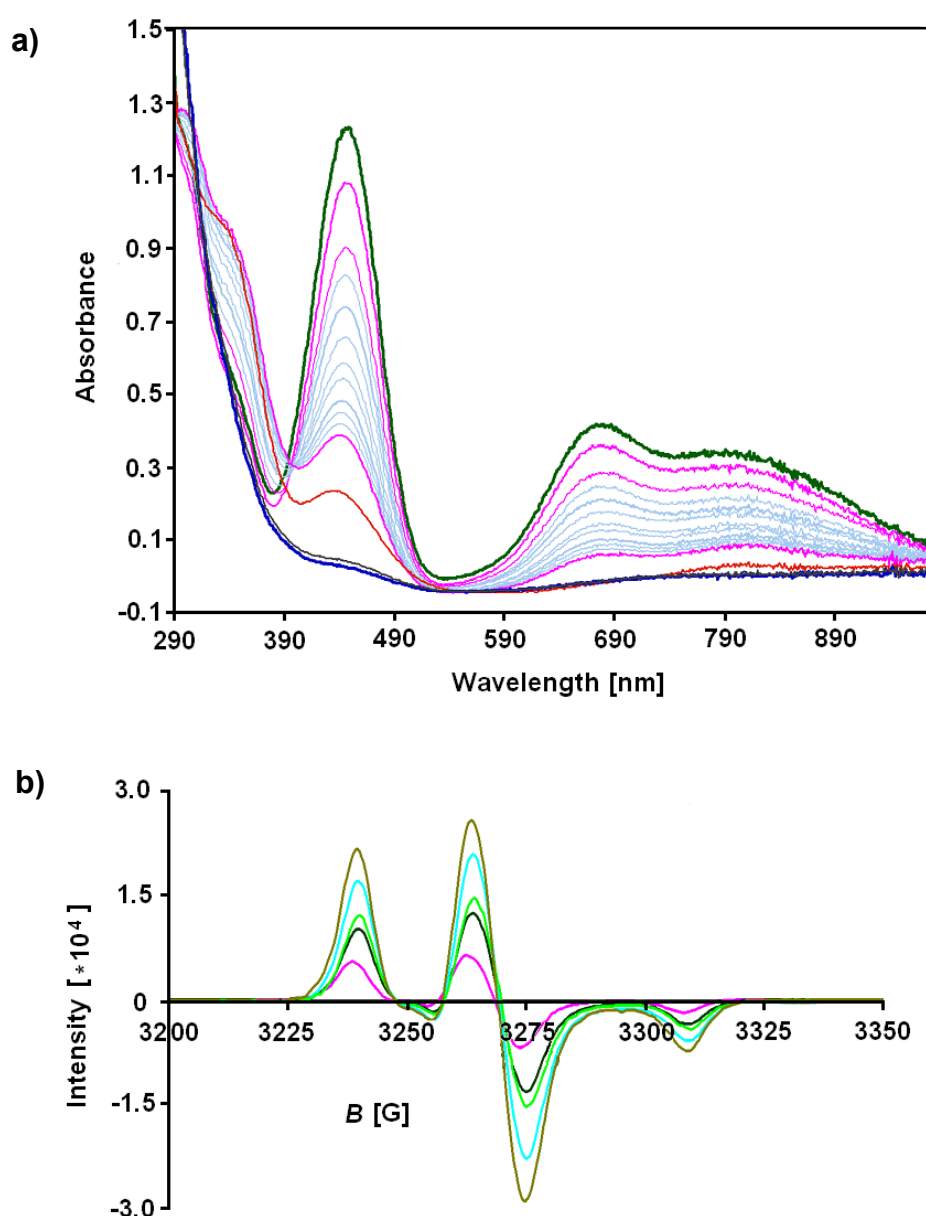
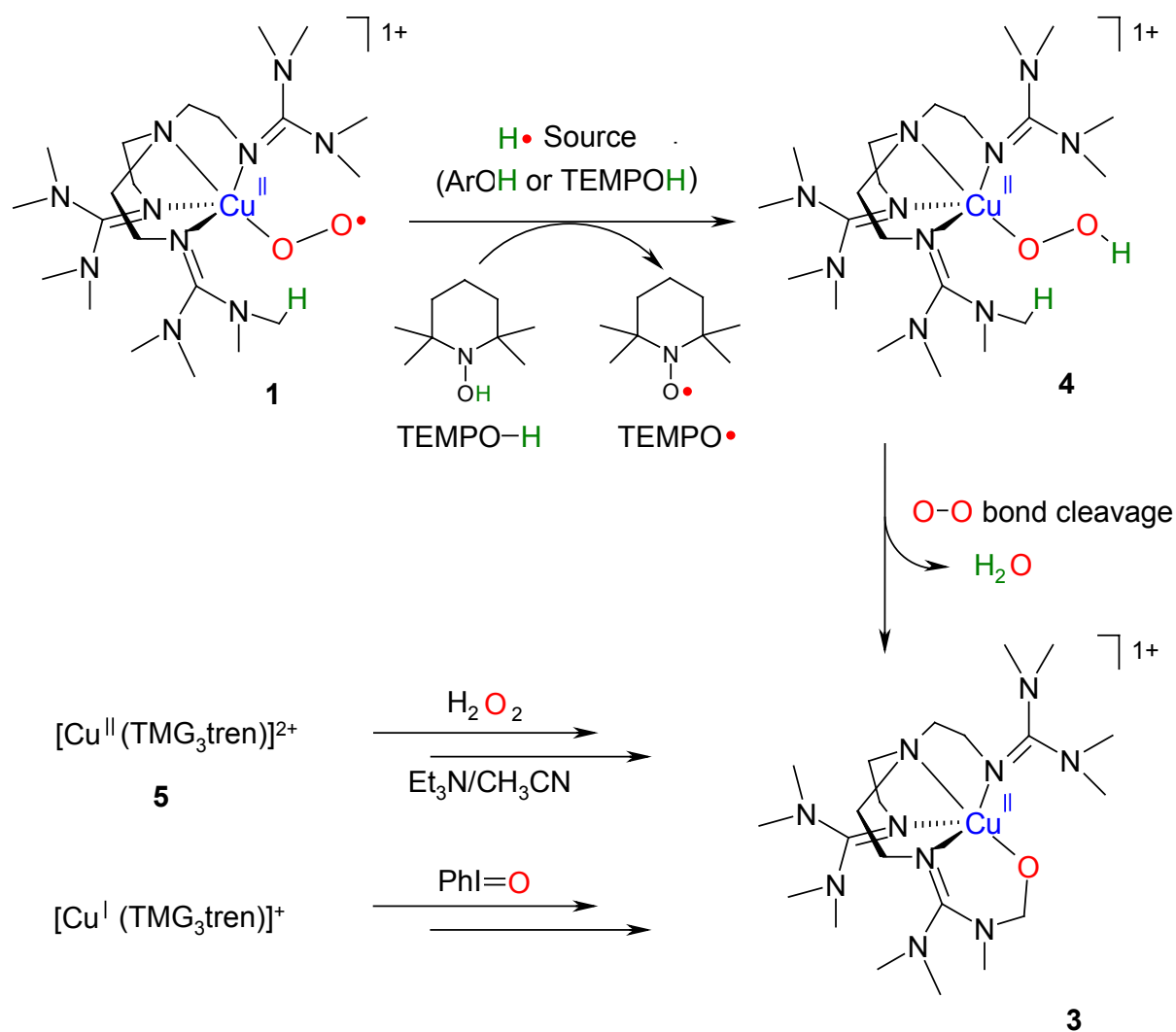


Figure 2.3.2: a) UV-vis and b) EPR spectroscopic monitoring of the reaction of [Cu^{II}(TMG₃tren)(O₂⁻)]⁺ (**1**) with TEMPO-H. In (a), the starting spectrum is green and the final spectrum is dark blue; in (b), the starting spectrum is pink and the final spectrum is light green.

The presence of an isosbestic point suggests that **1** directly converts to the new complex formulated as hydroperoxo complex $[\text{Cu}^{\text{II}}(\text{TMG}_3\text{tren})(\text{OOH}^-)]^+$ (**4**, Scheme 2.3.2). Support for this supposition comes from EPR spectroscopy. During the UV-vis monitoring at $-80\text{ }^\circ\text{C}$, aliquots of the solution were transferred to EPR sample tubes and immediately frozen at 77K. The EPR spectra thus obtained (as a function of time) confirm the increasing intensity of the signal arising from TEMPO^\bullet as the reaction progresses (Figure 2.3.2b). Comparisons of EPR intensity to authentic TEMPO^\bullet suggest the reaction yield to be approximately 90 %. Using ESI-MS or EPR spectroscopy to characterize reaction solutions from which the TEMPO^\bullet product has been separated out by extraction,^[66] the formation of $[\text{Cu}^{\text{II}}(\text{TMG}_3\text{trenO}^-)]^+$ (**3**, Scheme 2.3.2) was confirmed by comparison of data to the crystallographically characterized **3** (see above). The results thus strongly support the view that a hydroperoxo complex derived from **1** forms and is active in the hydroxylation of the *N*-methyl ligand.

More support comes from finding that the same chemistry occurs by treating a copper(II) analogue with hydrogen peroxide (Scheme 2.3.2). The complex $[\text{Cu}^{\text{II}}(\text{TMG}_3\text{tren})]^{2+}$ (**5**) was synthesized as the bis-perchlorate salt and isolated after reacting $\text{Cu}^{\text{II}}(\text{ClO}_4)_2 \cdot 6\text{H}_2\text{O}$ with the ligand TMG_3tren in acetonitrile. Addition of a small excess of $\text{H}_2\text{O}_2/\text{Et}_3\text{N}$ to a greenish-blue acetonitrile solution of **5** at $-40\text{ }^\circ\text{C}$ rapidly leads to a dark green product solution, which, after workup was confirmed to be authentic **3**. The formation of ^{18}O -labeled **3** (as determined by ESI-MS) when $\text{H}_2^{18}\text{O}_2$ was employed in this reaction^[66] further implicates formation of a $\text{Cu}^{\text{II}}(\text{OOH}^-)$ species that leads to the hydroxylation.

In light of the possibility that high-valent copper oxo species may be involved in copper-mediated O_2 activation (see above), we carried out the reaction of iodosylbenzene with the cuprous complex $[\text{Cu}^{\text{I}}(\text{TMG}_3\text{tren})]^+$.^[28] PhIO and its analogues have been extensively employed as oxo-transfer reagents to generate high-valent metal oxo complexes through reactions with reduced species {i.e. $\text{PhIO} + [\text{M}^{\text{n+}}-(\text{ligand})] \rightarrow [\text{M}^{\text{n+2}}=\text{O}^{2-}](\text{ligand}) + \text{PhI}$; $\text{M} = \text{heme, non-heme Fe, Mn, etc.}$).^[70-73] Interestingly, $[\text{Cu}^{\text{I}}(\text{TMG}_3\text{tren})]^+$ ^[28] also produces alkoxo species **3** in near quantitative yields upon reaction with PhIO (Scheme 2.3.2).^[66, 74] This observation suggests the possibility that a high-valent Cu oxo (or perhaps a $\text{Cu}(\text{OIPh})$ species)^[75] forms during the hydroxylation reaction.



Scheme 2.3.2: Varying pathways to produce hydroxylated product **3**.

In summary, we have described a novel example of a copper-dioxygen adduct that undergoes a reaction reminiscent of certain copper monooxygenases, that is, O-atom transfer from a dioxygen-derived species to the *N*-methyl group of the ligand in $[\text{Cu}^{\text{II}}(\text{TMG}_3\text{tren})(\text{O}_2^{\cdot-})]^+$ (**1**). The hydroxylated product has been captured as the alkoxide complex $[\text{Cu}^{\text{II}}(\text{TMG}_3\text{trenO}^-)]^+$ (**3**). The $\text{Cu}^{\text{II}}(\text{O}_2^{\cdot-})$ moiety in **1** is not able to effect this reaction, but when a hydrogen-atom donor (i.e. a phenols or TEMPO-H) is added, the hydroxylation reaction occurs. A hydroperoxo complex $[\text{Cu}^{\text{II}}(\text{TMG}_3\text{tren})(\text{OOH}^-)]^+$ (**4**) is thus implicated as the active species formed by such a reaction,^[68, 69] as further supported by the observation that ligand hydroxylation occurs when $[\text{Cu}^{\text{II}}(\text{TMG}_3\text{tren})]^{2+}$ (**5**) is subjected to basic hydrogen peroxide.

Thus, while these $[\text{Cu}^{\text{II}}(\text{ligand})(\text{O}_2^{\cdot-})]^+$ complexes (**1** and **2**) can effect phenolic H-atom abstractions and subsequent phenol oxidation or oxygenation, a copper(II)

hydroperoxo (but not an analogue with an end-on superoxo ligand) can effect C-H activation, that is, O₂-derived hydroxylation of a methyl group. As we have suggested in reports concerning the chemistry of mono- or dinuclear copper(II) hydroperoxo complexes,^[52, 53, 76, 77] the true oxidant may be the (Cu^{II})_nOOH moiety or a species derived from it, such as a high-valent copper oxo moiety (see above).^[48, 58-60] This possibility is hinted at but certainly not proven by the results of reactions using PhIO. Additional experimental and theoretical research is required to provide further deeper insights into the dioxygen activation chemistry described.

2.4 Selected parts of supporting information for chapter 2.3

2.4.1 Synthesis of $[\text{Cu}^{\text{I}}(\text{TMG}_3\text{tren})]\text{B}(\text{C}_6\text{F}_5)_4$

TMG₃tren (0.150 g, 0.341 mmol) and $[\text{Cu}^{\text{I}}(\text{CH}_3\text{CN})_4]\text{B}(\text{C}_6\text{F}_5)_4$.^[78] (0.309 g, 0.341 mmol) were placed in a 100 mL Schlenk flask under argon and 4 mL deoxygenated MeTHF was added. After 1 h of stirring, deoxygenated pentane (70 mL) was added to the stirring solution resulting in a white cloudy mixture. Additional time was provided for the white powder to settle. The supernatant was decanted under argon atmosphere, and the solid obtained was recrystallized three times from MeTHF/pentane. The solid was dried in vacuum for 2 h yielding 0.298 g (74 %) of product. Anal. Calcd. For $[\text{Cu}^{\text{I}}(\text{TMG}_3\text{tren})]\text{B}(\text{C}_6\text{F}_5)_4$; C₄₅H₄₈BCuF₂₀N₁₀: C, 45.68; H, 4.09; N, 11.84. Found: C, 45.24; H, 3.43; N, 11.55.

2.4.2 Generation of $[\text{Cu}^{\text{II}}(\text{TMG}_3\text{tren})(\text{O}_2)]\text{B}(\text{C}_6\text{F}_5)_4$

$[\text{Cu}^{\text{I}}(\text{TMG}_3\text{tren})]\text{B}(\text{C}_6\text{F}_5)_4$ (0.008 g, 0.007 mmol) was dissolved in 3.0 mL MeTHF inside the drybox and was taken in a Schlenk cuvette. Dioxygen was subsequently bubbled with a long needle syringe through the -80 °C solution of $[\text{Cu}^{\text{I}}(\text{TMG}_3\text{tren})]\text{B}(\text{C}_6\text{F}_5)_4$ for 10 s and the change in the absorption was followed by UV-vis spectroscopy. Colorless solution of $[\text{Cu}^{\text{I}}(\text{TMG}_3\text{tren})]\text{B}(\text{C}_6\text{F}_5)_4$ turned to a brilliant green solution due to formation of an end-on bound mononuclear copper(II)-superoxo species, $[\text{Cu}^{\text{II}}(\text{TMG}_3\text{tren})(\text{O}_2)]\text{B}(\text{C}_6\text{F}_5)_4$. The complex $[\text{Cu}^{\text{II}}(\text{TMG}_3\text{tren})(\text{O}_2)]^+$ had been previously characterized by X-ray crystallography and also by resonance Raman and UV-vis spectroscopy.^[11, 29] Application of a vacuum/argon purge to the solution of $[\text{Cu}^{\text{II}}(\text{TMG}_3\text{tren})(\text{O}_2)]\text{B}(\text{C}_6\text{F}_5)_4$ lead to a change from bright green to colorless copper(I) solution ($[\text{Cu}^{\text{I}}(\text{TMG}_3\text{tren})]\text{B}(\text{C}_6\text{F}_5)_4$); as decrease in the absorption features due to $[\text{Cu}^{\text{II}}(\text{TMG}_3\text{tren})(\text{O}_2)]\text{B}(\text{C}_6\text{F}_5)_4$ occurred. This oxygenation-superoxo formation/deoxygenation-copper(I) (re)formation cycle can be repeated several times. The product $[\text{Cu}^{\text{II}}(\text{TMG}_3\text{tren})(\text{O}_2)]\text{B}(\text{C}_6\text{F}_5)_4$ was sensitive towards temperature and released O₂ completely upon warming up to room temperature. In addition, during the decomposition, the bridging peroxo species was never observed.

2.4.3 Reaction of $[\text{Cu}^{\text{II}}(\text{TMG}_3\text{tren})(\text{O}_2)]\text{B}(\text{C}_6\text{F}_5)_4$ with *p*-MeO-2,6- $^t\text{Bu}_2$ -phenol

$[\text{Cu}^{\text{I}}(\text{TMG}_3\text{tren})]\text{B}(\text{C}_6\text{F}_5)_4$ (0.015 g, 0.013 mmol) was dissolved in 3 mL MeTHF inside the drybox and was taken in a Schlenk cuvette. The cuvette was cooled to $-80\text{ }^\circ\text{C}$ and dioxygen was bubbled for 10 s whereupon colorless solution turned to green solution of $[\text{Cu}^{\text{II}}(\text{TMG}_3\text{tren})(\text{O}_2)]\text{B}(\text{C}_6\text{F}_5)_4$. Excess dioxygen was removed carefully via vacuum/argon purging. *p*-MeO-2,6- $^t\text{Bu}_2$ -phenol (0.003 g, 0.013 mmol) was dissolved in 75 μL MeTHF inside the drybox and was added anaerobically to $[\text{Cu}^{\text{II}}(\text{TMG}_3\text{tren})(\text{O}_2)]\text{B}(\text{C}_6\text{F}_5)_4$ via a microliter syringe. The resulting mixture was bubbled with argon for 5 s at $-80\text{ }^\circ\text{C}$ and was kept cold for 48 h. The EPR spectrum of this solution (Figure 2.4.1b) exhibited a spectrum characteristic of a phenoxyl radical (X-band spectrometer ($\nu = 9.776\text{ GHz}$); $g = 2.006$) and corresponding UV-vis spectrum contained a characteristic absorption ($\lambda_{\text{max}} \sim 407\text{ nm}$) of the substituted phenoxyl radical MeO-2,6-Phenoxy (Figure 2.4.1a). The MeO-2,6-Phenoxy species was produced in $\sim 37\%$ yield as was determined from the known extinction coefficient^[79] at 403 nm ($\epsilon\ 1,560$). Resulting solution was washed three times with pentane (90 mL) and the supernatant was dried over Na_2SO_4 . This pentane solution was reduced in volume by rotary evaporation and was analyzed by GC and GC-MS confirming (Figure 2.4.2 and Figure 2.4.3) the formation of 2,6- $^t\text{Bu}_2$ -benzoquinone (yield $\sim 22\%$) and MeO-TBHP (authentic commercial 2,6- $^t\text{Bu}_2$ -benzoquinone was also used for comparison). When $^{18}\text{O}_2$ was employed to generate $[\text{Cu}^{\text{II}}(\text{TMG}_3\text{tren})(^{18}\text{O}_2)]\text{B}(\text{C}_6\text{F}_5)_4$ and a similar follow-up procedures were performed; $\sim 68\%$ ^{18}O -atom incorporation in 2,6- $^t\text{Bu}_2$ -benzoquinone (Figure 2.4.4) and $\sim 85\%$ ^{18}O -atom incorporation (Figure 2.4.5) in MeO-TBHP occur.

After pentane washing, copper product was further purified by recrystallization from MeTHF/pentane. X-ray quality crystals of this compound $[\text{Cu}^{\text{II}}(\text{TMG}_3\text{trenO})]\text{B}(\text{C}_6\text{F}_5)_4$ were obtained (Figure 2.2.2) by pentane diffusion into the MeTHF solution. The green crystals weighed 0.012 g (yield, $\sim 80\%$) after vacuum-drying for 1 h. Anal. Calcd. For $[\text{Cu}^{\text{II}}(\text{TMG}_3\text{trenO})]\text{B}(\text{C}_6\text{F}_5)_4 \cdot (\text{MeTHF})_{0.5}$; $\text{C}_{47.5}\text{H}_{52}\text{BCuF}_{20}\text{N}_{10}\text{O}_{1.5}$: C, 45.96; H, 4.22; N, 11.28. Found: C, 46.03; H, 3.90; N, 10.83. ESI-MS of $[\text{Cu}^{\text{II}}(\text{TMG}_3\text{trenO})]^+$ (518.19, $\text{M}^+ = [\text{Cu}^{\text{II}}(\text{TMG}_3\text{trenO})]^+$, see Figure 2.4.6). When the formation of $[\text{Cu}^{\text{II}}(\text{TMG}_3\text{tren})(\text{O}_2)]\text{B}(\text{C}_6\text{F}_5)_4$ was carried out with $^{18}\text{O}_2$ and a similar procedure was followed (see above), the positive ion peak clusters shifted to $m/z\ 520.27$ (Figure 2.4.7) due to the formation of $[\text{Cu}^{\text{II}}(\text{TMG}_3\text{tren}^{18}\text{O})]^+$. The analysis confirmed $\sim 99\%$ ^{18}O -atom incorporation in $[\text{Cu}^{\text{II}}(\text{TMG}_3\text{tren}^{18}\text{O})]^+$ occurred.

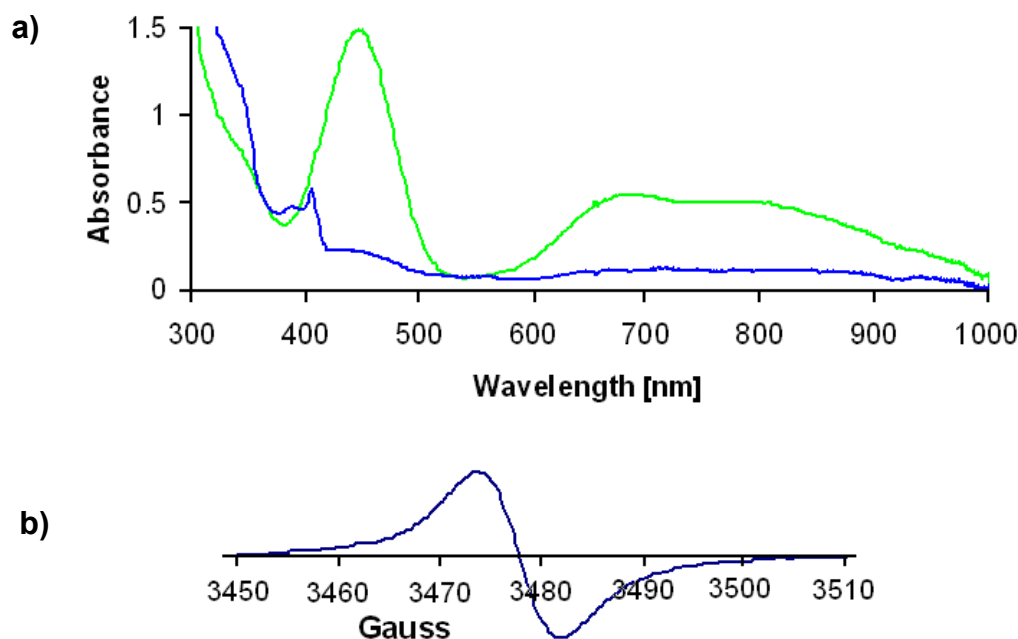


Figure 2.4.1: a) UV-vis spectra of $[\text{Cu}^{\text{II}}(\text{TMG}_3\text{tren})(\text{O}_2^-)]\text{B}(\text{C}_6\text{F}_5)_4$ at $-80\text{ }^\circ\text{C}$ in MeTHF (green) and the reaction of this superoxo complex with *p*-MeO-2,6- $^t\text{Bu}_2$ -phenol (See synthetic procedures above) indicating the formation of phenoxyl radical MeO-2,6-Phenoxy ($\lambda_{\text{max}} \sim 407\text{ nm}$) (blue). b) EPR spectrum of phenoxyl radical, MeO-2,6-Phenoxy (See synthetic procedures above) from the reaction of $[\text{Cu}^{\text{II}}(\text{TMG}_3\text{tren})(\text{O}_2)]\text{B}(\text{C}_6\text{F}_5)_4$ with *p*-MeO-2,6- $^t\text{Bu}_2$ -phenol. $g = 2.006$.

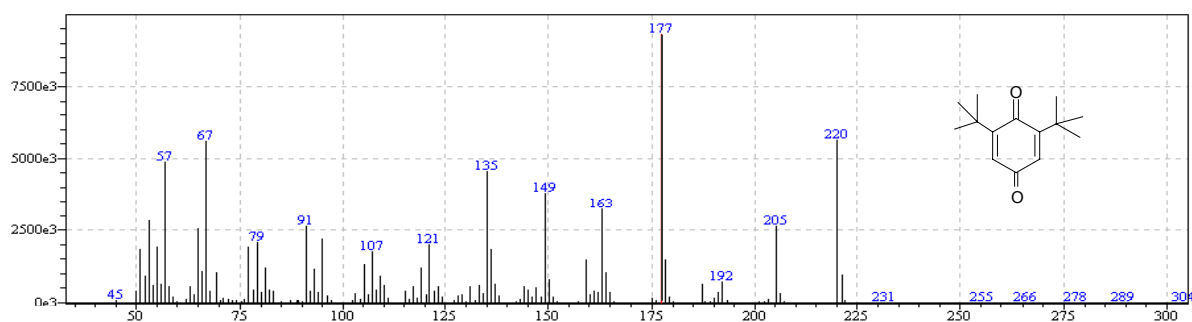


Figure 2.4.2: GC-MS spectrum of 2,6- $^t\text{Bu}_2$ -benzoquinone (See synthetic procedures above), $m/z = 220$, from the reaction of $[\text{Cu}(\text{TMG}_3\text{tren})\text{O}_2]\text{B}(\text{C}_6\text{F}_5)_4$ with *p*-MeO-2,6- $^t\text{Bu}_2$ -phenol.

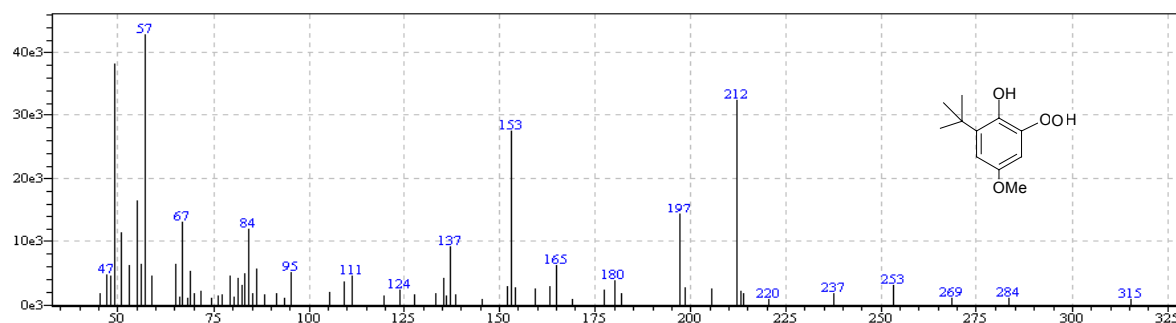


Figure 2.4.3: GC-MS spectrum of MeO-TBHP (See synthetic procedures above), $m/z = 212$, from the reaction of $[\text{Cu}(\text{TMG}_3\text{tren})\text{O}_2]\text{B}(\text{C}_6\text{F}_5)_4$ with p -MeO-2,6- $t\text{Bu}_2$ -phenol.

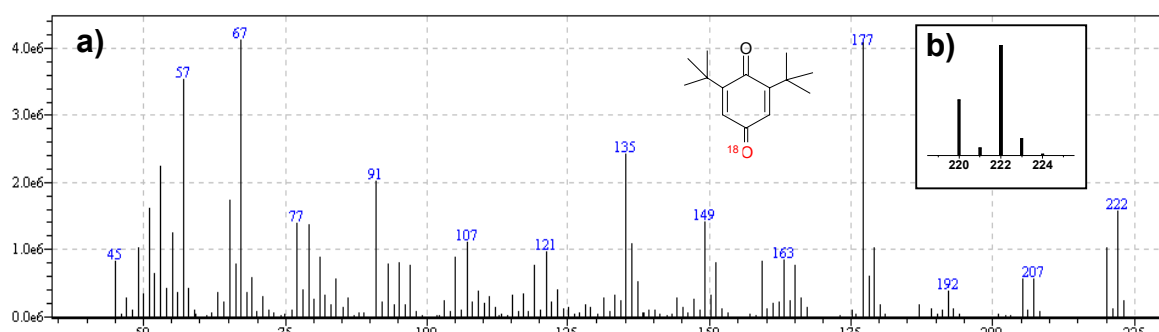


Figure 2.4.4: a) GC-MS spectrum of 2,6- $t\text{Bu}_2$ -benzoquinone (See synthetic procedures above) from the reaction of $[\text{Cu}(\text{TMG}_3\text{tren})\text{O}_2]\text{B}(\text{C}_6\text{F}_5)_4$ with p -MeO-2,6- $t\text{Bu}_2$ -phenol. b) Expected Mass pattern for 68 % ^{18}O incorporation into 2,6- $t\text{Bu}_2$ -benzoquinone (by Isotope Pattern Calculator v4.5).

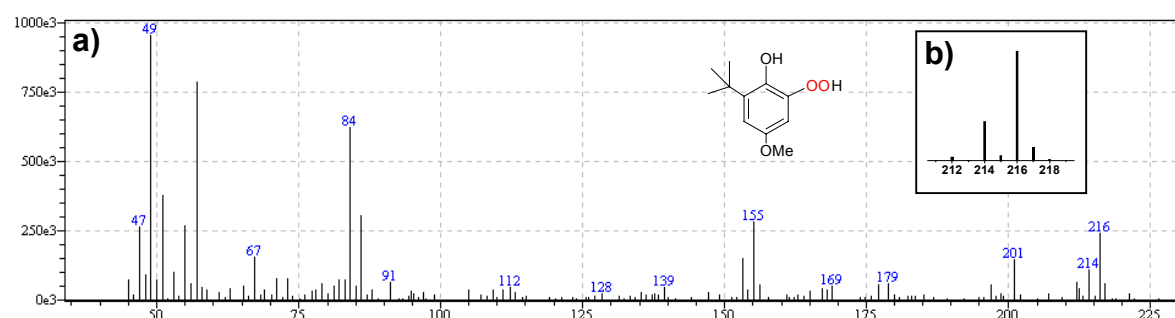


Figure 2.4.5: a) GC-MS spectrum of MeO-TBHP (See synthetic procedures above) from the reaction of $[\text{Cu}(\text{TMG}_3\text{tren})\text{O}_2]\text{B}(\text{C}_6\text{F}_5)_4$ with p -MeO-2,6- $t\text{Bu}_2$ -phenol. b) Expected mass pattern for 85 % ^{18}O incorporation into MeO-TBHP (by Isotope Pattern Calculator v4.5).

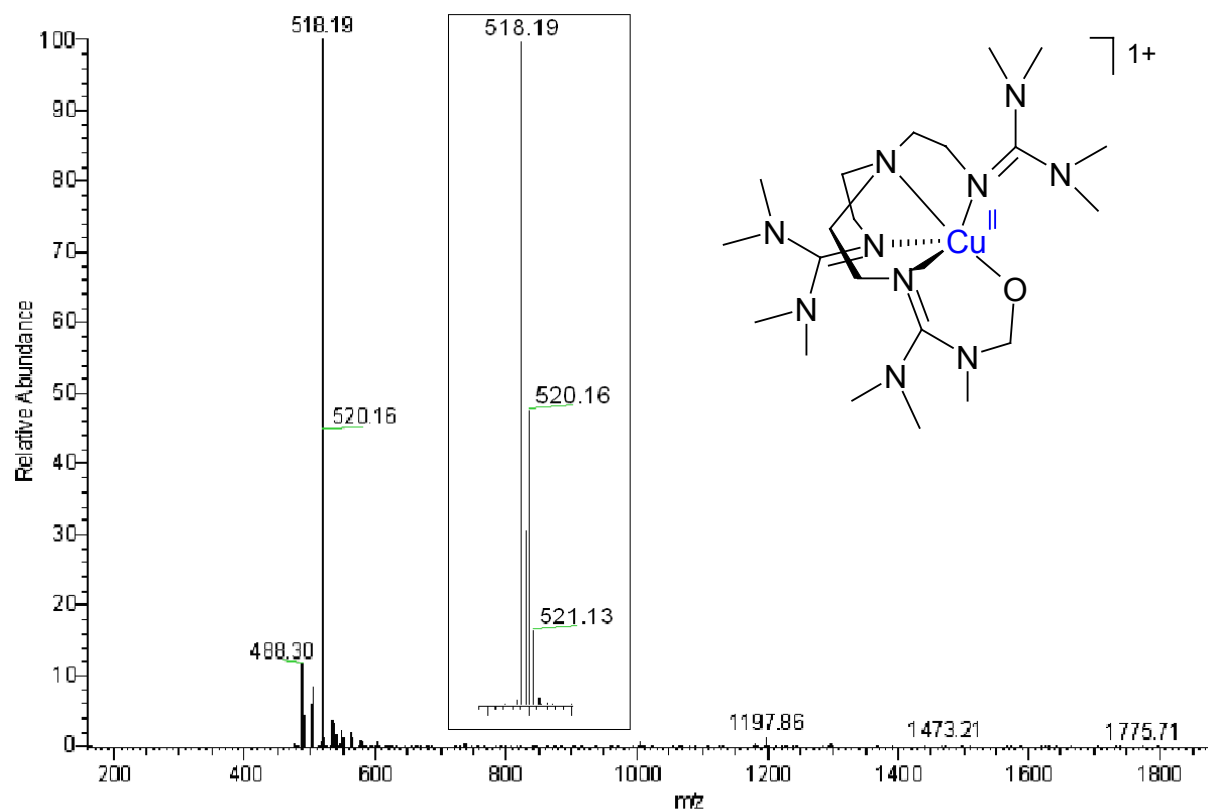


Figure 2.4.6: ESI-MS spectrum of $[\text{Cu}^{\text{II}}(\text{TMG}_3\text{trenO})]^+$ in MeOH with dominant peak at m/z = 518.19. Inset shows the $^{63,65}\text{Cu}$ -pattern around 518 peak.

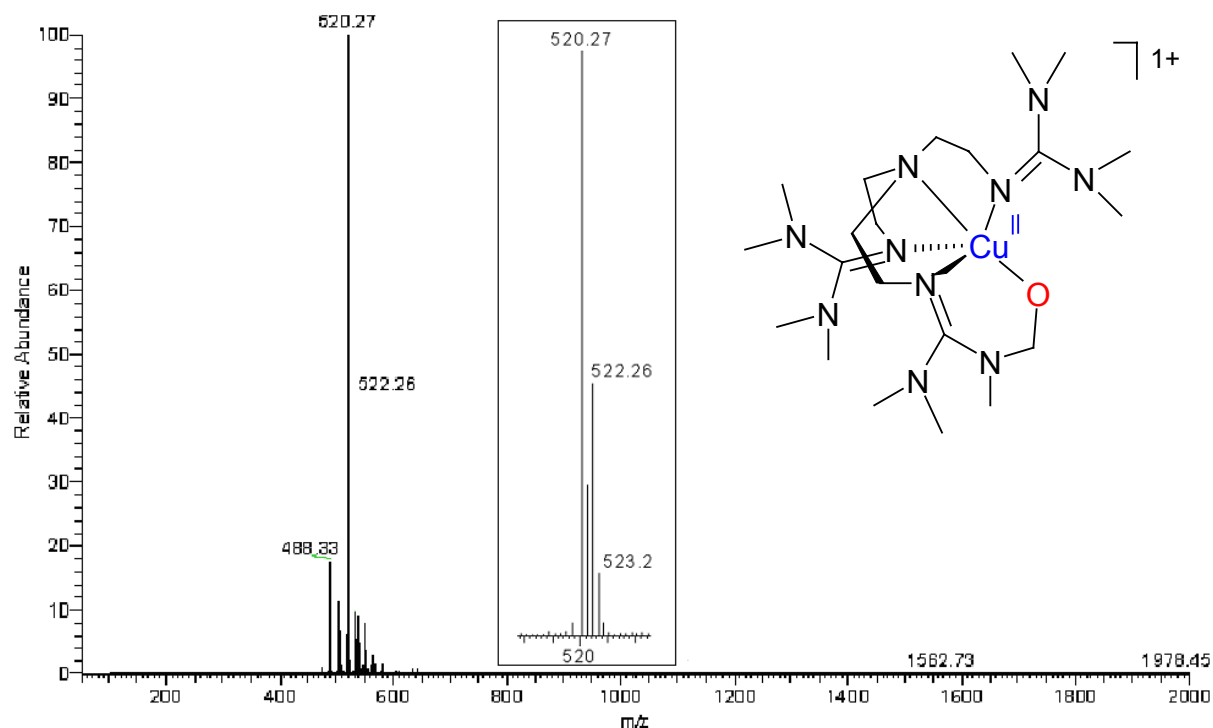


Figure 2.4.7: ESI-MS spectrum of $[\text{Cu}^{\text{II}}(\text{TMG}_3\text{tren}^{18}\text{O})]^+$ in MeOH with dominant peak at m/z = 520.27. Inset shows the $^{63,65}\text{Cu}$ -pattern around 520 peak.

2.4.4 Reaction of $[\text{Cu}^{\text{II}}(\text{TMG}_3\text{tren})(\text{O}_2)]\text{B}(\text{C}_6\text{F}_5)_4$ with 2,4,6- $^t\text{Bu}_3$ -phenol

In a 25 mL Schlenk flask, 4 mL MeTHF solution of $[\text{Cu}^{\text{I}}(\text{TMG}_3\text{tren})]\text{B}(\text{C}_6\text{F}_5)_4$ (0.018 g, 0.015 mmol) was prepared in the drybox and cooled to $-80\text{ }^\circ\text{C}$ outside on the benchtop. With a long needle, dioxygen was bubbled through the solution for 10 s and excess dioxygen was removed carefully via evacuation and purging with argon. A solution of 2,4,6- $^t\text{Bu}_3$ -phenol (0.004 g, 0.015 mmol) was prepared in 100 μL MeTHF and was added to the solution of $[\text{Cu}^{\text{II}}(\text{TMG}_3\text{tren})(\text{O}_2)]\text{B}(\text{C}_6\text{F}_5)_4$. Resulting mixture was bubbled with argon for 5 s and was kept at $-80\text{ }^\circ\text{C}$ for 48 h. The reaction solution was washed three times with pentane (150 mL) and the supernatant was dried over Na_2SO_4 . The copper product (0.012 g, yield ~65 %) was characterized as $[\text{Cu}^{\text{II}}(\text{TMG}_3\text{trenO})]\text{B}(\text{C}_6\text{F}_5)_4$ by comparable ESI and EPR spectrum to that of $[\text{Cu}^{\text{II}}(\text{TMG}_3\text{trenO})]\text{B}(\text{C}_6\text{F}_5)_4$ (see above, Figure 2.4.6). After reducing the volume of the pentane solution, GC and GC-MS analysis confirmed the formation of 2,6- $^t\text{Bu}_2$ -benzoquinone (also, compared with authentic commercial 2,6- $^t\text{Bu}_2$ -benzoquinone) in ~35 % yield. When $^{18}\text{O}_2$ was employed to generate $[\text{Cu}^{\text{II}}(\text{TMG}_3\text{tren})(^{18}\text{O}_2)]\text{B}(\text{C}_6\text{F}_5)_4$ and a similar follow-up procedures were performed; ~65 % ^{18}O -atom incorporation in 2,6- $^t\text{Bu}_2$ -benzoquinone occurred (Figure 2.4.8).

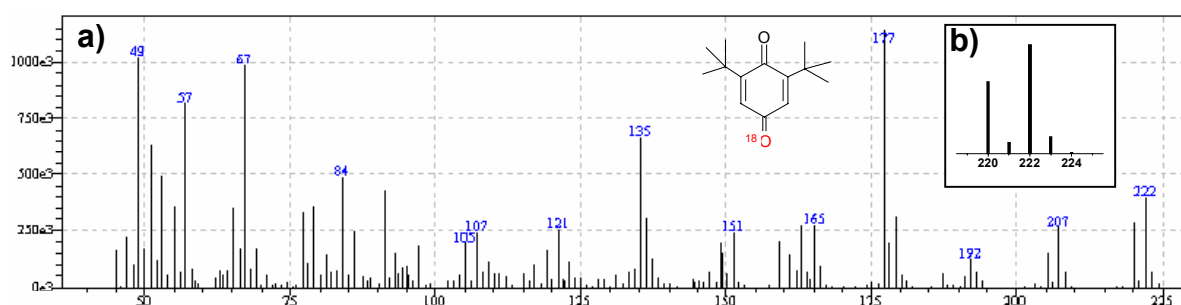


Figure 2.4.8: a) GC-MS spectrum of 2,6- $^t\text{Bu}_2$ -benzoquinone (See synthetic procedures above) from the reaction of $[\text{Cu}(\text{TMG}_3\text{tren})\text{O}_2]\text{B}(\text{C}_6\text{F}_5)_4$ with 2,4,6- $^t\text{Bu}_3$ -phenol. b) Expected Mass pattern for 65 % ^{18}O incorporation into 2,6- $^t\text{Bu}_2$ -benzoquinone (by Isotope Pattern Calculator v4.5).

2.4.5 Reaction of $[\text{Cu}^{\text{II}}(\text{TMG}_3\text{tren})(\text{O}_2)]\text{B}(\text{C}_6\text{F}_5)_4$ (1) with 2,6- $^t\text{Bu}_2$ -phenol

$[\text{Cu}^{\text{I}}(\text{TMG}_3\text{tren})]\text{B}(\text{C}_6\text{F}_5)_4$ (0.012 g, 0.010 mmol) was dissolved in 3.5 mL MeTHF inside the drybox and was taken in a 25 mL Schlenk flask. After cooling the flask to $-80\text{ }^\circ\text{C}$ in a dry-ice/acetone bath, dioxygen was bubbled through the solution for 10 s. Excess O_2 was removed carefully via evacuation and purging with argon. A solution of 2,6- $^t\text{Bu}_2$ -phenol (0.002 g, 0.010 mmol) was prepared in 100 μL MeTHF and was

added anaerobically to the solution of $[\text{Cu}^{\text{II}}(\text{TMG}_3\text{tren})(\text{O}_2)]\text{B}(\text{C}_6\text{F}_5)_4$. The resulting mixture was bubbled with argon for 5 s to ensure thorough mixing with the substrate at $-80\text{ }^\circ\text{C}$ and the reaction was kept cold for 48 h. After pentane (80 mL) washing, Na_2SO_4 drying and reducing the volume of pentane by rotary evaporation, GC and GC-MS analysis were performed. The analysis confirmed the formation of 2,6- $^t\text{Bu}_2$ -benzoquinone (compared with commercial 2,6- $^t\text{Bu}_2$ -benzoquinone) in $\sim 33\%$ yield. The reaction of $[(\text{TMG}_3\text{tren})\text{Cu}^{\text{II}}(\text{O}_2)]\text{B}(\text{C}_6\text{F}_5)_4$ with 2,6- $^t\text{Bu}_2$ -phenol leads to substantial (0.009 g, yield $\sim 75\%$) formation of $[(\text{TMG}_3\text{trenO})\text{Cu}^{\text{II}}]\text{B}(\text{C}_6\text{F}_5)_4$, as determined by comparison of ESI-MS and EPR spectroscopic signatures of the dark green crystalline solids obtained with $[\text{Cu}(\text{TMG}_3\text{trenO})]^+$ formed in the $[\text{Cu}^{\text{II}}(\text{TMG}_3\text{tren})(\text{O}_2)]\text{B}(\text{C}_6\text{F}_5)_4/p\text{-MeO-2,6-}^t\text{Bu}_2\text{-phenol}$ reaction.

2.4.6 Reaction of 2,4- $^t\text{Bu}_2$ -phenol with $[\text{Cu}^{\text{II}}(\text{TMG}_3\text{tren})(\text{O}_2)]\text{B}(\text{C}_6\text{F}_5)_4$

In a 25 mL Schlenk flask 4 mL MeTHF solution of $[\text{Cu}^{\text{I}}(\text{TMG}_3\text{tren})]\text{B}(\text{C}_6\text{F}_5)_4$ (0.017 g, 0.014 mmol) was prepared in the drybox and cooled to $-80\text{ }^\circ\text{C}$. With a long needle, dioxygen was bubbled through the solution for 5 s and excess dioxygen was removed carefully via evacuation and purging with argon. A solution of 2,4- $^t\text{Bu}_2$ -phenol (0.003 g, 0.015 mmol) in 100 μL MeTHF was added to this solution with stirring and the reaction mixture was kept cold for 48 h. After washing three times with pentane (120 mL), the supernatant was dried over Na_2SO_4 . Pentane solution was reduced in volume by rotary evaporation and was analyzed by GC and GC-MS confirming (Figure 2.4.9) the formation of 4,4',6,6'-tetra- ^tBu -2,2'-biphenol ($\sim 10\%$ yield, authentic commercial biphenol was used for comparison). The copper product (0.011 g, yield $\sim 65\%$) was characterized as $[\text{Cu}^{\text{II}}(\text{TMG}_3\text{trenO})]\text{B}(\text{C}_6\text{F}_5)_4$ by comparable ESI and EPR spectrum to that of crystallographically characterized $[\text{Cu}^{\text{II}}(\text{TMG}_3\text{trenO})]\text{B}(\text{C}_6\text{F}_5)_4$ (see above, Figure 2.4.6).

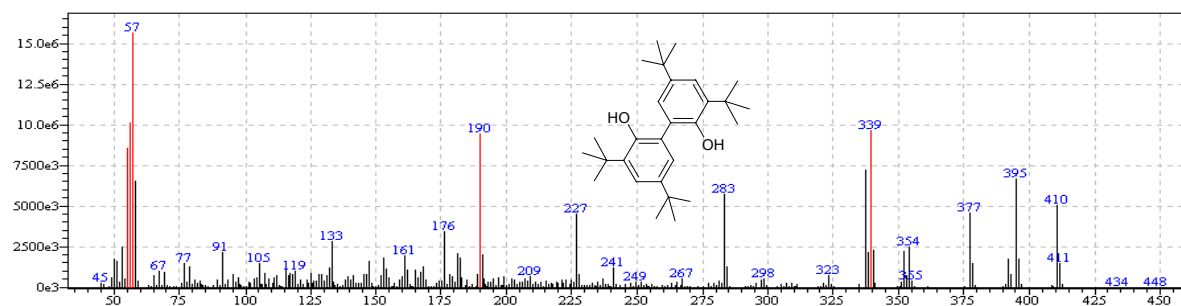


Figure 2.4.9: GC-MS spectrum of 4,4',6,6'-tetra- ^tBu -2,2'-biphenol (See synthetic procedures above) from the reaction of $[\text{Cu}(\text{TMG}_3\text{tren})\text{O}_2]\text{B}(\text{C}_6\text{F}_5)_4$ with 2,4- $^t\text{Bu}_2$ -phenol.

2.4.7 Reaction of $[\text{Cu}^{\text{II}}(\text{TMG}_3\text{tren})(\text{O}_2^-)]\text{B}(\text{C}_6\text{F}_5)_4$ with 3,5- $^t\text{Bu}_2$ -Catechol

$[\text{Cu}^{\text{I}}(\text{TMG}_3\text{tren})]\text{B}(\text{C}_6\text{F}_5)_4$ (0.011 g, 0.009 mmol) in 4.8 mL MeTHF was prepared in a Schlenk flask inside the drybox. Out on the bench top, the flask was cooled to $-80\text{ }^\circ\text{C}$ and dioxygen was then bubbled through the solution for 5 s. Excess dioxygen was removed carefully via evacuation and purging with argon. A solution of 3,5- $^t\text{Bu}_2$ -Catechol (0.002 g, 0.009 mmol) in 60 μL MeTHF was added to this solution with stirring and the resulting mixture was kept cold for 12 h. Resulting solution was washed three times with pentane (80 mL) and the supernatant was dried over Na_2SO_4 . The ESI and EPR spectroscopic studies confirm the copper product formation as $[\text{Cu}^{\text{II}}(\text{TMG}_3\text{trenO})]\text{B}(\text{C}_6\text{F}_5)_4$ (0.008 g, yield ~72 %). This pentane solution was reduced in volume by rotary evaporation and was analyzed by GC and GC-MS confirming the formation of 3,5- $^t\text{Bu}_2$ -benzoquinone in ~20 % yield (authentic commercial 3,5- $^t\text{Bu}_2$ -benzoquinone was also used for comparison).

2.4.8 Synthesis of $[\text{Cu}^{\text{II}}(\text{TMG}_3\text{tren})]^{2+}$

Ligand TMG_3tren (0.242 g, 0.550 mmol) was treated with $\text{Cu}^{\text{II}}(\text{ClO}_4)_2 \cdot 6\text{H}_2\text{O}$ (0.203 g, 0.549 mmol) (Aldrich) in acetonitrile (20 mL) for 25 min at room temperature.^[28] The bright greenish blue complex was precipitated by diethylether addition (100 mL) after reducing the volume of acetonitrile to 4 mL. The supernatant was decanted. The resulting crystalline solid was (re)dissolved in acetonitrile, washed two more times with diethylether (70 mL) and dried under vacuum for 12 h to afford $[\text{Cu}^{\text{II}}(\text{TMG}_3\text{tren})](\text{ClO}_4)_2$, (0.332 g, 86 % yield). Anal. Calcd. $[\text{Cu}^{\text{II}}(\text{TMG}_3\text{tren})](\text{ClO}_4)_2$; $\text{C}_{21}\text{H}_{48}\text{Cl}_2\text{CuN}_{10}\text{O}_8$: C, 35.87; H, 6.88; N, 19.92. Found: C, 35.93; H, 6.70; N, 19.80.

2.4.9 Reaction of $[\text{Cu}^{\text{II}}(\text{TMG}_3\text{tren})](\text{ClO}_4)_2$ with $\text{H}_2\text{O}_2/\text{Et}_3\text{N}$

Complex $[\text{Cu}^{\text{II}}(\text{TMG}_3\text{tren})](\text{ClO}_4)_2$ (0.101 g, 0.136 mmol) in 25 mL acetonitrile were prepared in a Schlenk flask and cooled to $-40\text{ }^\circ\text{C}$ on the bench top. Addition of Et_3N (90 μL , 0.683 mmol) and 50 wt % H_2O_2 (41 μL , 0.683 mmol) produces a light green solution. The ESI-MS spectra of this solution confirmed the formation of the alkoxide- Cu^{II} complex $[\text{Cu}^{\text{II}}(\text{TMG}_3\text{trenO})]^+$, (ESI-MS data, similar as Figure 2.4.6). Further confirmation comes from the formation of $[\text{Cu}^{\text{II}}(\text{TMG}_3\text{tren}^{18}\text{O})]^+$, when $\text{H}_2^{18}\text{O}_2$ was employed to generate $[\text{Cu}^{\text{II}}(\text{TMG}_3\text{tren}^{18}\text{O})]^+$ (ESI-MS data, similar as Figure 2.4.7).

2.4.10 Reaction of $[\text{Cu}^{\text{I}}(\text{TMG}_3\text{tren})]\text{B}(\text{C}_6\text{F}_5)_4$ with PhIO ^[74]

$[\text{Cu}^{\text{I}}(\text{TMG}_3\text{tren})]\text{B}(\text{C}_6\text{F}_5)_4$ (0.022 g, 0.018 mmol) was dissolved in 2.0 mL CH_3CN inside the drybox and was taken in a 100 mL Schlenk flask. In a separate Schlenk flask, PhIO (0.012g, 0.054 mmol) was taken with 4.0 mL CH_3CN under argon. With a long needle syringe 2.0 mL of this CH_3CN solution (0.006g, 0.027 mmol) was introduced anaerobically into the solution of $[\text{Cu}^{\text{I}}(\text{TMG}_3\text{tren})]\text{B}(\text{C}_6\text{F}_5)_4$ and was stirred for 30 min. The reaction solution turned to nice green which was washed three times with pentane (150 mL). The copper product (0.020 g, yield ~90 %) was characterized as $[\text{Cu}^{\text{II}}(\text{TMG}_3\text{trenO})]\text{B}(\text{C}_6\text{F}_5)_4$ by comparable ESI and EPR spectrum to that of $[\text{Cu}^{\text{II}}(\text{TMG}_3\text{trenO})]\text{B}(\text{C}_6\text{F}_5)_4$ (see above, Figure 2.4.6).

2.4.11 Reaction of $[\text{Cu}^{\text{II}}(\text{TMG}_3\text{tren})(\text{O}_2^-)]\text{B}(\text{C}_6\text{F}_5)_4$ with TEMPO-H

$[\text{Cu}^{\text{I}}(\text{TMG}_3\text{tren})]\text{B}(\text{C}_6\text{F}_5)_4$ (0.050 g, 0.042 mmol) in 20 mL MeTHF were prepared in a Schlenk flask inside the drybox. Outside on the bench top, the flask was cooled to $-80\text{ }^\circ\text{C}$ and dioxygen was then bubbled through the solution for 10 s to generate the green solution $[\text{Cu}^{\text{II}}(\text{TMG}_3\text{tren})(\text{O}_2)]\text{B}(\text{C}_6\text{F}_5)_4$. Excess dioxygen was removed carefully via evacuation/argon purging and the initial spectrum was recorded. A solution of TEMPO-H^[80] (0.007 g, 0.044 mmol) in 200 μL MeTHF was added to this green solution and argon was purged for 5 s to ensure thorough mixing. The reaction was kept cold for 1 h and the UV-vis spectrum was recorded with time (Figure 2.3.2a). The final spectrum confirmed the complete disappearance of the superoxo species at 447 nm. Resulting green copper solution was washed three times with pentane (180 mL). Copper product was further purified by recrystallization from MeTHF/pentane. When this concentrated copper product (with TEMPO-H and product generated from it) was (re)dissolved in MeTHF and layered with pentane, it results in crushing out of copper product only. This copper product was characterized as $[\text{Cu}^{\text{II}}(\text{TMG}_3\text{trenO})]\text{B}(\text{C}_6\text{F}_5)_4$ by comparable ESI and EPR spectrum to that of crystallographically characterized $[\text{Cu}^{\text{II}}(\text{TMG}_3\text{trenO})]\text{B}(\text{C}_6\text{F}_5)_4$ (see above, Figure 2.4.6). In a separate set of experiment, similar procedure (as above) was followed; the solution was transferred to EPR sample tubes with respect to time and frozen immediately at 77K. The EPR spectra (Figure 2.3.2b) confirmed increased intensity (hence increased formation) of TEMPO \cdot signal (compared with commercial TEMPO \cdot) as the reaction progress. Authentic TEMPO \cdot was also used to determine the yield (~90%) of TEMPO \cdot generated from the reaction of TEMPO-H and $[\text{Cu}^{\text{II}}(\text{TMG}_3\text{trenO}_2)]\text{B}(\text{C}_6\text{F}_5)_4$.

Chapter 3 – Peroxo Complexes

This chapter includes two manuscripts that are ready for submission. These two manuscripts have been obtained in cooperation with my colleagues Dr. Ildikó Kerezsi, Dr. Simon Foxon, Dr. Markus Weitzer and Dipl.-Chem. Alexander Beitat (research group of Prof. Dr. Siegfried Schindler) and the following research groups. Their individual participation in these projects is highly acknowledged:

- Dr. Patrick K. Wick at the ETH Hönggerberg Zürich (Schweiz).
- Prof. Dr. Felix Tuczek and Dipl.-Chem. Ole Sander at the Christian Albrechts Universität Kiel.

Furthermore, I would like to thank Thomas Waitz for recording and evaluation of the TG measurements and Dipl.-Chem. Volker Lutz for the GC-MS measurements.

3.1 Reversible Binding of Dioxygen by Copper(I) Complexes with Tripodal Tetraamine Ligands

This work is ready for submission to *Inorganic Chemistry*.

Christian Würtele, Ildikó Kerezsi, Alexander Beitat, Markus Weitzer, Simon Foxon,
Patrick K. Wick and Siegfried Schindler

3.1.1 Abstract

Crystal structures of copper(I) and copper(II) complexes with the tetradentate tripodal ligands tris(2-pyridylmethyl)amine (tmpa), 2-dimethyl-aminoethyl)bis(2-pyridylmethyl)-amine (Me₂uns-penp), bis(2-dimethyl-aminoethyl)(2-pyridylmethyl)amine (Me₄apme) and tris(2-dimethylaminoethyl)amine (Me₆tren) using tetraphenylborate as anion are reported. Cyclic voltammetry was used to measure the redox potentials of all complexes in acetone and acetonitrile. At low temperatures in propionitrile, the copper(I) complexes [Cu^IL(RCN)]⁺ with these ligands first reversibly bind dioxygen to form 1:1 Cu-O₂ species which then further react reversibly with a second [Cu^IL(RCN)]⁺ ion to form the dinuclear 2:1 Cu₂O₂ peroxo complexes. These reactions can be observed using low temperature stopped-flow techniques. The spectral characteristics and full kinetic and thermodynamic results for the reaction of [Cu^I(Me₂uns-penp)(RCN)]⁺ and [Cu^I(Me₄apme)(RCN)]⁺ with dioxygen are reported and are compared with the results for the reaction of [Cu^I(tmpa)(RCN)]⁺ and [Cu^I(Me₆tren)(RCN)]⁺ with dioxygen.

3.1.2 Keywords

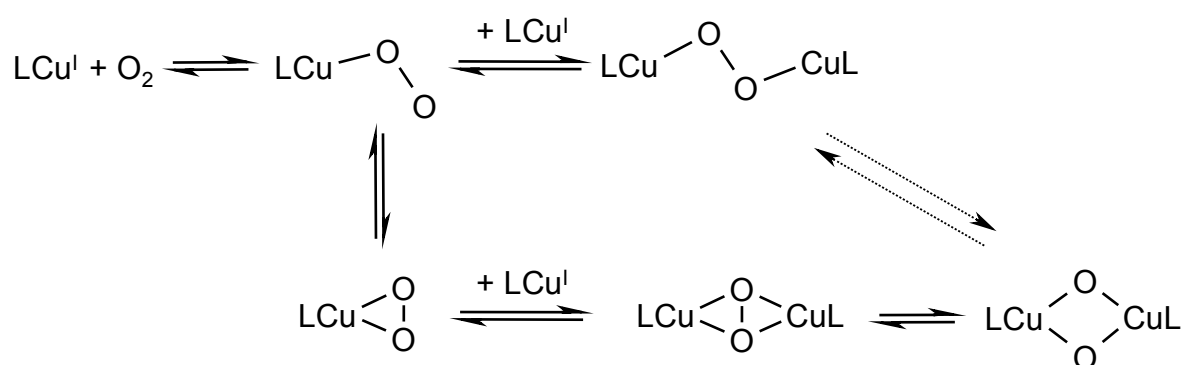
Copper, Tripodal Ligands, Dioxygen, Peroxo Complexes, Kinetics.

3.1.3 Introduction

The interaction of dioxygen with copper complexes is of fundamental meaning for biological, chemical and industrial purposes.^[3, 6, 7, 30, 48, 81-83] Quite a large number of copper containing proteins is involved in vital processes in organisms, e. g. hemocyanin (dioxygen carrier in the blood of arthropods and molluscs), tyrosinase (a monooxygenase that catalyses ortho-hydroxylation of phenols to the according

chatechols), or dopamine β -monooxygenase (responsible for the hydroxylation of dopamine to yield epinephrine).^{[3, 7] [6, 33, 81-84]}

Low molecular weight copper complexes have been synthesized and investigated in regard to their potential to model the active site and the function of such copper proteins.^[6, 7, 30, 65] These model complexes not only can provide better understanding of the biological systems but they also assist in the development of new homogeneous catalysts for selective oxidations under mild conditions.^[85, 86] It is not surprising that binding and activation of dioxygen lead to different copper "oxygen adduct" complexes, all of which in principle can act as the reactive species. Therefore it is important to understand the nature of these different adduct complexes as well as the mechanisms of their generation. A general mechanistic framework of some of the possible reactions is presented in Scheme 1.

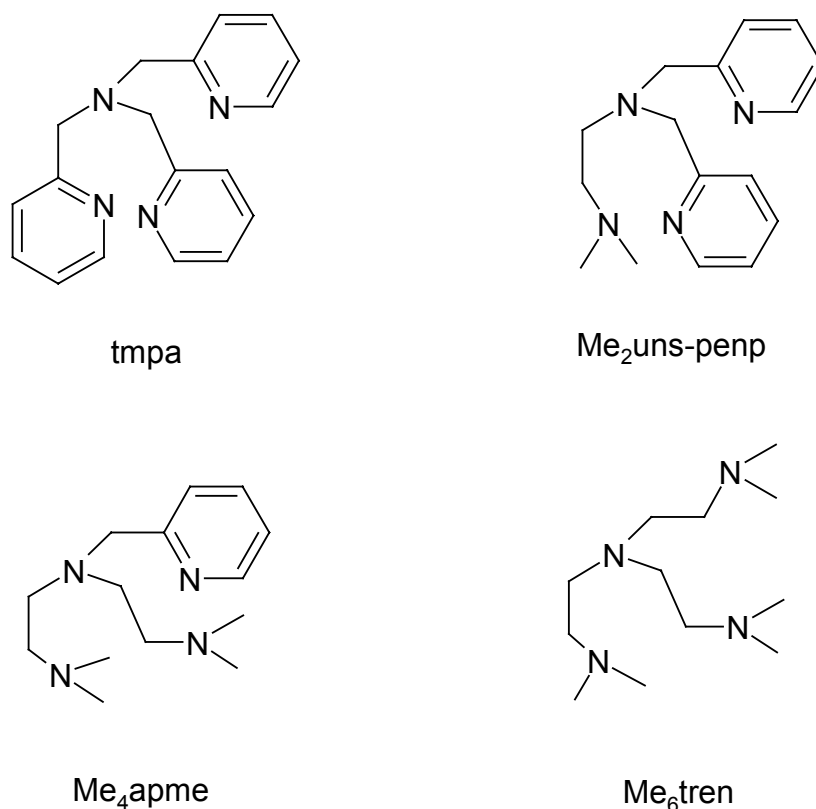


Scheme 3.1.1: Some possible reaction pathways for the oxidation of copper(I) complexes with dioxygen.

According to Scheme 3.1.1, dioxygen reacts with a Cu(I) complex to first form an end-on mononuclear superoxo complex. This intermediate usually can only be observed as a transient species because it can either form immediately a side-on superoxo complex or dimerise to the according peroxo complexes in subsequent reactions.^[48, 65] Further reactions can occur such as bond cleavage of the peroxide leading to copper oxo complexes or (not shown in Scheme 3.3.1) protonation reactions as well as formation of trinuclear or tetranuclear product complexes.^[6, 7, 30, 48, 81, 82] The course of these reactions depends on ligand, solvent and temperature. Therefore, kinetic and thermodynamic parameters are very important in the understanding of the reactivity of copper(I) complexes with dioxygen.^[19, 26, 87] Spectroscopic, structural and electrochemical data as well as theoretical calculations

are required additionally to complement kinetic information and thus can provide a complete mechanistic picture.^[3, 6, 7, 19, 48, 65, 81, 82, 88] Currently however, still many open questions remain regarding the detailed mechanism of the activation of dioxygen and predictions for the development of optimized systems so far cannot be made. Furthermore, the number of copper complexes that might become useful as catalysts for selective oxidations in the future so far is rather limited.

Copper complexes of a family of pyridyl-alkylamine tripodal tetradentate ligands, the 'parent' ligand being tris(2-pyridylmethyl)amine (tmpa, Scheme 3.1.2; sometimes abbreviated as tpa in the literature) and closely related ligands^[24] have been widely employed in order to explore and understand the thermodynamic and kinetic aspects of the reaction of copper(I) compounds with dioxygen.^[7, 11, 12, 20, 39, 89-91] The properties of these complexes were strongly affected by donor atoms, sterical hindrance and chelate ring size.^[7] Using the copper(I) complex $[\text{Cu}(\text{tmpa})\text{CH}_3\text{CN}]^+$, it was possible for the first time to model reversible dioxygen binding of a copper protein and furthermore to obtain the copper peroxo complex $[\text{Cu}_2(\text{tmpa})_2(\text{O}_2)]^{2+}$, that could be structurally characterized (at low temperatures).^[12, 19, 24, 26, 87, 88]



Scheme 3.1.2: The tripodal ligands tmpa, Me₂uns-penp, Me₄apme and Me₆tren.

It was discovered previously that similar to the reaction of $[\text{Cu}(\text{tmpa})(\text{CH}_3\text{CN})]^+$ with O_2 , the copper(I) complex of the analogous aliphatic ligand tris(2-dimethylaminoethyl)amine (Me_6tren , Scheme 3.1.2), also supports the formation of a copper superoxo and peroxo complex at low temperatures.^[3, 25] In a detailed mechanistic study differences in the kinetic behavior during the oxidation of the two complexes were observed.^[39] Especially these differences were responsible for the larger stabilization of the transient end-on superoxo copper complex, $[\text{Cu}(\text{Me}_6\text{tren})(\text{O}_2)]^+$, that could be therefore characterized for the first time using Resonance Raman spectroscopy. Furthermore, work based on this result allowed the full characterization of an end-on superoxo copper complex using a tren derivative as ligand.^[11, 29]

A preliminary kinetic study of the oxygenation reaction of the copper(I) complex of 2-dimethyl-aminoethyl)bis(2-pyridylmethyl)amine ($\text{Me}_2\text{uns-penp}$, Scheme 3.3.1) had demonstrated that the lifetime of the transient peroxo complex in propionitrile is much larger in comparison with the related complexes of tmpa and Me_6tren .^[26] It could be observed spectroscopically (and by eye due to its intensive blue color) for a short time in solution at ambient temperatures. This stability is quite surprising and in contrast to the expectations that there would be a systematic increase/decrease of the stability of the superoxo/peroxo copper complexes of the ligands shown in Scheme 3.1.2 (going from tmpa to Me_6tren). Due to this result we became interested in a detailed kinetic investigation of the copper(I) complexes of the tetradentate tripodal ligands $\text{Me}_2\text{uns-penp}$ and bis(2-dimethyl-aminoethyl)(2-pyridylmethyl)amine (Me_4apme , Scheme 3.1.2) thus hoping to gain a better understanding of these reactions.

3.1.4 Experimental Section

3.1.4.1 Materials and Methods

Reagents and solvents used were of commercially available reagent quality unless otherwise stated. The ligands tmpa, $\text{Me}_2\text{uns-penp}$, Me_4apme and Me_6tren were prepared according to the literature.^[25, 26, 92] The copper(I) complexes $[\text{Cu}(\text{tmpa})]\text{BPh}_4$ (**1**), $[\text{Cu}(\text{Me}_2\text{uns-penp})(\text{CH}_3\text{CN})]\text{PF}_6$, $[\text{Cu}(\text{Me}_2\text{uns-penp})]\text{BPh}_4$ (**2**), $[\text{Cu}(\text{Me}_4\text{apme})]\text{BPh}_4$ (**3**), $[\text{Cu}(\text{Me}_6\text{tren})]\text{BPh}_4$ (**4**) and the copper(II) complexes $[\text{Cu}(\text{tmpa})\text{Cl}]\text{BPh}_4$ (**5**), $[\text{Cu}(\text{Me}_2\text{uns-penp})\text{Cl}]\text{BPh}_4$ (**6**), $[\text{Cu}(\text{Me}_4\text{apme})\text{Cl}]\text{BPh}_4$ (**7**) and

[Cu(Me₆tren)Cl]BPh₄ (**8**) were synthesized analogous to previously reported methods.^[21, 26, 93] Propionitrile (Merck) was purified following published procedures.^[19] Prior to the measurements the dioxygen-free propionitrile was distilled, collected and strictly kept under an argon atmosphere.

3.1.4.2 Stopped-Flow Experiments

Rapid kinetic studies were performed using two SF-21 variable-temperature stopped-flow units (Hi-Tech Scientific, 10 or 2 mm path length cell) combined with a TIDAS/NMC301-MMS/16 VIS/500-1 diode array spectrometer (J&M; 256 diodes, 300-1100 nm, 0.8 ms minimum sampling time or TIDAS-16 HQ/UV-Vis 512/16B diode array spectrometer J&M, 507 diodes, 300-720 nm, 1.3 ms minimum sampling time). Data acquisition (up to 256 complete spectra and up to four different time bases) was performed using the Kinspec program (J&M). For numerical analysis, all data were pretreated by factor analysis using the Specfit program (SPECFIT/32 is a trademark of Spectrum Software Associates, copyright 2000-2002 Spectrum Software Associates; R. Binstead and A. D. Zuberbühler).^[94]

Weighed samples of copper(I) complex were transferred into a glass vessel which was modified for air-sensitive manipulations and fit exactly on the adapter units of the stopped-flow instrument. Freshly distilled propionitrile was transferred to this and another vessel in a glove box (Braun, Garching, Germany; water and dioxygen less than 1 ppm) under a nitrogen or argon atmosphere. The propionitrile in the second vessel was bubbled with dry dioxygen (grade 4.8, Messer Griesheim, Germany) for at least 20 min. (the solubility of dioxygen in propionitrile was determined previously).^[19] To obtain variable O₂ concentrations in solution, a gas mixing unit was employed which consisted of two MKS PR-4000 control towers equipped with MKS general purpose Mass-Flow Controllers of type 1179A calibrated for either 200 sccm N₂ (used for O₂ regulation) or 500 sccm N₂ (used for argon regulation). The regulated amounts of argon and O₂ were mixed and yielded a specific O₂/argon ratio. The mixed gases were passed through a drying column and then bubbled through the solution to yield a specific concentration of O₂ in the solvent. The solubility of dioxygen in propionitrile has been determined previously.^[19] After that the stopcocks were closed, the gas-saturated solution was equilibrated by shaking the glass vessel at room temperature and any pressure inside was released by briefly opening the stopcock. Then the two glass vessels were mounted on the stopped-flow instrument.

During the whole time of the measurements, argon and dioxygen were purged slowly through the connecting tubes of the two glass vessels containing the copper(I)- and the O₂-solution, respectively.

At least four series with different concentrations of Cu(I) and/or O₂ were measured between -92 °C and room temperatures. The maximum timebase of the data collection was up to 80 s for [Cu(Me₂uns-penp)(CH₃CN)]PF₆ and up to 220 s for [Cu(Me₄apme)B(Ph)₄].

3.1.4.3 Electrochemistry

All cyclic voltammetry experiments were performed under Argon, with a Princeton BAS Model 263 instrumentation, using a 1 mM solution of the copper(I) complex (tetraphenylborate as anion) in acetone or acetonitrile. Electrodes employed were glassy carbon (working electrode), Ag/AgCl (reference electrode) and a platinum wire (auxiliary electrode). Ferrocene was used as an internal reference (0.4971/0.5884 V in acetone; 0.4315/0.5272 V in acetonitrile).

3.1.4.4 X-ray crystallography

The X-ray crystallographic data were collected on a STOE IPDS-diffractometer equipped with a low temperature unit (Karlsruher Glastechnisches Werk). Mo-K_α radiation ($\lambda = 0.71069$ Å) and a graphite monochromator was used. All single crystals for measurements at -80 °C were mounted on the tip of a glass rod in inert oil, single crystals for measurements at room temperature were placed inside of a glass capillary. Cell parameters were refined by using up to 5000 reflections, collected with the ϕ -oscillation mode, if not mentioned otherwise. No absorption corrections were applied. The structures were solved by Direct Methods in SHELXS97, and refined by using full-matrix least squares in SHELXL97.^[95] The hydrogen atoms were positioned geometrically and all non-hydrogen atoms were refined anisotropically. The refinement of **1**, **3**, **6a** showed two complex molecules and two tetraphenylborate anions in the independent unit, the refinement of **8** showed one half of a molecule in the independent unit and the refinement of **5** showed a "wiggly" acetone solvent molecule in the independent unit of the elementary cell. The less accurate refinement for **3** was a consequence of the fact that we only obtained very small crystals for this compound and therefore had problems with the measured data sets. Crystallographic

data for the structures reported in this paper have been deposited with the Cambridge Crystallographic Data Centre as supplementary publication no. CCDC-697812 for **1**, CCDC-697813 for **2**, CCDC-697814 for **3**, CCDC-697815 for **5**, CCDC-697816 for **6a**, CCDC-697817 for **6b**, CCDC-697818 for **7** and CCDC-697819 for **8**. Copies of the data can be obtained, free of charge from The Cambridge Crystallographic Data Centre via www.ccdc.cam.ac.uk/data_request/cif.

3.1.5 Results and Discussion

3.1.5.1 Synthesis and characterization

The ligands and complexes were synthesized analogous according to published procedures without any serious problems. The copper(I) complexes were prepared either as the PF_6^- or BPh_4^- salts. To exclude possible anion effects in our studies we prepared and characterized the whole series of the copper(I)/(II) complexes using tetraphenylborate as anion.

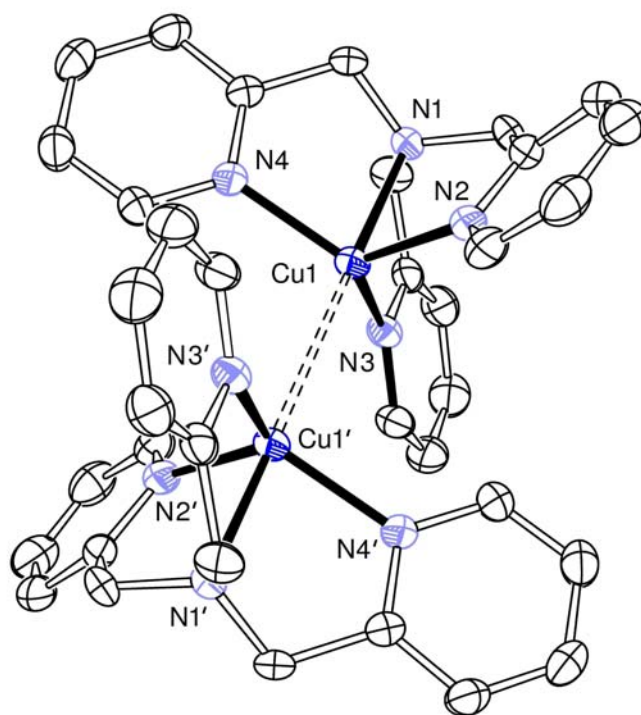


Figure 3.1.1: Molecular structure of the cation of $[\text{Cu}(\text{tpma})]\text{BPh}_4$ (**1**). ORTEP plot with thermal ellipsoids set at 50 % probability (hydrogen atoms and tetraphenylborate anion are not shown). Selected bond lengths [Å] and angles [°]: Cu1---Cu' 2.8341(9), Cu1-N1 2.199(2), Cu1-N2 2.037(2), Cu1-N3 2.034(2), Cu1-N4 2.072(3); N1-Cu1-Cu' 177.65(7), N1-Cu1-N2 81.64(8), N2-Cu1-N3 121.24(9), N2-Cu1-N4 116.47(9).

We did not expect any unusual observations, however very surprisingly we found that the expected complex $[\text{Cu}(\text{tmpa})(\text{CH}_3\text{CN})]\text{BPh}_4$ was not obtained in crystalline form (this has been expected because $[\text{Cu}(\text{tmpa})(\text{CH}_3\text{CN})]\text{ClO}_4$ as well as an analogous complex with PF_6^- as anion have been structurally characterized previously)^[89, 96] but instead $[\text{Cu}(\text{tmpa})]\text{BPh}_4$ was isolated (Figure 3.3.1).

That acetonitrile as an additional ligand is missing here would not have been so surprising (from different copper(I) complexes this phenomena is well known),^[20, 25] however in contrast to our expectations the copper(I) ions of two complex units get into very close contact. While this cannot be called a real bond it cannot be neglected.^[97] Different examples of such copper copper interactions are known, however, in all these examples the two copper ions are bridged by a coordinated ligand.^[97-105] The most related example has been described by Lippard and coworkers.^[98] Thus instead of an additional coordinated acetonitrile the fifth axial position of a trigonal bipyramid is occupied by a second copper(I) ion. In contrast this was not observed for the copper(I) complexes of $\text{Me}_2\text{uns-penp}$, Me_4apme and Me_6tren ; the molecular structures for $[\text{Cu}(\text{Me}_2\text{uns-penp})]^+$ and $[\text{Cu}(\text{Me}_4\text{apme})]^+$ are shown in Figures 3.1.2 and 3.1.3. The crystal structure of $[\text{Cu}(\text{Me}_6\text{tren})]\text{BPh}_4$ (**4**) will be reported in another context elsewhere.

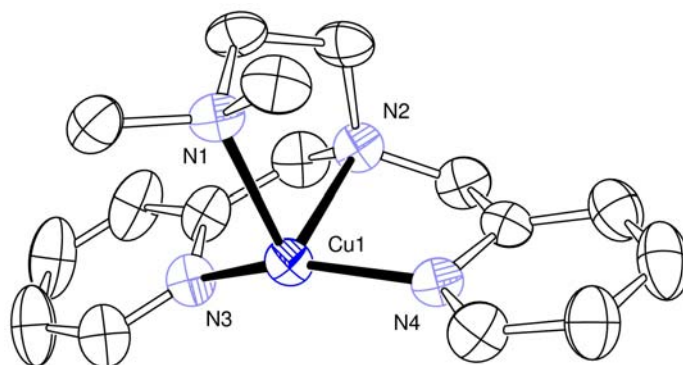


Figure 3.1.2: Molecular structure of the cation of $[\text{Cu}(\text{Me}_2\text{uns-penp})]\text{BPh}_4$ (**2**). ORTEP plot with thermal ellipsoids set at 50 % probability (hydrogen atoms and tetraphenylborate anion are not shown). Selected bond lengths [Å] and angles [°]: Cu1-N1 2.188(3), Cu1-N2 2.189(3), Cu1-N3 1.956(3), Cu1-N4 1.944(4); N1-Cu1-N2 85.04(13), N1-Cu1-N3 100.47(14), N3-Cu1-N4 148.83(15).

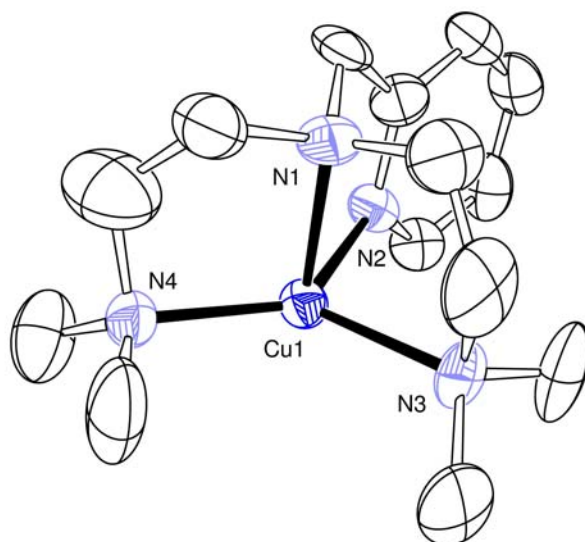


Figure 3.1.3: Molecular structure of the cation of $[\text{Cu}(\text{Me}_4\text{apme})]\text{BPh}_4$ (**3**). ORTEP plot with thermal ellipsoids set at 50 % probability (hydrogen atoms and tetraphenylborate anion are not shown). Selected bond lengths [\AA] and angles [$^\circ$]: Cu1-N1 2.156(7), Cu1-N2 2.004(6), Cu1-N3 2.132(7), Cu1-N4 2.048(9); N1-Cu1-N2 84.0(3), N2-Cu1-N3 103.0(3), N3-Cu1-N4 120.0(3).

In none of these complexes acetonitrile molecules are coordinated as additional ligands. Again this was different for the previously crystallographically characterized complex $[\text{Cu}(\text{Me}_2\text{uns-penp})(\text{CH}_3\text{CN})]\text{PF}_6$,^[26] however, the crystal structures are similar with some small differences in bond lengths and angles (as expected due to the coordinated acetonitrile molecule). For the ligand Me_4apme no complexes have been reported so far and similar to the complex with Me_6tren as ligand (see below) our efforts to obtain $[\text{Cu}(\text{Me}_4\text{apme})(\text{CH}_3\text{CN})]\text{PF}_6$ as a solid material were unsuccessful due to problems with disproportionation of the complex at higher concentrations in solution. The crystal structure of the copper(I) complex of Me_6tren has been reported previously by us and here we had already observed that no additional acetonitrile was coordinated in the perchlorate complex (as well as in the PF_6^- complex according to elemental analysis).^[25] Interestingly in here, the perchlorate ion is weakly coordinated, pointing with three of its dioxygen atoms towards the copper(I) ion and thus completing again the fifth position in a trigonal bipyramidal geometry. Compared with *tmpa* the axial amine nitrogen coordinates stronger to the copper(I) ion if the pyridine arms are replaced with aliphatic amine arms. This is observed in the bond lengths ranging from 2.20 (*tmpa*), 2.19 ($\text{Me}_2\text{uns-penp}$), 2.16 (Me_4apme) to 2.15 (Me_6tren). Most important is the fact that using tetraphenylborate as an anion

did allow the facile synthesis of the complexes of the ligands Me₄apme and Me₆tren. While the copper(I) complexes with the ligands tmpa and Me₂uns-penp are quite stable in the solid state and in solution (under inert conditions) copper(I) complexes with the ligands Me₄apme and Me₆tren show a strong tendency towards disproportionation if other anions than tetraphenylborate (such as perchlorate and PF₆⁻, triflate or BF₄⁻) are used.

In contrast the copper(II) complexes of the investigated ligands did not show anything unusual. Chloride ions were provided as additional coordinating ions together with tetraphenylborate as anions. Molecular structures of the four complexes are shown in Figures 3.1.4-3.1.7. Crystallographic data are presented in Chapter 4.

The crystal structures of **5**, **6** and **8** are very similar to those published previously for [Cu(tmpa)Cl]PF₆, [Cu(Me₂uns-penp)Cl]ClO₄ and [Cu(Me₆tren)Cl]ClO₄.^[25, 26, 106] No copper(II) complexes have been described so far for the ligand Me₄apme. The molecular geometry of **5**, **6** and **7** can be best described as trigonal bipyramidal according to the structural parameter τ assigned previously.^[107] However, for **6** (and for [Cu(Me₂uns-penp)Cl]ClO₄ described previously) a slightly distorted square pyramidal geometry is adopted.

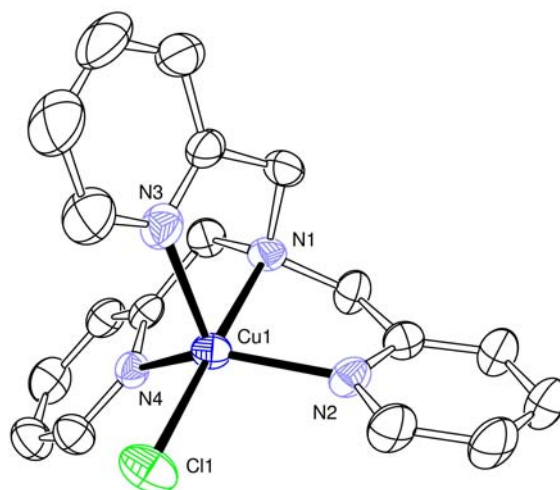


Figure 3.1.4: Molecular structure of the cation of [Cu(tmpa)Cl]BPh₄ (**5**). ORTEP plot with thermal ellipsoids set at 50 % probability (hydrogen atoms and tetraphenylborate anion are not shown). Selected bond lengths [Å] and angles [°]: Cu1-Cl1 2.2321(12), Cu1-N1 2.046(3), Cu1-N2 2.032(7), Cu1-N3 2.114(3), Cu1-N4 2.034(3); N1-Cu1-Cl1 178.51(10), N1-Cu1-N2 81.31(12), N2-Cu1-N3 111.47(13), N2-Cu1-N4 134.24(12).

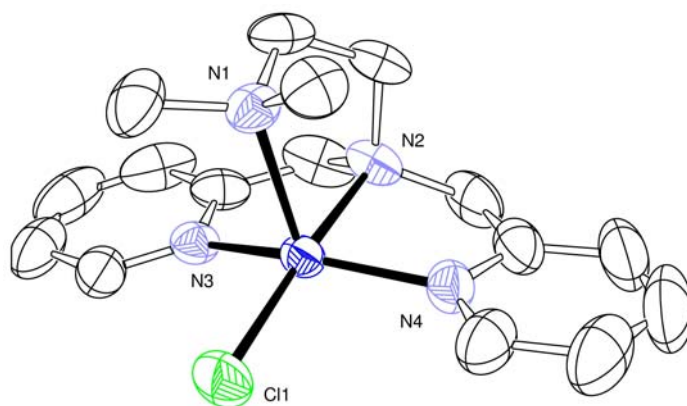


Figure 3.1.5: Molecular structure of the cation $[\text{Cu}(\text{Me}_2\text{uns-penp})\text{Cl}]\text{BPh}_4$ (**6a**). ORTEP plot with thermal ellipsoids set at 50 % probability (hydrogen atoms and tetraphenylborate anion are not shown). Selected bond lengths [\AA] and angles [$^\circ$]: Cu1-Cl1 2.2342(9), Cu1-N1 2.2463(19), Cu1-N2 2.051(2), Cu1-N3 2.016(2), Cu1-N4 2.014(2); N2-Cu1-Cl1 176.02(6), N1-Cu1-N2 85.07(8), N1-Cu1-N3 92.97(8), N3-Cu1-N4 154.82(9).

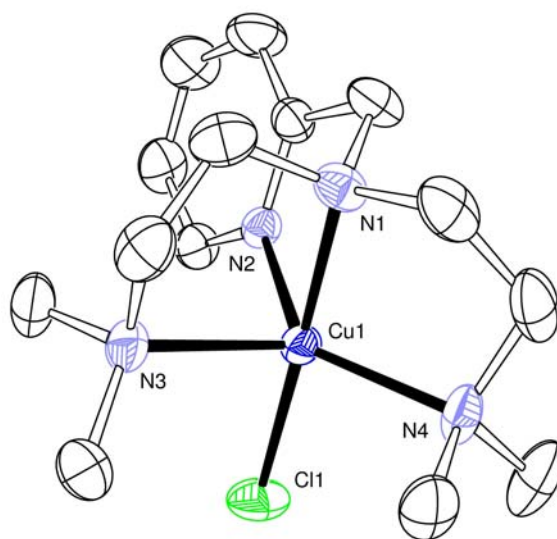


Figure 3.1.6: Molecular structure of the cation of $[\text{Cu}(\text{Me}_4\text{apme})\text{Cl}]\text{BPh}_4$ (**7**). ORTEP plot with thermal ellipsoids set at 50 % probability (hydrogen atoms and tetraphenylborate anion are not shown). Selected bond lengths [\AA] and angles [$^\circ$]: Cu1-Cl1 2.2387(6), Cu1-N1 2.0400(17), Cu1-N2 2.0607(16), Cu1-N3 2.2247(18), Cu1-N4 2.0715(18); N1-Cu1-Cl1 177.93(5), N1-Cu1-N2 81.40(7), N1-Cu1-N3 8.49(7), N2-Cu1-N3 102.02(7), N2-Cu1-N4 136.45(7).

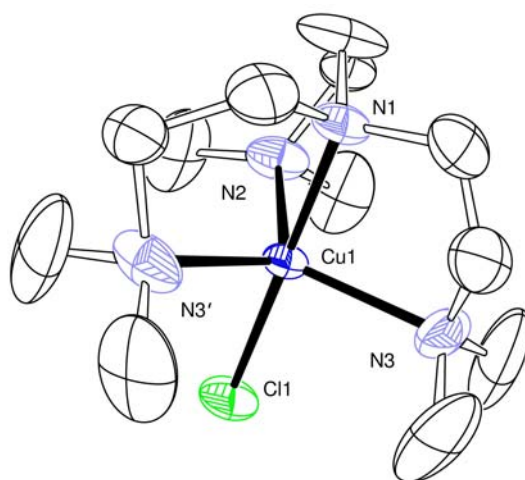


Figure 3.1.7: Molecular structure of the cation of $[\text{Cu}(\text{Me}_6\text{tren})\text{Cl}]\text{BPh}_4$ (**8**). ORTEP plot with thermal ellipsoids set at 50 % probability (hydrogen atoms and tetraphenylborate anion are not shown). Selected bond lengths [Å] and angles [°]: Cu1-Cl1 2.2081(11), Cu1-N1 2.025(3), Cu1-N2 2.170(3), Cu1-N3 2.152(3); N1-Cu1-Cl1 179.20(10), N1-Cu1-N2 84.49(13), N2-Cu1-N3 119.17(10).

Copper(II) chloride complexes are interesting in regard to their possible role to provide information on the crystal structure of dioxygen adduct complexes if these complexes are not stable enough to be isolated. This has proved to be correct for the tmpa and the Bz_3tren system for which the peroxo complexes as well as the chlorido complexes could be structurally characterized.^[12, 21, 22, 106] Therefore, this information can be used for the other ligand systems for which we could not obtain crystals of the formed peroxo complexes.

3.1.5.2 Electrochemistry

To gain more information on the redox behavior of the four complexes cyclic voltammetry was performed on them under the same conditions in acetonitrile and acetone. The cyclic voltammograms are shown in Figures 3.1.8 and 3.1.9. Data of the measured redox potentials are provided in Table 3.1.1 and 3.1.2.

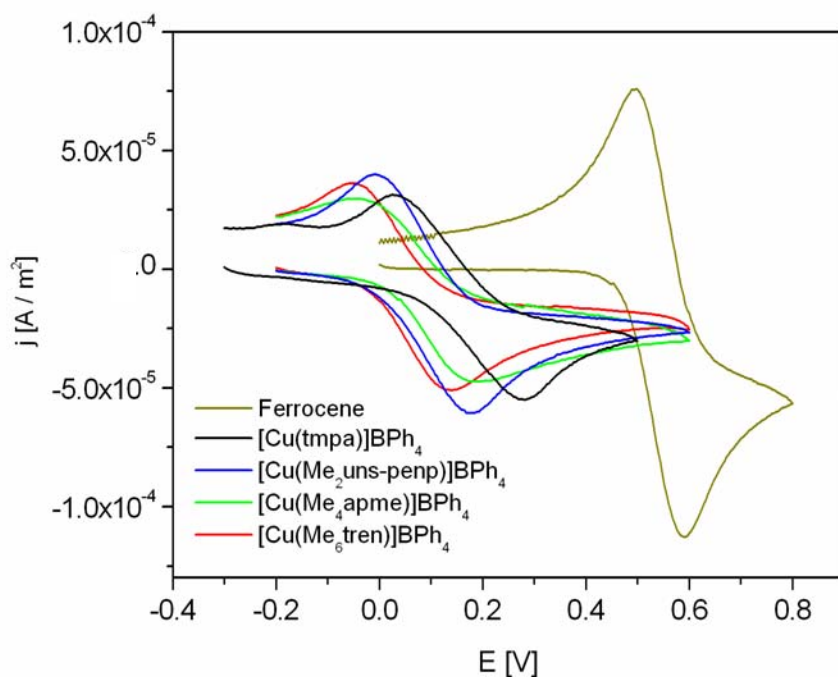


Figure 3.1.8: Cyclic voltammogram for $[\text{Cu}(\text{L})]\text{BPh}_4$ in acetone at room temperature; $[\text{complex}] = 1 \text{ mmol/L}$; $[\text{electrolyte}] ([\text{NBu}_4]\text{BF}_4) = 0.1 \text{ mol/L}$.

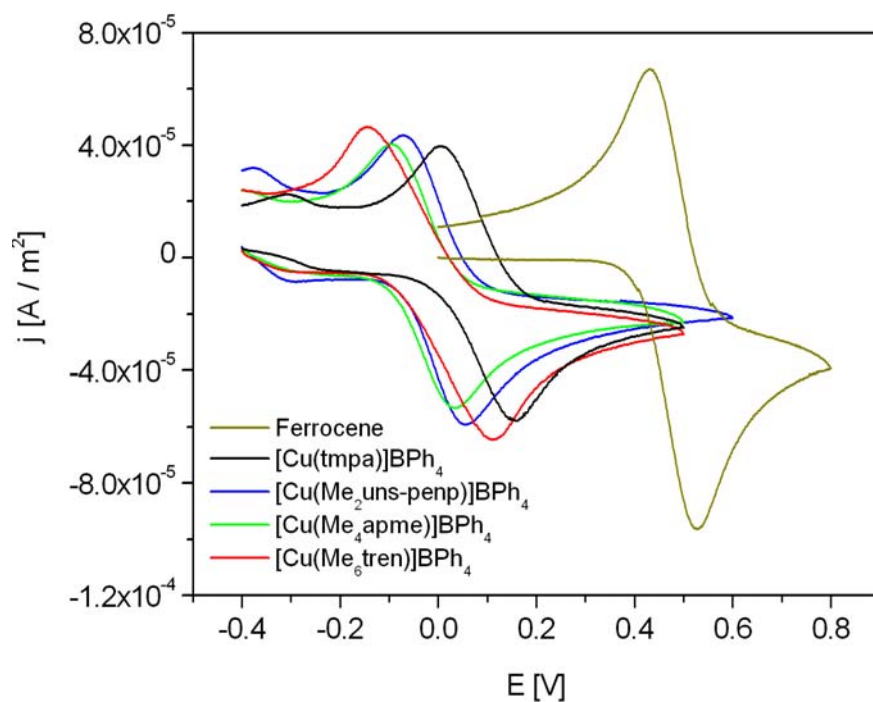


Figure 3.1.9: Cyclic voltammogram for $[\text{Cu}(\text{L})]\text{BPh}_4$ in acetonitrile at room temperature; $[\text{complex}] = 1 \text{ mmol/L}$; $[\text{electrolyte}] ([\text{NBu}_4]\text{BF}_4) = 0.1 \text{ mol/L}$.

Table 3.1.1: Cyclic voltammetry for [Cu(L)]BPh₄ in acetone ^[a]

Compound	E_p^{red} [V]	E_p^{ox} [V]	$E_{1/2}$ [V]	ΔE [mV]
[Cu(Me ₆ tren)]BPh ₄	-0.0533	0.1400	0.0434	193.3
[Cu(Me ₄ apme)]BPh ₄	-0.0460	0.1878	0.0709	233.8
[Cu(Me ₂ uns-penp)]BPh ₄	-0.0061	0.1766	0.0853	182.7
[Cu(tmpa)]BPh ₄	0.0367	0.2759	0.1563	239.2
Ferrocene	0.4971	0.5884	0.5428	91.3

Table 3.1.2: Cyclic voltammetry for [Cu(L)]BPh₄ in acetonitrile ^[a]

Compound	E_p^{red} [V]	E_p^{ox} [V]	$E_{1/2}$ [V]	ΔE [mV]
[Cu(Me ₆ tren)]BPh ₄	-0.1429	0.1129	-0.0150	255.8
[Cu(Me ₄ apme)]BPh ₄	-0.0950	0.0319	-0.0316	126.9
[Cu(Me ₂ uns-penp)]BPh ₄	-0.0711	0.0548	-0.0082	125.9
[Cu(tmpa)]BPh ₄	-0.0068	0.1606	0.0769	167.4
Ferrocene	0.4315	0.5272	0.4794	95.7

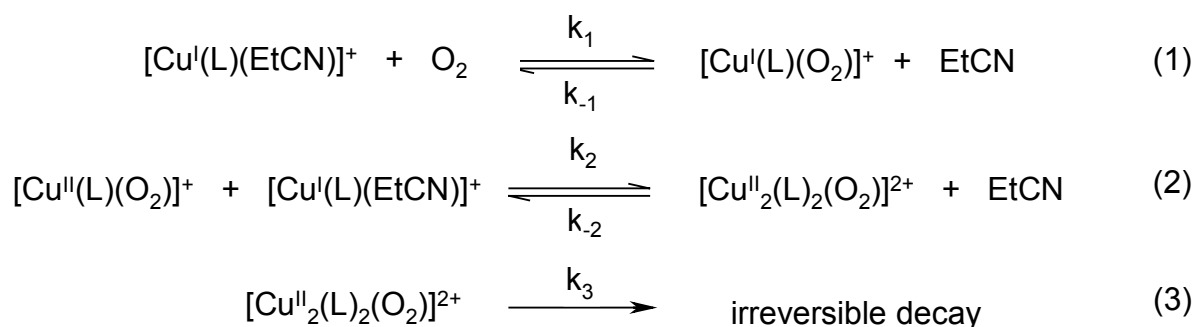
^[a] All potentials measured with a glassy carbon electrode vs. Ag/AgCl using [NBu₄]BF₄ (0.1 mol/L) as electrolyte. [$E_{1/2} = (E_p^{\text{red}} + E_p^{\text{ox}})/2$; $\Delta E = E_p^{\text{ox}} - E_p^{\text{red}}$].

From the results of these measurements it is clear that the redox potentials are becoming more positive for the oxidations from **4** to **1**. This is expected and has been observed previously, that aromatic nitrogen donor atoms support the copper(I) state and thus facilitate reduction of the copper(II) complexes as well as making it harder to oxidize the copper(I) complexes. The redox potential of [Cu(tmpa)(CH₃CN)]PF₆ in acetonitrile has been reported previously (-0.40 V vs. Fc/Fc⁺) and fits perfectly well with our results.^[40]

Unfortunately, so far all our efforts to perform electrochemistry on the peroxo complexes formed during oxidation of the copper(I) complexes at low temperatures in the electrochemical compartment were unsuccessful.

3.1.5.3 Kinetic Measurements

Previous detailed mechanistic studies on the reactions of the copper(I) complexes $[\text{Cu}(\text{tmpa})(\text{CH}_3\text{CN})]^+$ and $[\text{Cu}(\text{Me}_6\text{tren})]^+$ with dioxygen allowed the postulation of the well supported mechanism shown in Scheme 3.1.3 (due to the fact that the reactions were investigated in propionitrile as solvent, propionitrile is involved as an additional ligand in these oxidation processes).^[19, 39, 40] Detailed kinetic and thermodynamic data have been reported and are presented in Table 3.1.3 and 3.1.4.



Scheme 3.1.3: Reaction of $[\text{LCu}(\text{EtCN})]^+$ and O_2 in propionitrile (L = tmpa; Me₂uns-penp; Me₄apme; Me₆tren)

Table 3.1.3: Kinetic parameters for O_2 interaction with $[\text{LCu}(\text{RCN})]^+$ in propionitrile; L = tmpa,^[40] Me₂uns-penp, Me₄apme and Me₆tren).^[39]

parameter	temperature	L = tmpa	L = Me ₂ uns-penp	L = Me ₄ apme ⁺	L = Me ₆ tren
k_1 ($\text{M}^{-1}\text{s}^{-1}$)	183 K	$(1.18 \pm 0.01) \times 10^4$	$(3.3 \pm 0.3) \times 10^5$	$(7.0 \pm 0.6) \times 10^5$	$(9.5 \pm 0.4) \times 10^4$
	223 K	$(5.0 \pm 0.3) \times 10^5$	$(2.3 \pm 0.3) \times 10^6$	$(5.7 \pm 0.7) \times 10^6$	$(8.7 \pm 0.4) \times 10^5$
	298 K	$(5.8 \pm 0.8) \times 10^7$	$(2.2 \pm 0.5) \times 10^7$	$(7 \pm 2) \times 10^7$	$(1.2 \pm 0.1) \times 10^7$
ΔH^\ddagger (kJmol^{-1})		31.6 ± 0.5	14.7 ± 0.8	16.2 ± 0.8	17.1 ± 0.6
ΔS^\ddagger ($\text{JK}^{-1}\text{mol}^{-1}$)		10 ± 3	-55 ± 4	-40 ± 4	-52 ± 3
k_2 (s^{-1})	183 K	$(1.59 \pm 0.01) \times 10^1$	$(5.6 \pm 0.5) \times 10^0$	$(2.3 \pm 0.3) \times 10^0$	$(7.0 \pm 0.3) \times 10^{-2}$
	223 K	$(2.7 \pm 0.2) \times 10^4$	$(3.2 \pm 0.3) \times 10^3$	$(1.3 \pm 0.2) \times 10^3$	$(1.28 \pm 0.05) \times 10^2$
	298 K	$(1.5 \pm 0.2) \times 10^8$	$(5 \pm 1) \times 10^6$	$(2.0 \pm 0.6) \times 10^6$	$(7.7 \pm 0.9) \times 10^5$
ΔH^\ddagger (kJmol^{-1})		61.5 ± 0.5	52.1 ± 0.8	52 ± 1	62.0 ± 0.6
ΔS^\ddagger ($\text{JK}^{-1}\text{mol}^{-1}$)		118 ± 3	58 ± 4	50 ± 6	76 ± 3
k_3 ($\text{M}^{-1}\text{s}^{-1}$)	183 K	$(1.34 \pm 0.02) \times 10^4$	$(7.9 \pm 0.4) \times 10^4$	$(4.7 \pm 0.1) \times 10^4$	$(1.53 \pm 0.04) \times 10^4$
	223 K	$(2.33 \pm 0.02) \times 10^5$	$(8.6 \pm 0.4) \times 10^5$	$(4.1 \pm 0.1) \times 10^5$	$(1.38 \pm 0.02) \times 10^5$
	298 K	$(6.7 \pm 0.2) \times 10^6$	$(1.41 \pm 0.07) \times 10^5$	$(5.2 \pm 0.2) \times 10^6$	$(1.85 \pm 0.06) \times 10^6$
ΔH^\ddagger (kJmol^{-1})		22.6 ± 0.1	18.5 ± 0.2	16.6 ± 0.1	17.0 ± 0.2
ΔS^\ddagger ($\text{JK}^{-1}\text{mol}^{-1}$)		-38.6 ± 0.6	-46.1 ± 0.8	-60.6 ± 0.6	-67.9 ± 0.9
k_4 (s^{-1})	183 K	$(2.0 \pm 0.2) \times 10^{-5}$	$(1.97 \pm 0.01) \times 10^{-5}$	$(5 \pm 1) \times 10^{-07}$	$(5.8 \pm 0.9) \times 10^{-5}$
	223 K	$(9.1 \pm 0.4) \times 10^{-2}$	$(5.22 \pm 0.02) \times 10^{-2}$	$(6.2 \pm 0.5) \times 10^{-3}$	$(1.28 \pm 0.07) \times 10^{-1}$
	298 K	$(1.6 \pm 0.1) \times 10^3$	$(4.82 \pm 0.01) \times 10^2$	$(3.1 \pm 0.3) \times 10^2$	$(9.6 \pm 0.7) \times 10^2$
ΔH^\ddagger (kJmol^{-1})		69.8 ± 0.6	65.2 ± 0.4	78 ± 1	63.7 ± 0.8
ΔS^\ddagger ($\text{JK}^{-1}\text{mol}^{-1}$)		51 ± 3	25 ± 2	63 ± 6	26 ± 3

Table 3.1.4: Thermodynamic parameters for O₂ interaction with [LCu(RCN)]⁺ in propionitrile; L = tmpa,^[40] Me₂uns-penp, Me₄apme and Me₆tren).^[39]

parameter	temperature	L = tmpa	L = Me ₂ uns-penp	L = Me ₄ -apme	L = Me ₆ tren
K ₁ (M ⁻¹)	183 K	(7.42 ± 0.04) × 10 ²	(5.9 ± 0.4) × 10 ⁴	(3.3 ± 0.1) × 10 ⁵	(1.35 ± 0.04) × 10 ⁶
	223 K	(2.20 ± 0.04) × 10 ¹	(7.2 ± 0.7) × 10 ²	(2.39 ± 0.08) × 10 ³	(6.8 ± 0.1) × 10 ³
	298 K	(3.8 ± 0.2) × 10 ⁻¹	(4.5 ± 0.8) × 10 ⁰	(8.2 ± 0.3) × 10 ⁰	(1.55 ± 0.05) × 10 ¹
ΔH° (kJmol ⁻¹)		-29.8 ± 0.2	-37.4 ± 0.7	-41.8 ± 0.2	-44.9 ± 0.2
ΔS° (JK ⁻¹ mol ⁻¹)		-108 ± 1	-113 ± 4	-123 ± 1	-128 ± 1
K ₂ (M ⁻¹)	183 K	(6.7 ± 0.7) × 10 ⁸	(4.1 ± 0.3) × 10 ⁹	(8.4 ± 0.3) × 10 ¹⁰	(1.4 ± 0.3) × 10 ⁸
	223 K	(2.6 ± 0.1) × 10 ⁶	(1.6 ± 0.1) × 10 ⁷	(6.5 ± 0.4) × 10 ⁷	(8.6 ± 0.5) × 10 ⁵
	298 K	(4.2 ± 0.3) × 10 ³	(2.7 ± 0.2) × 10 ⁴	(1.69 ± 0.06) × 10 ⁴	(2.5 ± 0.2) × 10 ³
ΔH° (kJmol ⁻¹)		-47.2 ± 0.6	-47.1 ± 0.2	-61 ± 2	-46.7 ± 0.9
ΔS° (JK ⁻¹ mol ⁻¹)		-89 ± 2	-73 ± 1	-123 ± 6	-94 ± 3

From our previous investigations on [Cu(Me₂uns-penp)(CH₃CN)]⁺ we furthermore know that this complex reacts according to the same mechanism.^[26] As expected and described below the same reaction scheme can be applied for the oxidation of [Cu(Me₄apme)]⁺.

At low temperatures, the mononuclear Cu(I) complex first reversibly binds dioxygen to form a labile 1:1 Cu-O₂ species, which then further reacts reversibly with a second Cu(I) center to form the dinuclear 2:1 Cu₂O₂ adduct. The behavior of the two reactions differs in detail and thus the relative stabilities of the 1:1 or 1:2 adducts depend largely on the coordinated ligand. Especially, when the temperature is increased from low temperatures (approximately -90 °C) to ambient temperatures the rate of the irreversible decay of the peroxo complexes increases and thus eliminates (for most of these compounds) the possibility to observe the copper peroxo complex at room temperature.

Time resolved UV-vis spectra of the reaction of [Cu(Me₄apme)]BPh₄ with dioxygen in propionitrile at -92.2 °C are shown in Figure 3.1.10. As expected these absorbance changes are very similar to the UV-vis spectra of the other three copper complexes and thus the absorbance maxima at 412 nm and 537 can be assigned to the superoxo complex, [Cu(Me₄apme)(O₂)]⁺, and the peroxo complex, [Cu₂(Me₄apme)₂(O₂)]⁺, accordingly.

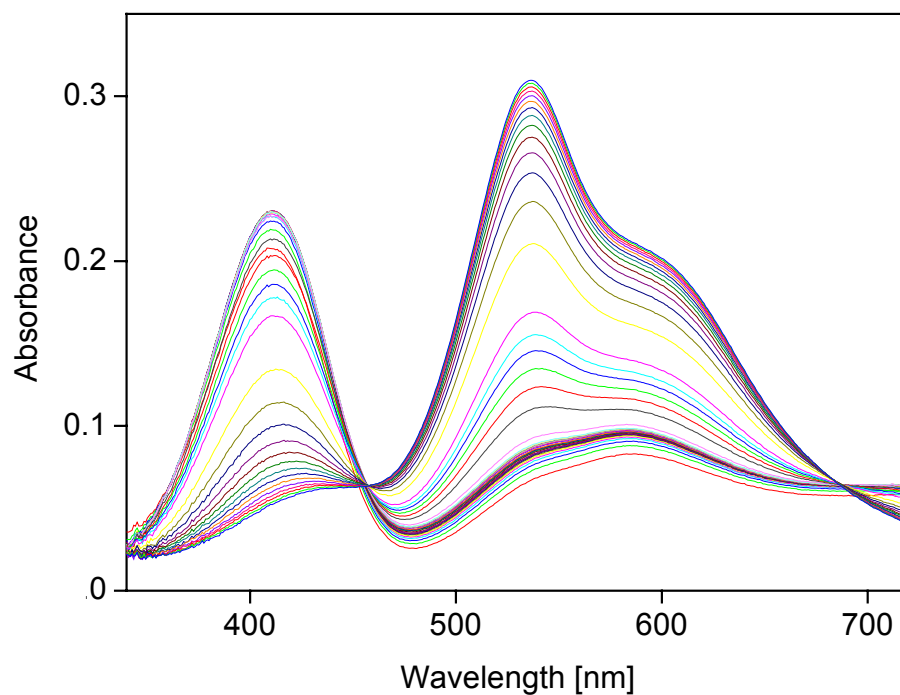


Figure 3.1.10: Time dependent, low temperature UV-vis spectra for the oxygenation reaction of $[\text{Cu}(\text{Me}_4\text{apme})]^+$ at $-92.2\text{ }^\circ\text{C}$ in propionitrile. $[\text{Cu}(\text{I})] = 0.270\text{ mM}$, $[\text{O}_2] = 1.10\text{ mM}$, path length: 2 mm.

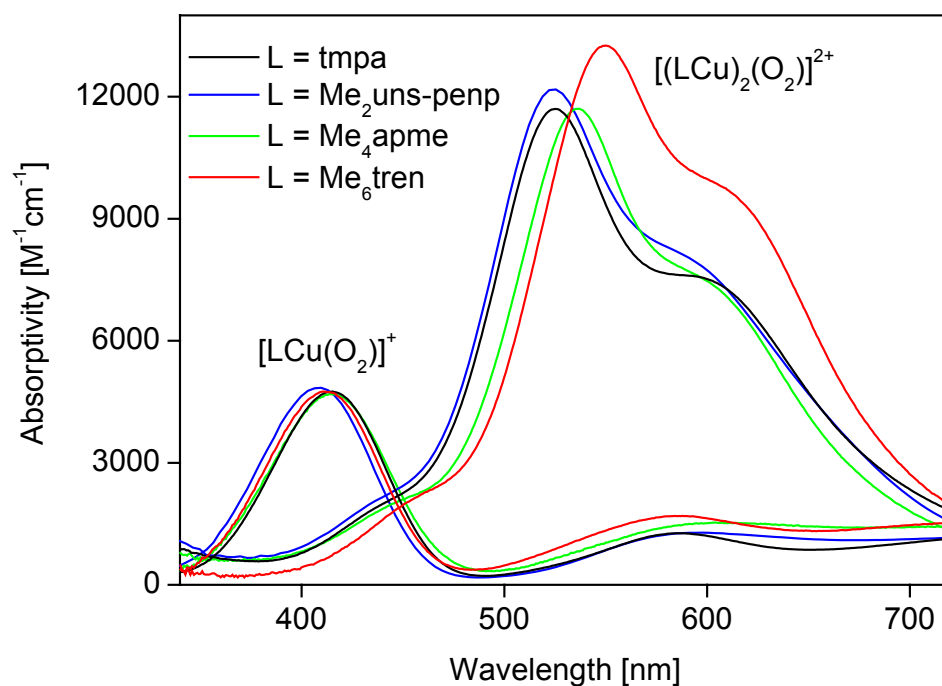


Figure 3.1.11: Calculated spectra for the $[\text{LCu}(\text{O}_2)]^+$ and $[(\text{LCu})_2\text{O}_2]^{2+}$ adducts.

Numerical analysis permits calculation of the spectra of all four $[\text{LCu}(\text{O}_2)]^+$ and $[(\text{LCu})_2(\text{O}_2)]^+$ complexes. The spectroscopic features are very similar. In all four cases the superoxo species has an absorbance maximum at about 410–415 nm with nearly identical ϵ values (Fig. 3.1.11, Table 3.1.5).

Table 3.1.5: UV-vis spectroscopic data for superoxo and peroxo copper(II) complexes.

L	$[\text{LCu}(\text{O}_2)]^+$		$[(\text{LCu})_2(\text{O}_2)]^+$	
	λ_{max} [nm]	ϵ [$\text{M}^{-1}\text{cm}^{-1}$]	λ_{max} [nm]	ϵ [$\text{M}^{-1}\text{cm}^{-1}$]
tmpa	415	4.8×10^3	525	1.15×10^4
$\text{Me}_2\text{uns-penp}$	410	4.8×10^3	525	1.22×10^4
Me_4apme	414	4.7×10^3	537	1.17×10^4
Me_6tren	412	4.8×10^3	552	1.35×10^4

For $[\text{tmpaCu}(\text{O}_2)]^+$ the absorbance band has been assigned in the past as a LMCT transition.^[6, 19, 108] Furthermore, the spectra of all trans- μ -peroxo complexes, with the exception of $[(\text{Me}_6\text{trenCu})_2(\text{O}_2)]^+$, are nearly identical (Fig. 3.1.11). The calculated ϵ values at λ_{max} are presented in Table 3.1.5. Absorbance maxima are assigned to copper(II) LMCT transitions. The slightly different behavior observed for $[\text{Cu}_2(\text{Me}_6\text{tren})_2(\text{O}_2)]^+$ observation might be explained by minor geometrical differences in the CuOOCu adducts and consequently different transition energies.

3.1.5.4 Kinetic and Thermodynamic Parameters

As for the previously investigated tmpa and Me_6tren systems, low temperature stopped-flow techniques allowed the detailed time resolved spectroscopic study of the formation of the copper superoxo and peroxo complexes with the ligands $\text{Me}_2\text{uns-penp}$ and Me_4apme (time resolved spectra thus obtained for the reaction of $[\text{Cu}(\text{Me}_4\text{apme})]\text{BPh}_4$ with dioxygen are shown in Fig. 3.1.10). The model used for data fitting in Specfit consists of two equilibria $K_1 = k_1/k_{-1}$ and $K_2 = k_2/k_{-2}$ and an unspecific decomposition reaction k_3 (Scheme 3.1.3). The formation of the superoxo species is observable only at the lowest temperatures. At higher temperatures, the equilibrium K_1 is established within the mixing time of the instrument. The ratio of

k_1/k_{-1} can be calculated by keeping the spectrum of minority species (Cu(I) or superoxo species) and the extrapolated k_1 fixed. The back reaction k_{-1} is fixed in such a way that the calculated spectrum of the majority species is not a linear addition of both species. The back reaction k_{-2} and therefore K_2 can be calculated from data obtained at $-80\text{ }^\circ\text{C}$ ($[\text{Cu}(\text{Me}_2\text{uns-penp})(\text{CH}_3\text{CN})_4]^+$) and from $-52\text{ }^\circ\text{C}$ ($[\text{Cu}(\text{Me}_4\text{apme})(\text{CH}_3\text{CN})_4]^+$). Activation enthalpies ΔH^\ddagger and entropies ΔS^\ddagger for the reactions of both complexes compared with the reactions of tmpa and Me₆tren complexes are presented in Table 3.1.3, in addition with individual rate constants calculated for 183, 223 and 298 K (Figures 3.2.5 – 3.2.8). By combination of the appropriate kinetic parameters for the corresponding forward and backward reactions, thermodynamic parameters have also been derived. Reaction enthalpies ΔH° and entropies ΔS° are shown in the Table 3.1.4 (Figures 3.2.9 and 3.2.10).

3.1.5.5 Formation and Dissociation of the Cu-O₂ 1:1 adducts

Our expectation that the stability of copper “dioxygen adducts” would be increased by replacing the aromatic groups with aliphatic groups in the ligand was fulfilled for the superoxo complex (1:1 species) and partly for the peroxo complexes (1:2 compound). This means the superoxo complex with the ligand Me₆tren is the most stable, at low temperature (183 K) approximately four times more stable than the analogous complex with Me₄apme, 20 times than with Me₂uns-penp and almost 3 orders of magnitude than with tmpa. This stabilization is based on enthalpy, reaction entropies being similar (Table 3.1.3). This is a consequence primarily due to a reduction of the rate of dissociation $k_{-1} = (1.59 \pm 0.01) \times 10^1 \text{ s}^{-1}$ (tmpa), $k_{-1} = (5.6 \pm 0.5) \times 10^0 \text{ s}^{-1}$ (Me₂uns-penp), $k_{-1} = (2.3 \pm 0.3) \times 10^0 \text{ s}^{-1}$ (Me₄apme), $k_{-1} = (7.0 \pm 0.3) \times 10^{-2} \text{ s}^{-1}$ (Me₆tren) at 183 K, Table 3.1.4 (Figure 3.2.6). The rate of formation increased in the low temperature region from tmpa to Me₄apme but for Me₆tren less than for Me₂uns-penp and Me₄apme $k_1 = (1.18 \pm 0.01) \times 10^4 \text{ s}^{-1}$ (tmpa), $k_1 = (3.3 \pm 0.3) \times 10^5 \text{ s}^{-1}$ (Me₂uns-penp), $k_1 = (7.0 \pm 0.6) \times 10^5 \text{ s}^{-1}$ (Me₄apme), $k_1 = (9.5 \pm 0.4) \times 10^4 \text{ s}^{-1}$ (Me₆tren) at 183 K, Table 3.1.3 (Figure 3.2.5).

The activation enthalpy favors the formation of $[\text{Cu}(\text{Me}_2\text{uns-penp})(\text{O}_2)]^+$ and least of all the formation of $[\text{Cu}(\text{tmpa})(\text{O}_2)]^+$ ($\Delta H^\ddagger = 14.7 \pm 0.8 \text{ kJmol}^{-1}$ (Me₂uns-penp), $\Delta H^\ddagger = 16.2 \pm 0.8 \text{ kJmol}^{-1}$ (Me₄apme), $\Delta H^\ddagger = 17.1 \pm 0.6 \text{ kJmol}^{-1}$ (Me₆tren) vs. $\Delta H^\ddagger = 31.6 \pm 0.5 \text{ kJmol}^{-1}$ (tmpa), Table 3.1.3). The activation entropies have similar negative

values except for the copper tmpa complex ($\Delta S^\ddagger = -55 \pm 4 \text{ kJmol}^{-1}$ ($\text{Me}_2\text{uns-penp}$), $\Delta S^\ddagger = -40 \pm 4 \text{ kJmol}^{-1}$ (Me_4apme), $\Delta S^\ddagger = -52 \pm 3 \text{ kJmol}^{-1}$ (Me_6tren) vs. $\Delta S^\ddagger = 10 \pm 3 \text{ kJmol}^{-1}$ (tmpa), Table 3.1.4, Figure 3.2.5).

The Eyring plot of the data for k_{-1} leads to parallel lines for the complexes of $\text{Me}_2\text{uns-penp}$ and Me_4apme (Figure 3.2.6) or rather for tmpa and Me_6tren complexes. Accordingly the activation enthalpies are nearly identical for $\text{Me}_2\text{uns-penp}$ and Me_4apme or rather for tmpa and Me_6tren complexes. However, there is a small difference between our results and the earlier determined activation enthalpies ($\Delta H^\ddagger = 52.1 \pm 0.8 \text{ kJmol}^{-1}$ ($\text{Me}_2\text{uns-penp}$), $\Delta H^\ddagger = 52 \pm 1 \text{ kJmol}^{-1}$ (Me_4apme), $\Delta H^\ddagger = 61.5 \pm 0.5 \text{ kJmol}^{-1}$ (tmpa) vs. $\Delta H^\ddagger = 62.0 \pm 0.6 \text{ kJmol}^{-1}$ (Me_6tren), Table 3.1.4).

3.1.5.6 Formation and Dissociation of the Cu-O₂ 2:1 Adducts

Weitzer et. al observed that in contrast to the formation of superoxo complexes, the replacement of tmpa by Me_6tren leads to a relatively small, but significant, destabilization of the peroxo complex.^[39] As discussed above we observed in our investigations that the copper superoxo complexes are stabilized by the four ligands in the following order: $\text{Me}_6\text{tren} > \text{Me}_4\text{apme} > \text{Me}_2\text{uns-penp} > \text{tmpa}$ (Table 3.1.4). In contrast, a comparison of the stability of the peroxo complexes clearly showed that $[\text{Cu}_2(\text{Me}_2\text{uns-penp})_2(\text{O}_2)]^{2+}$ is the most persistent at higher temperatures, confirming our previous preliminary investigations on this complex.^[26] The stability of the peroxo complexes in propionitrile follows the order: $[\text{Cu}_2(\text{Me}_2\text{uns-penp})_2(\text{O}_2)]^{2+} > [\text{Cu}_2(\text{Me}_4\text{apme})_2(\text{O}_2)]^{2+} > [\text{Cu}_2(\text{tmpa})_2(\text{O}_2)]^{2+} > [\text{Cu}_2(\text{Me}_6\text{tren})_2(\text{O}_2)]^{2+}$.

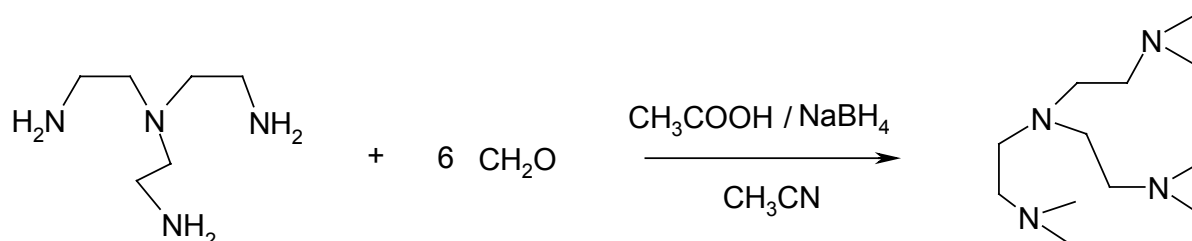
3.1.6 Conclusion

Our systematic kinetic investigations showed that the stability of end-on copper superoxo complexes is clearly increased if more aliphatic N-donor atoms are present. Thus, $[\text{Cu}(\text{Me}_6\text{tren})\text{O}_2]^+$ is most persistent under the conditions applied. This systematic increase/decrease of stabilities is not observed for the according Cu/O₂ 2:1 adducts: here the peroxo complexes do not follow such an order and $[\text{Cu}_2(\text{Me}_2\text{uns-penp})_2(\text{O}_2)]^{2+}$ turned out to be the most persistent complex at room temperature. The kinetic data for the reactions of dioxygen with the copper(I) complexes with the ligands tmpa, $\text{Me}_2\text{uns-penp}$, Me_4apme and Me_6tren in

propionitrile are similar. They clearly explain the different stabilities of the superoxo complexes, however fail to fully describe the stability of the formed peroxo complexes. Here the decomposition reactions seem to play an important part and it will be necessary to investigate these in more detail in the future. However, a likely explanation is indicated by the crystal structure of the copper(II) complexes with the ligand Me₂uns-penp (**6** and [Cu(Me₂uns-penp)Cl]ClO₄). Here a square pyramidal geometry is adopted with the additional ligand in the equatorial plane. While this does not seem to play an important role for the superoxo complex it might be quite relevant for the formation of the sterically more demanding peroxo complex. If this complex adopts such a coordination geometry the equatorial peroxo ligand should be coordinated much stronger compared with the coordination as an axial ligand in a trigonal bipyramidal environment. However, further studies are necessary to proof this assumption.

3.2 Selected parts of supporting information and unpublished results for chapter 3.1

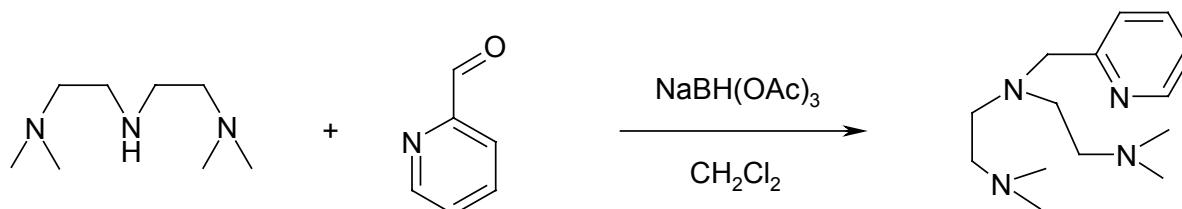
3.2.1 Synthesis of Me₆tren (tris(2-dimethylaminoethyl)amine)^[92]



To aqueous formaldehyde (49.0 mL, 37 %, 637 mmol) was added a solution of tris(2-aminoethyl)amine (3.0 mL, 19.9 mmol) and 135 mL of acetic acid in acetonitrile (600 mL) and allowed to stir for 1 h. Subsequently, the reaction mixture was cooled to 0 °C by using an ice bath and sodium borohydride (10.0 g, 264 mmol) was slowly added. After 48 h of stirring, all solvents were removed, the residue was made strongly basic by using aqueous sodium hydroxide (3 mol/L), and extracted with CH₂Cl₂ (3 × 50 mL). The organic fractions were combined, dried over anhydrous MgSO₄ and the solvent removed. The residue was dissolved in pentane, filtered and removal of the solvent in vacuum gave Me₆tren as a yellow oil. The oil was purified by using Kugelrohr-distillation yielding 2.93 g, 12.7 mmol (64 %) of Me₆tren as a colorless oil.

¹H-NMR (400 MHz, CDCl₃/TMS, δ/ppm): 2.55 (t, 6H, (Me)₂NCH₂), 2.32 (t, 6H, NCH₂), 2.16 (s, 16H, NCH₃).

3.2.2 Synthesis of Me₄apme (bis(2-dimethyl-aminoethyl)(2-pyridylmethyl)-amine)^[92]

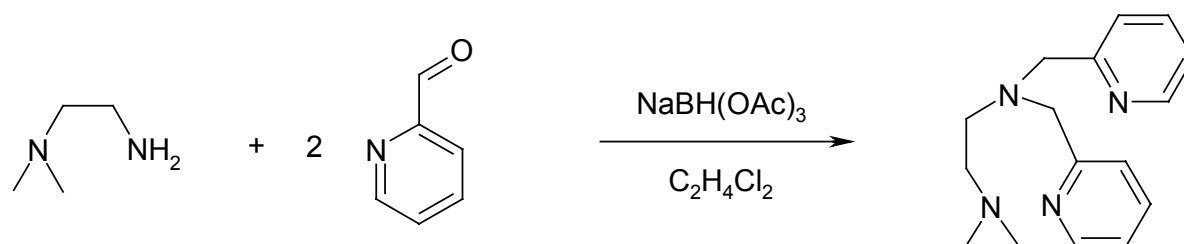


In a 250 mL round-bottom flask, pyridine-2-carboxyaldehyde (1.18 g, 11.0 mmol) was added to a mixture of 1.96 g (12.3 mmol) of bis[2-(dimethylamino)-ethyl]amine and 3.66 g (17.2 mmol) of sodium triacetoxyborohydride in CH₂Cl₂ (100 mL) and allowed to stir for 12 h. The reaction was quenched by the addition of an aqueous solution of

sodium hydroxide (3 mol/L). The organic layer was separated and the aqueous layer was extracted with CH_2Cl_2 (3×100 mL). The organic fractions were combined, dried over anhydrous MgSO_4 and the solvent was removed. The residue was dissolved in THF (100 mL) and treated with NaH (0.6 g, 25 mmol). After being stirred for 2 h, the solvent was removed and the residue was extracted with pentane (3×50 mL). The solution was filtered and removal of the solvent in vacuum resulted a brown oil. The oil was purified by using Kugelrohr-distillation yielding 1.02 g, 4.07 mmol (37 %) of Me_4apme as a yellow oil.

^1H -NMR (400 MHz, CDCl_3/TMS , δ/ppm): 8.47 (d, 1H, 6-PyH), 7.59 (t, 1H, 4-PyH), 7.43 (d, 1H, 3-PyH), 7.09 (t, 1H, 5-PyH), 3.75 (s, 2H, PyCH_2), 2.62 (t, 4H, $(\text{Me})_2\text{NCH}_2$), 2.38 (t, 4H, NCH_2), 2.15 (s, 12H, NCH_3).

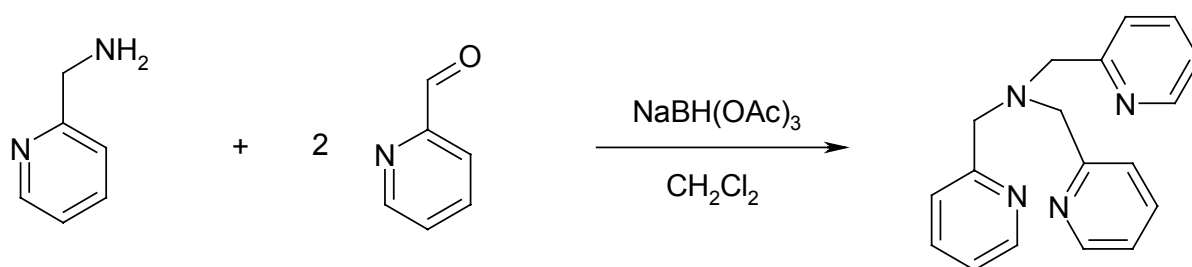
3.2.3 Synthesis of $\text{Me}_2\text{uns-penp}$ (2-dimethyl-aminoethyl)bis(2-pyridylmethyl)-amine)



N,N-dimethylethylenediamine (8.8 g, 0.1 mol), 2-pyridinecarboxaldehyde (21.4 g, 0.2 mol) were placed in 1,2-dichloroethane (300 mL) in a 2 L round-bottom flask. $\text{NaBH}(\text{OAc})_3$ (60 g, 0.28 mol) was added and the cloudy solution was stirred at room temperature for 2 days. The reaction was quenched by the addition of a 2M aqueous solution of NaOH (300 mL). The organic layer was separated and the aqueous layer was extracted with CH_2Cl_2 (3×100 mL). The organic fractions were combined and washed with a saturated aqueous solution of NaCl (150 mL). The organic fraction was dried over anhydrous Na_2SO_4 . Filtration and removal of the solvent in vacuum yielded $\text{Me}_2\text{uns-penp}$ as a golden colored oil (23.0 g, 94.9 mmol, 85 %).

^1H -NMR (400 MHz, CDCl_3/TMS , δ/ppm): 8.52 (d, 2H, 6-PyH), 7.65 (t, 2H, 4-PyH), 7.53 (d, 2H, 3-PyH), 7.14 (m, 2H, 5-PyH), 3.86 (s, 4H, PyCH_2), 2.71 (t, 2H, $(\text{Me})_2\text{NCH}_2$), 2.48 (t, 2H, NCH_2), 2.17 (s, 6H, NCH_3).

3.2.4 Synthesis of tmpa (tris(2-pyridylmethyl)amine)^[92]



2-(Aminomethyl)pyridine (1.62 g, 16 mmol) and sodium triacetoxyborohydride (9.36 g, 44 mmol) were placed in CH_2Cl_2 (150 mL) in a 250 mL round-bottom flask. Pyridine-2-carboxaldehyde (3.37 g, 32 mmol) was added and the solution was stirred at room temperature. After 20 h a saturated aqueous sodium hydrogen carbonate solution was added. After 15 min of stirring, extraction of the mixture using ethyl acetate was performed (3×50 mL). The organic fractions were dried over anhydrous Na_2SO_4 . Filtration and removal of the solvent in vacuum yielded tmpa as a yellow solid (3.82 g, 13.15 mmol, 83.3 %).

$^1\text{H-NMR}$ (400 MHz, CDCl_3/TMS , δ/ppm): 8.55 (d, 3H, 6-PyH), 7.84 (t, 3H, 4-PyH), 7.79 (d, 3H, 3-PyH), 7.24 (m, 3H, 5-PyH), 3.87 (s, 6H, NCH_2).

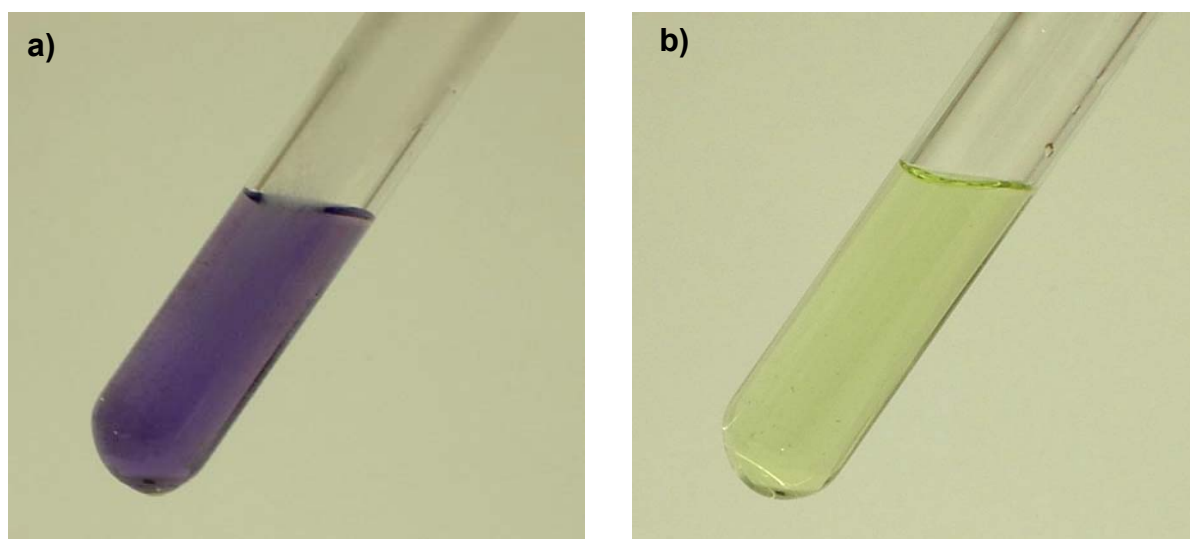


Figure 3.2.1: The photographs show the warming/cooling cycles of the peroxo complex of tmpa. a) Blue solution of $[\text{Cu}^{\text{II}}_2(\text{tmpa})_2(\text{O}_2)]^{2+}$ (~ 0.25 mmol) in propionitrile at -80°C b) After warming to room temperature, the solution changed color to yellow and $[\text{Cu}^{\text{I}}(\text{tmpa})]^+$ was reformed. These cycles can be repeated many times without any evidence of major decomposition reactions.

3.2.5 Synthesis of $[\text{Cu}(\text{Me}_6\text{tren})]\text{BPh}_4$

Under the inert atmosphere of a glove box Me_6tren (0.20 g, 0.87 mmol) was dissolved in acetone (2 mL) to which of a solution of $[\text{Cu}(\text{CH}_3\text{CN})_4]\text{PF}_6$ (0.30 g, 0.81 mmol in acetone (4 mL) was added. To the formed complex of $[\text{Cu}(\text{Me}_6\text{tren})]\text{PF}_6$ was added a solution of NaBPh_4 (0.28 g, 0.82 mmol) in acetone (2 mL). The complex $[\text{Cu}(\text{Me}_6\text{tren})]\text{BPh}_4$ was precipitated by addition of diethyl ether (approximately 20 mL). The white solid was filtered and washed with diethyl ether. The solid was dried in vacuum for 1 h yielding 0.48 g (96.6 %) of product (Figure 3.2.2a). X-ray quality crystals of this compound $[\text{Cu}(\text{Me}_6\text{tren})]\text{BPh}_4$ were obtained (Figure 3.4.1) by ether diffusion into the acetone solution.

3.2.6 Synthesis of $[\text{Cu}(\text{Me}_4\text{apme})]\text{BPh}_4$

Under the inert atmosphere of a glove box Me_4apme (0.20 g, 0.80 mmol) was dissolved in acetone (2 mL) to which of a solution of $[\text{Cu}(\text{CH}_3\text{CN})_4]\text{PF}_6$ (0.29 g, 0.78 mmol in acetone (4 mL) was added. To the formed complex of $[\text{Cu}(\text{Me}_4\text{apme})]\text{PF}_6$ was added a solution of NaBPh_4 (0.28 g, 0.82 mmol) in acetone (2 mL). The complex $[\text{Cu}(\text{Me}_4\text{apme})]\text{BPh}_4$ was precipitated by addition of diethyl ether (approximately 20 mL). The yellow solid was filtered and washed with diethyl ether. The solid was dried in vacuum for 1 h yielding 0.44 g (89.1 %) of product (Figure 3.2.2b). X-ray quality crystals of this compound $[\text{Cu}(\text{Me}_4\text{apme})]\text{BPh}_4$ were obtained (Figure 3.1.3) by ether diffusion into the acetone / THF solution.

3.2.7 Synthesis of $[\text{Cu}(\text{Me}_2\text{uns-penp})]\text{BPh}_4$

Under the inert atmosphere of a glove box $\text{Me}_2\text{uns-penp}$ (0.20 g, 0.74 mmol) was dissolved in acetone (2 mL) to which of a solution of $[\text{Cu}(\text{CH}_3\text{CN})_4]\text{PF}_6$ (0.27 g, 0.72 mmol in acetone (4 mL) was added. To the formed complex of $[\text{Cu}(\text{Me}_2\text{uns-penp})]\text{PF}_6$ was added a solution of NaBPh_4 (0.28 g, 0.82 mmol) in acetone (2 mL). The complex $[\text{Cu}(\text{Me}_2\text{uns-penp})]\text{BPh}_4$ was precipitated by addition of diethyl ether (approximately 20 mL). The yellow solid was filtered and washed with diethyl ether. The solid was dried in vacuum for 1 h yielding 0.46 g (97.8 %) of product (Figure 3.2.2c). X-ray quality crystals of this compound $[\text{Cu}(\text{Me}_2\text{uns-penp})]\text{BPh}_4$ were obtained (Figure 3.1.2) by ether diffusion into the acetone solution.

3.2.8 Synthesis of $[\text{Cu}(\text{tmpa})]\text{BPh}_4$

Under the inert atmosphere of a glove box tmpa (0.20 g, 0.69 mmol) was dissolved in acetone (2 mL) to which of a solution of $[\text{Cu}(\text{CH}_3\text{CN})_4]\text{PF}_6$ (0.25 g, 0.67 mmol) in acetone (4 mL) was added. To the formed complex of $[\text{Cu}(\text{tmpa})]\text{PF}_6$ was added a solution of NaBPh_4 (0.28 g, 0.82 mmol) in acetone (2 mL). The complex $[\text{Cu}(\text{tmpa})]\text{BPh}_4$ was precipitated by addition of diethyl ether (approximately 20 mL). The yellow solid was filtered and washed with diethyl ether. The solid was dried in vacuum for 1 h yielding 0.41 g (90.9 %) of product (Figure 3.2.2d). X-ray quality crystals of this compound $[\text{Cu}(\text{tmpa})]\text{BPh}_4$ were obtained (Figure 3.1.1) by ether diffusion into the acetone solution.

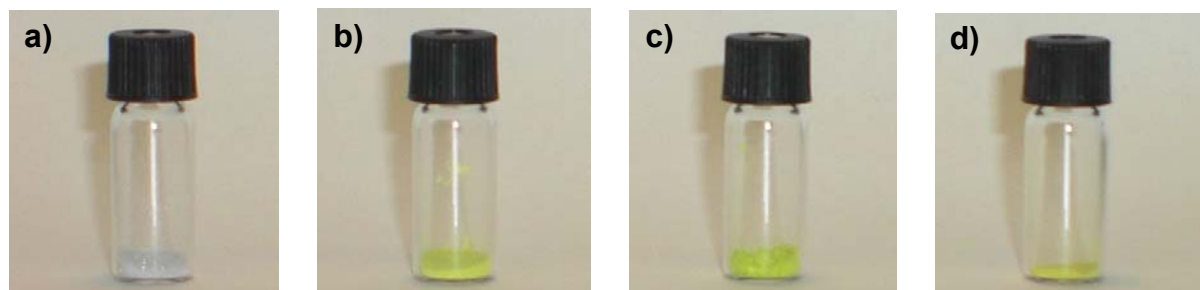


Figure 3.2.2: The photographs show the four air sensitive copper(I)-complexes under argon. a) $[\text{Cu}(\text{Me}_6\text{tren})]\text{BPh}_4$, b) $[\text{Cu}(\text{Me}_4\text{apme})]\text{BPh}_4$, c) $[\text{Cu}(\text{Me}_2\text{uns-penp})]\text{BPh}_4$, d) $[\text{Cu}(\text{tmpa})]\text{BPh}_4$

3.2.9 Synthesis of $[\text{Cu}(\text{Me}_6\text{tren})\text{Cl}]\text{BPh}_4$

Ligand Me_6tren (0.10 g, 0.44 mmol) was dissolved in methanol (4 mL) to which a solution of $\text{CuCl}_2 \cdot 2 \text{H}_2\text{O}$ (0.08 g, 0.47 mmol) in methanol (4 mL) was added. After 10 min of stirring a solution of NaBPh_4 (0.15 g, 0.44 mmol) in methanol was added. The complex $[\text{Cu}(\text{Me}_6\text{tren})\text{Cl}]\text{BPh}_4$ was precipitated as a greenish colored solid. The solid was filtered and dried in vacuum for 2 h yielding 0.24 g (84.1 %) of the product (Figure 3.2.3a). X-ray quality crystals of this compound $[\text{Cu}(\text{Me}_6\text{tren})\text{Cl}]\text{BPh}_4$ were obtained (Figure 3.1.7) by slow evaporation of an acetone solution.

3.2.10 Synthesis of $[\text{Cu}(\text{Me}_4\text{apme})\text{Cl}]\text{BPh}_4$

Ligand Me_4apme (0.10 g, 0.40 mmol) was dissolved in methanol (4 mL) to which a solution of $\text{CuCl}_2 \cdot 2 \text{H}_2\text{O}$ (0.07 g, 0.40 mmol) in methanol (4 mL) was added. After 10 min of stirring a solution of NaBPh_4 (0.14 g, 0.41 mmol) in methanol was added. The

complex $[\text{Cu}(\text{Me}_4\text{apme})\text{Cl}]\text{BPh}_4$ was precipitated as a greenish colored solid. The solid was filtered and dried in vacuum for 2 h yielding 0.22 g (82.5 %) of the product (Figure 3.2.3b). X-ray quality crystals of this compound $[\text{Cu}(\text{Me}_4\text{apme})\text{Cl}]\text{BPh}_4$ were obtained (Figure 3.1.6) by ether diffusion into an acetone solution.

3.2.11 Synthesis of $[\text{Cu}(\text{Me}_2\text{uns-penp})\text{Cl}]\text{BPh}_4$

Ligand $\text{Me}_2\text{uns-penp}$ (0.10 g, 0.37 mmol) was dissolved in methanol (4 mL) to which a solution of $\text{CuCl}_2 \cdot 2 \text{H}_2\text{O}$ (0.06 g, 0.35 mmol) in water/methanol (5 mL) was added. After 10 min of stirring a solution of NaBPh_4 (0.12 g, 0.35 mmol) in methanol was added. The complex $[\text{Cu}(\text{Me}_2\text{uns-penp})\text{Cl}]\text{BPh}_4$ was precipitated as a greenish colored solid. The solid was filtered and dried in vacuum for 2 h yielding 0.20 g (82.9 %) of product (Figure 3.2.3c). X-ray quality crystals of this compound $[\text{Cu}(\text{Me}_2\text{uns-penp})\text{Cl}]\text{BPh}_4$ were obtained in two different crystal systems by slow evaporation of a water/methanol solution (Figure 3.1.5: triclinic, green colored; Figure 3.2.4: monoclinic, blue colored).

3.2.12 Synthesis of $[\text{Cu}(\text{tmpa})\text{Cl}]\text{BPh}_4$

Ligand tmpa (0.10 g, 0.35 mmol) was dissolved in methanol (4 mL) to which a solution of $\text{CuCl}_2 \cdot 2 \text{H}_2\text{O}$ (0.06 g, 0.35 mmol) in methanol (4 mL) was added. After 10 min of stirring a solution of NaBPh_4 (0.12 g, 0.35 mmol) in methanol was added. The complex $[\text{Cu}(\text{tmpa})\text{Cl}]\text{BPh}_4$ was precipitated as a greenish colored solid. The solid was filtered and dried in vacuum for 2 h yielding 0.18 g (72.6 %) of the product (Figure 3.2.3d). X-ray quality crystals of this compound $[\text{Cu}(\text{tmpa})\text{Cl}]\text{BPh}_4$ were obtained (Figure 3.1.4) by slow evaporation of an acetone solution.

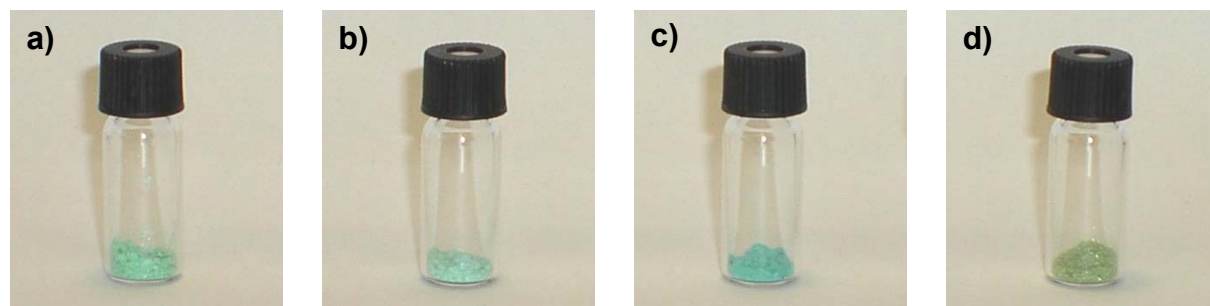


Figure 3.2.3: The photographs show the four copper(II)-complexes. a) $[\text{Cu}(\text{Me}_6\text{tren})\text{Cl}]\text{BPh}_4$, b) $[\text{Cu}(\text{Me}_4\text{apme})\text{Cl}]\text{BPh}_4$, c) $[\text{Cu}(\text{Me}_2\text{uns-penp})\text{Cl}]\text{BPh}_4$, d) $[\text{Cu}(\text{tmpa})\text{Cl}]\text{BPh}_4$.

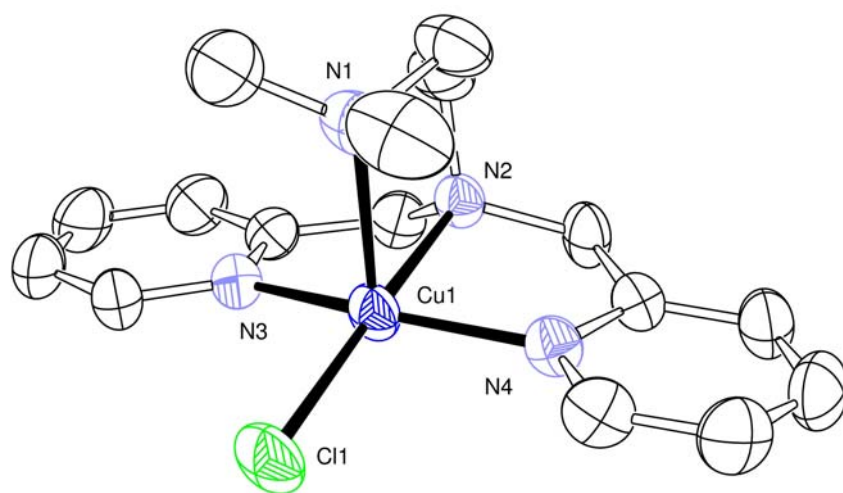


Figure 3.2.4: Molecular structure of the cation of $[\text{Cu}(\text{Me}_2\text{uns-penp})\text{Cl}]\text{BPh}_4$ (**6b**). ORTEP plot with thermal ellipsoids set at 50 % probability (hydrogen atoms and tetraphenylborate anion are not shown). Selected bond lengths [\AA] and angles [$^\circ$]: Cu1-Cl1 2.2381(7), Cu1-N1 2.329(2), Cu1-N2 2.0541(17), Cu1-N3 2.004(2), Cu1-N4 1.998(2); N2-Cu1-Cl1 175.65(6), N1-Cu1-N2 84.77(8), N1-Cu1-N3 99.34(9), N3-Cu1-N4 159.95(8).

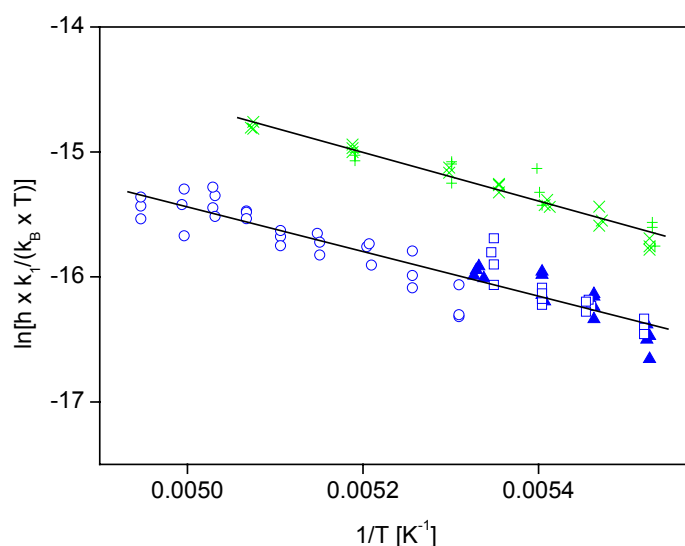


Figure 3.2.5: Eyring plots for k_1 pertaining to the formation of $[\text{LCu}(\text{O}_2)]^+$ from $[\text{LCu}(\text{EtCN})]^+$ in EtCN. k_B : Boltzman constant; h : Planck constant; L = $\text{Me}_2\text{uns-penp}$: \blacktriangle $[\text{Cu}(\text{I})] = 2.50 \times 10^{-4} \text{ M}$, $[\text{O}_2] = 1.00 \times 10^{-3} \text{ M}$; \square $[\text{Cu}(\text{I})] = 7.33 \times 10^{-4} \text{ M}$, $[\text{O}_2] = 1.00 \times 10^{-3} \text{ M}$; \circ $[\text{Cu}(\text{I})] = 8.97 \times 10^{-5} \text{ M}$, $[\text{O}_2] = 4.09 \times 10^{-4} \text{ M}$; L = Me_4apme : $+$ $[\text{Cu}(\text{I})] = 7.82 \times 10^{-4} \text{ M}$, $[\text{O}_2] = 1.10 \times 10^{-3} \text{ M}$; \times $[\text{Cu}(\text{I})] = 7.45 \times 10^{-4} \text{ M}$, $[\text{O}_2] = 4.40 \times 10^{-3} \text{ M}$

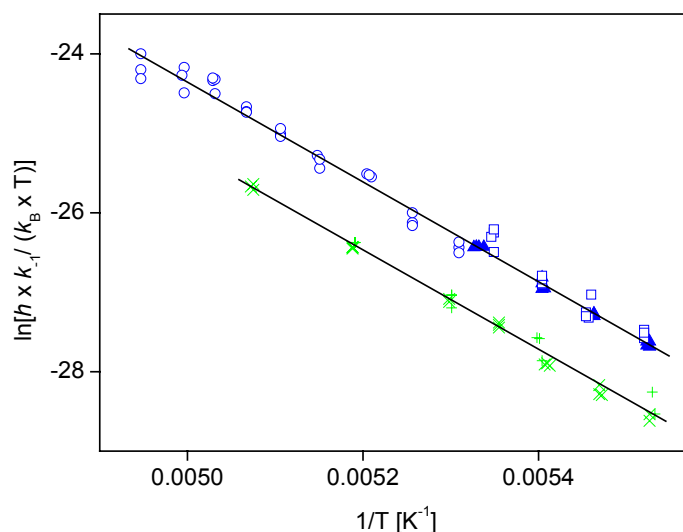


Figure 3.2.6: Eyring plots for k_{-1} pertaining to the formation of $[\text{LCu}(\text{O}_2)]^+$ from $[\text{LCu}(\text{EtCN})]^+$ in EtCN. k_B : Boltzman constant; h : Planck constant; L = Me₂uns-penp: \blacktriangle $[\text{Cu}(\text{I})] = 2.50 \times 10^{-4} \text{ M}$, $[\text{O}_2] = 1.00 \times 10^{-3} \text{ M}$; \square $[\text{Cu}(\text{I})] = 7.33 \times 10^{-4} \text{ M}$, $[\text{O}_2] = 1.00 \times 10^{-3} \text{ M}$; \circ $[\text{Cu}(\text{I})] = 8.97 \times 10^{-5} \text{ M}$, $[\text{O}_2] = 4.09 \times 10^{-4} \text{ M}$; L = Me₄apme: $+$ $[\text{Cu}(\text{I})] = 7.82 \times 10^{-4} \text{ M}$, $[\text{O}_2] = 1.10 \times 10^{-3} \text{ M}$; \times $[\text{Cu}(\text{I})] = 7.45 \times 10^{-4} \text{ M}$, $[\text{O}_2] = 4.40 \times 10^{-3} \text{ M}$

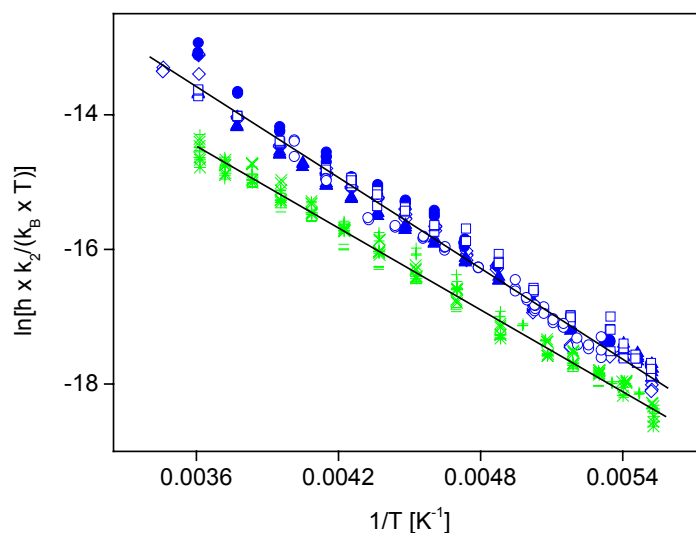


Figure 3.2.7: Eyring plots for k_2 pertaining to the formation of $[(\text{LCu})_2(\text{O}_2)]^{2+}$ in EtCN. k_B : Boltzman constant; h : Planck constant; L = Me₂uns-penp: \diamond $[\text{Cu}(\text{I})] = 2.47 \times 10^{-4} \text{ M}$, $[\text{O}_2] = 4.40 \times 10^{-3} \text{ M}$; \bullet $[\text{Cu}(\text{I})] = 7.48 \times 10^{-4} \text{ M}$, $[\text{O}_2] = 4.40 \times 10^{-3} \text{ M}$; \blacktriangle $[\text{Cu}(\text{I})] = 2.50 \times 10^{-4} \text{ M}$, $[\text{O}_2] = 1.00 \times 10^{-3} \text{ M}$; \square $[\text{Cu}(\text{I})] = 7.33 \times 10^{-4} \text{ M}$, $[\text{O}_2] = 1.00 \times 10^{-3} \text{ M}$; \circ $[\text{Cu}(\text{I})] = 8.97 \times 10^{-5} \text{ M}$, $[\text{O}_2] = 4.09 \times 10^{-4} \text{ M}$; L = Me₄apme: $-$ $[\text{Cu}(\text{I})] = 2.60 \times 10^{-4} \text{ M}$, $[\text{O}_2] = 4.40 \times 10^{-3} \text{ M}$; $*$ $[\text{Cu}(\text{I})] = 2.70 \times 10^{-4} \text{ M}$, $[\text{O}_2] = 1.10 \times 10^{-3} \text{ M}$; $+$ $[\text{Cu}(\text{I})] = 7.82 \times 10^{-4} \text{ M}$, $[\text{O}_2] = 1.10 \times 10^{-3} \text{ M}$; \times $[\text{Cu}(\text{I})] = 7.45 \times 10^{-4} \text{ M}$, $[\text{O}_2] = 4.40 \times 10^{-3} \text{ M}$

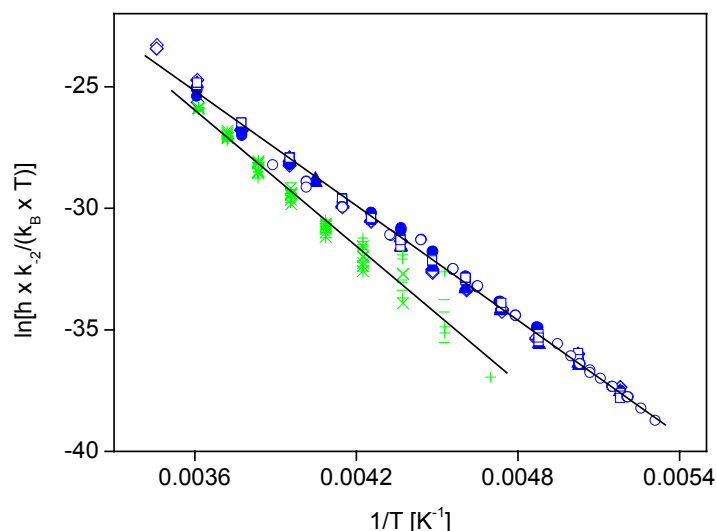


Figure 3.2.8: Eyring plots for k_2 pertaining to the formation of $[(\text{LCu})_2(\text{O}_2)]^{2+}$ in EtCN. k_B : Boltzman constant; h : Planck constant; L = Me₂uns-penp: \diamond $[\text{Cu(I)}] = 2.47 \times 10^{-4}$ M $[\text{O}_2] = 4.40 \times 10^{-3}$ M; \bullet $[\text{Cu(I)}] = 7.48 \times 10^{-4}$ M, $[\text{O}_2] = 4.40 \times 10^{-3}$ M; \blacktriangle $[\text{Cu(I)}] = 2.50 \times 10^{-4}$ M, $[\text{O}_2] = 1.00 \times 10^{-3}$ M; \square $[\text{Cu(I)}] = 7.33 \times 10^{-4}$ M, $[\text{O}_2] = 1.00 \times 10^{-3}$ M; \circ $[\text{Cu(I)}] = 8.97 \times 10^{-5}$ M, $[\text{O}_2] = 4.09 \times 10^{-4}$ M; L = Me₄apme: $-$ $[\text{Cu(I)}] = 2.60 \times 10^{-4}$ M, $[\text{O}_2] = 4.40 \times 10^{-3}$ M; $*$ $[\text{Cu(I)}] = 2.70 \times 10^{-4}$ M, $[\text{O}_2] = 1.10 \times 10^{-3}$ M; $+$ $[\text{Cu(I)}] = 7.82 \times 10^{-4}$ M, $[\text{O}_2] = 1.10 \times 10^{-3}$ M; \times $[\text{Cu(I)}] = 7.45 \times 10^{-4}$ M, $[\text{O}_2] = 4.40 \times 10^{-3}$ M

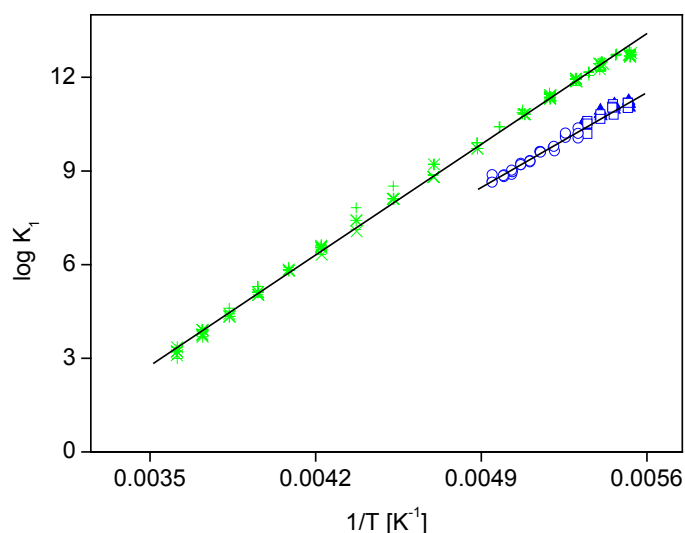


Figure 3.2.9: van't Hoff plots for K_1 pertaining to the formation of $[\text{LCu}(\text{O}_2)]^+$ from $[\text{LCu}(\text{EtCN})]^+$ in EtCN. L = Me₂uns-penp: \blacktriangle $[\text{Cu(I)}] = 2.50 \times 10^{-4}$ M, $[\text{O}_2] = 1.00 \times 10^{-3}$ M; \square $[\text{Cu(I)}] = 7.33 \times 10^{-4}$ M, $[\text{O}_2] = 1.00 \times 10^{-3}$ M; \circ $[\text{Cu(I)}] = 8.97 \times 10^{-5}$ M, $[\text{O}_2] = 4.09 \times 10^{-4}$ M; L = Me₄apme: $-$ $[\text{Cu(I)}] = 2.60 \times 10^{-4}$ M, $[\text{O}_2] = 4.40 \times 10^{-3}$ M; $*$ $[\text{Cu(I)}] = 2.70 \times 10^{-4}$ M, $[\text{O}_2] = 1.10 \times 10^{-3}$ M; $+$ $[\text{Cu(I)}] = 7.82 \times 10^{-4}$ M, $[\text{O}_2] = 1.10 \times 10^{-3}$ M; \times $[\text{Cu(I)}] = 7.45 \times 10^{-4}$ M, $[\text{O}_2] = 4.40 \times 10^{-3}$ M

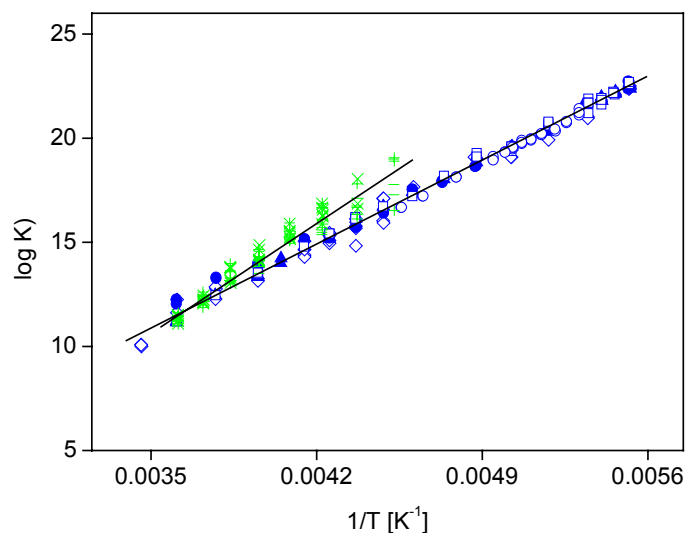


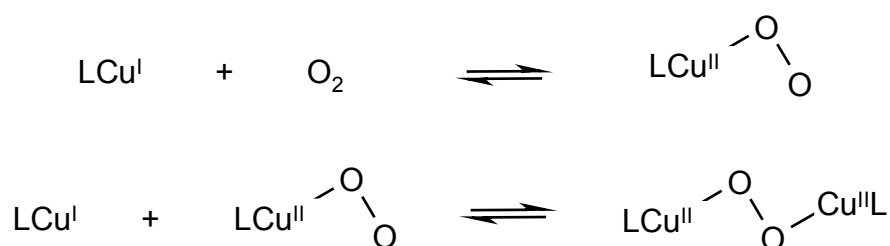
Figure 3.2.10: van't Hoff plots for K_2 pertaining to the formation of $[(\text{LCu})_2(\text{O}_2)]^{2+}$ in EtCN. L = Me₂uns-penp: \diamond $[\text{Cu}(\text{I})] = 2.47 \times 10^{-4} \text{ M}$, $[\text{O}_2] = 4.40 \times 10^{-3} \text{ M}$; \bullet $[\text{Cu}(\text{I})] = 7.48 \times 10^{-4} \text{ M}$, $[\text{O}_2] = 4.40 \times 10^{-3} \text{ M}$; \blacktriangle $[\text{Cu}(\text{I})] = 2.50 \times 10^{-4} \text{ M}$, $[\text{O}_2] = 1.00 \times 10^{-3} \text{ M}$; \square $[\text{Cu}(\text{I})] = 7.33 \times 10^{-4} \text{ M}$, $[\text{O}_2] = 1.00 \times 10^{-3} \text{ M}$; \circ $[\text{Cu}(\text{I})] = 8.97 \times 10^{-5} \text{ M}$, $[\text{O}_2] = 4.09 \times 10^{-4} \text{ M}$; L = Me₄apme: $-$ $[\text{Cu}(\text{I})] = 2.60 \times 10^{-4} \text{ M}$, $[\text{O}_2] = 4.40 \times 10^{-3} \text{ M}$; $*$ $[\text{Cu}(\text{I})] = 2.70 \times 10^{-4} \text{ M}$, $[\text{O}_2] = 1.10 \times 10^{-3} \text{ M}$; $+$ $[\text{Cu}(\text{I})] = 7.82 \times 10^{-4} \text{ M}$, $[\text{O}_2] = 1.10 \times 10^{-3} \text{ M}$; \times $[\text{Cu}(\text{I})] = 7.45 \times 10^{-4} \text{ M}$, $[\text{O}_2] = 4.40 \times 10^{-3} \text{ M}$

3.3 Extreme Stabilization of Copper Peroxo Complexes in the Solid State by Anion Encapsulation

This work is ready for submission to *Chemical Communications*.

Christian Würtele, Ole Sander, Felix Tuczek and Siegfried Schindler

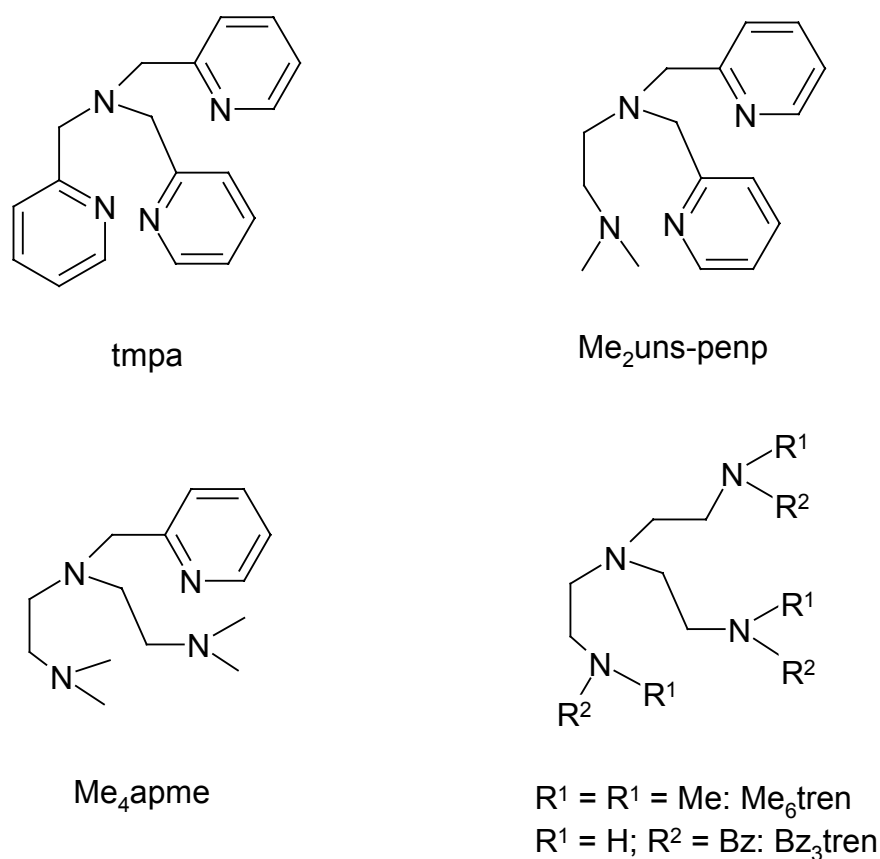
The interaction of copper(I) complexes with dioxygen has been studied intensively during the last 30 years in regard to the possible application of such compounds for the selective catalytic oxidation of organic substrates by air.^[6, 7, 30] Monooxygenases that contain copper ions in their active sites (e. g. tyrosinase or α -hydroxylating monooxygenase (PHM)) show selective hydroxylation reactions of organic substrates and thus created high interest in modeling the reactivity of these enzymes using low molecular weight copper complexes. It is well known that different copper "dioxygen adduct" complexes can form during the interaction of copper(I) compounds with dioxygen (Scheme 3.3.1, only the reaction pathways that are relevant for this paper are shown). However, so far it is not really clear which of these complexes are the active species in such oxidation processes. Only recently the initially formed end-on "dioxygen adduct complex" has been structurally characterized in PHM and shortly afterwards some of us obtained the same structural unit in $[\text{Cu}(\text{TMG}_3\text{tren})\text{O}_2]^+$ using tris(tetramethylguanidino)tren (TMG₃tren) as ligand.^[11, 38, 109]



Scheme 3.31: End-on copper superoxo and peroxo complexes.

Usually such end-on superoxo complexes cannot be isolated because they show a strong tendency to react further to the appropriate dinuclear peroxo complexes (Scheme 3.3.1). However, similar to the end-on superoxo species (as well as to other "dioxygen adduct" complexes) these dinuclear copper peroxo complexes can only be handled at low temperatures ($\sim -80^\circ\text{C}$).^[19, 26, 39] Synthetic efforts in the past,

sometimes assisted by theoretical calculations, have shown that it is possible to obtain copper peroxo complexes that persist for some time at room temperature by using specially designed ligands.^[110-112] Here it was possible to structurally characterize a dinuclear side-on peroxo complex, however this was not possible for the analogous end-on type shown in Scheme 3.3.1.^[112] For all of these complexes the increased stability was achieved by connecting mononuclear units to form a preorganized dinuclear system. In contrast, mononuclear copper complexes with tetradentate tripodal ligands (Scheme 3.3.2) only showed the formation of thermally very labile dinuclear copper complexes such as $[\text{Cu}_2(\text{tmpa})(\text{O}_2)](\text{PF}_6)_2$, the first crystallographically characterized copper peroxo complex.^[12, 19, 25, 26, 39] However, these complexes can be stabilized again much further if the mononuclear complexes are connected through an appropriate bridge.^[113, 114]



Scheme 3.3.2: Tetradentate tripodal ligands.

Previous findings by us and others demonstrated the importance of solvent effects for these oxidation reactions,^[25, 114] however more recently we realized that the “right” choice of anions seems to be extremely important as well. Using tetraphenylborate as anion first of all allowed us to obtain a quite stable copper(I) complex with Me₆tren

(Scheme 3.3.2) as ligand (the crystal structure and data of $[\text{Cu}(\text{Me}_6\text{tren})]\text{BPh}_4$ (**1**) are reported in the Supporting Material). This is in contrast to our previous report on the ClO_4^- or PF_6^- salts of this complex that were extremely labile towards disproportionation reactions.^[25]

To our great surprise this complex reacted in the solid state immediately with air to an extremely stable deep blue peroxo complex. This complex, $[\text{Cu}_2(\text{Me}_6\text{tren})(\text{O}_2)](\text{BPh}_4)_2$ (**2**), could be structurally characterized and the molecular structure of its cation is presented in Figure 3.3.1. It is quite similar to the only two other known peroxo complexes of this type, $[\text{Cu}_2(\text{tmpa})(\text{O}_2)](\text{PF}_6)_2$ and $[\text{Cu}_2(\text{Bz}_3\text{tren})(\text{O}_2)](\text{BPh}_4)_2$.^[12, 21, 22] However, crystal packing is quite different for these complexes and explains well the observed different stabilities discussed below. The cation of **2** is completely shielded by 8 BPh_4^- anions (Figure 3.3.2) and this encapsulation completely suppresses any further reactions in contrast to the accessible cation of $[\text{Cu}_2(\text{tmpa})(\text{O}_2)](\text{PF}_6)_2$.

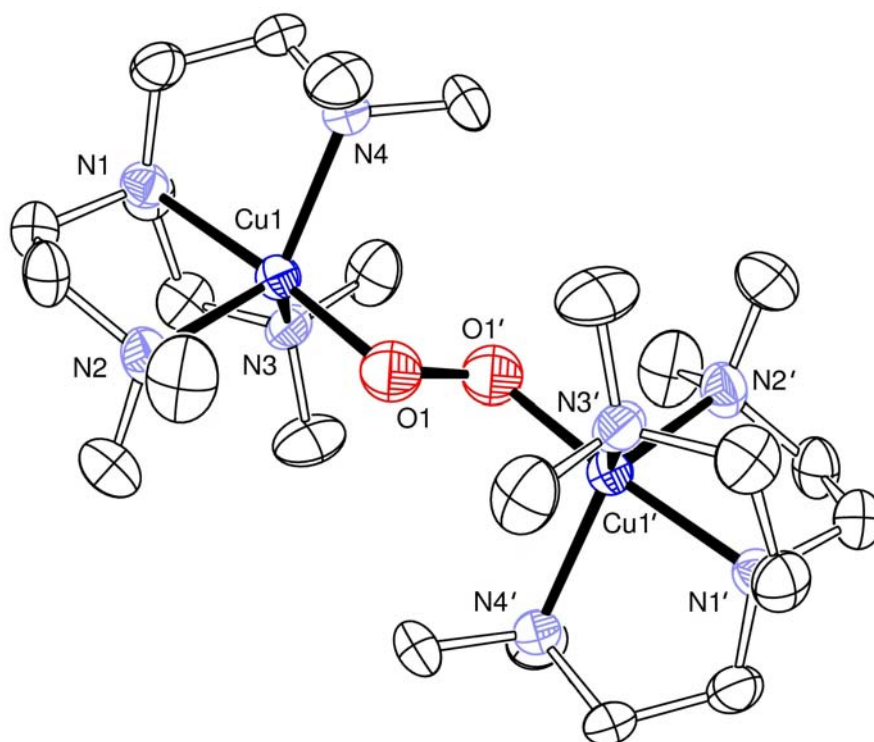


Figure 3.3.1: Molecular structure of $[\text{Cu}_2(\text{Me}_6\text{tren})_2(\text{O}_2)]^{2+}$. ORTEP plot with thermal ellipsoids set at 50 % probability (hydrogen atoms, acetone solvent molecules and anions are not shown). Selected bond lengths [Å] and angles [°]: O1-O1' 1.368(9), Cu1-O1 1.907(5), Cu1-Cu1' 4.590; Cu1-O1-O1' 116.5(5).

Furthermore, a comparison of the crystal structures of complexes **1** and **2** shows that it is easy for the copper ions to rearrange during the reaction with dioxygen to form the peroxo complex, thus explaining the facile oxidation in the solid state.

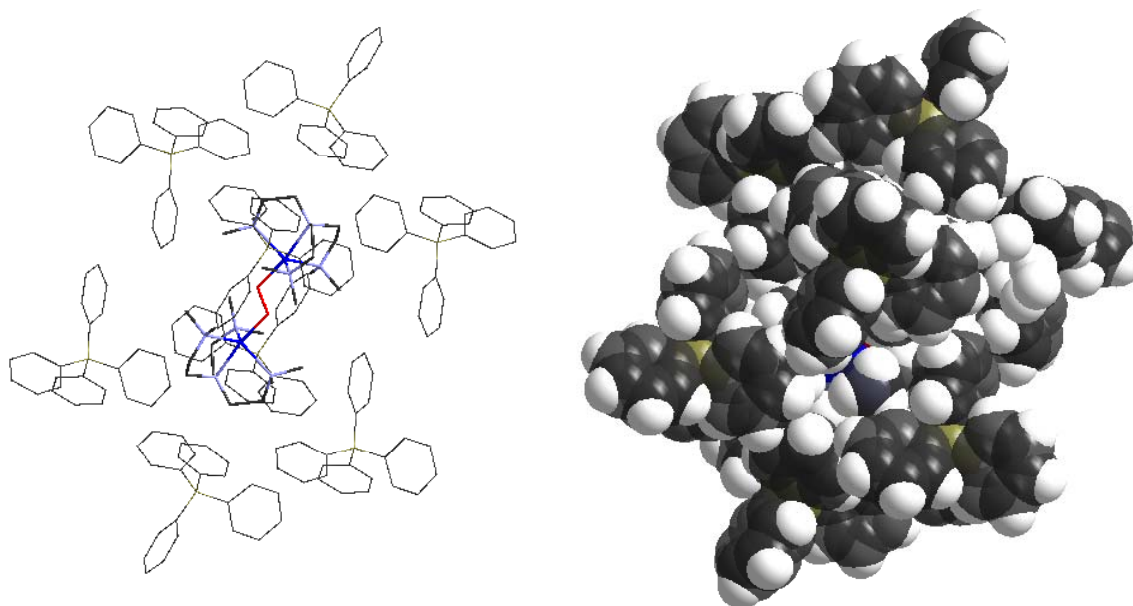


Figure 3.3.2: Anion shielding in **2**.

Peroxo complexes with the related ligands (Figure 3.3.2) tmpa, Me₂uns-penp and Me₄apme and tetraphenylborate as anion can be prepared in a similar way either by reactions in the solid state or by precipitation of these compounds from solution. All four peroxo complexes obtained in that way can be stored openly in air at room temperature for at least several months and the four samples are shown in Figure 4. Furthermore, it is even possible to heat these samples above 70 °C without any observable decomposition (see Supporting Information).



Figure 3.3.3: Photograph of the four peroxo complexes in vials under ambient conditions.

At this point it is interesting to note that in contrast to our findings it was not possible to stabilize the previously reported peroxo complex $[\text{Cu}_2(\text{Bz}_3\text{tren})(\text{O}_2)](\text{BPh}_4)_2$ ^[21, 22] in the same way. Again a closer look at the crystal structure explains this because due to the sterically demanding benzyl groups the same shielding/encapsulation of the peroxide cation for the ligands tmpa, $\text{Me}_2\text{uns-penp}$, Me_4apme and Me_6tren cannot be achieved in this complex.

While the solid peroxo complexes turned out to be extremely stable they immediately showed decomposition once dissolved at room temperature in solvents such as acetone or propionitrile. However, using precooled solvents and cooling the sample as well to $-80\text{ }^\circ\text{C}$, solutions of the peroxo complexes were stable and showed the same UV-vis spectra reported previously for these compounds (Table 1).^[6, 19, 21, 26, 39, 108]

Table 3.3.1: Spectroscopic Data: [a] Measurement at $-80\text{ }^\circ\text{C}$. [b] Measurement at room temperature with 568.2 nm laser excitation

Complexes	UV-vis bands ^[a]	$\nu(\text{O-O})$ ^[b]	$\nu(\text{Cu-O})$ ^[b]
	λ_{max} [nm] (acetone)	$\tilde{\nu}$ [cm^{-1}] (solid state)	$\tilde{\nu}$ [cm^{-1}] (solid state)
$[\text{Cu}_2(\text{Me}_6\text{tren})_2(\text{O}_2)]^{2+}$	558	820, 809	585, 541
$[\text{Cu}_2(\text{Me}_4\text{apme})_2(\text{O}_2)]^{2+}$	532	820, 809	580, 563
$[\text{Cu}_2(\text{Me}_2\text{uns-penp})_2(\text{O}_2)]^{2+}$	522	839, 819	561
$[\text{Cu}_2(\text{tmpa})_2(\text{O}_2)]^{2+}$	518	825	561

Additionally we measured resonance Raman spectra of all four solids and confirmed data obtained previously for some of these compounds in solution or in the solid state (Fig. 3.3.4 and Table 3.3.1).^[6, 21, 39, 108]

For all systems the O-O stretch appears to be split into two or more peaks. This is in contrast for $[\text{Cu}_2(\text{tmpa})(\text{O}_2)](\text{PF}_6)_2$ where only one O-O and one Cu-O stretch were observed.^[108] However, splitting of the O-O stretch into multiple peaks has been described previously in resonance Raman spectra of $[\text{Cu}_2(\text{Me}_6\text{tren})(\text{O}_2)](\text{ClO}_4)_2$ recorded in solution and the solid state.^[21, 22, 26] Furthermore, multiple splitting has

been observed for related copper peroxo complexes and has been assigned to the occurrence of different isomers.^[21, 22, 42, 115]

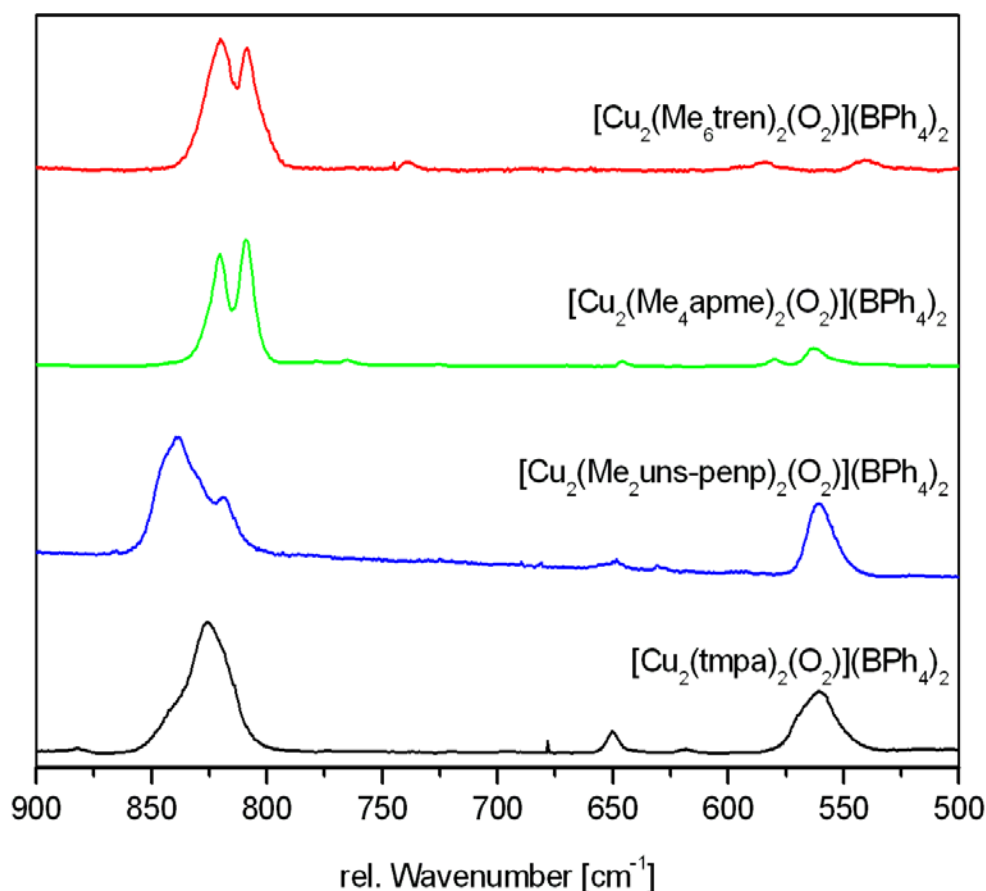


Figure 3.2.4: Solid state resonance Raman spectra of the four peroxo complexes with 568.2 nm laser excitation.

We could demonstrate with our work that peroxo complexes that have been regarded previously as extremely labile at high temperatures could be stabilized dramatically in the solid state. Because these complexes can be regarded as hydrogen peroxide in which the hydrogen atoms have been substituted by copper coordination units they might become quite useful in further studies on selective oxidation reactions. Furthermore, the fast solid state reactions of **1** with dioxygen might be applied for dioxygen detection/leakage in inert systems. It is very clear from our reported results that a statement per se on the thermal stability of such copper dioxygen adduct complexes is incorrect and only can be given in regard to the exact conditions applied.

3.3.1 Experimental Section

The synthesis, handling and spectroscopic characterization of the complexes discussed herein was performed according to published procedures,^[12, 21, 25, 39, 108] with slight modifications (see Supporting Information). CCDC 688486 (**1**) and CCDC 688485 (**2**) contains the supplementary crystallographic data for this paper. These data can be obtained free of charge from The Cambridge Crystallographic Data Centre via www.ccdc.cam.ac.uk/data_request/cif.

3.4 Supporting information for chapter 3.3 and continuing research for the peroxo complexes described

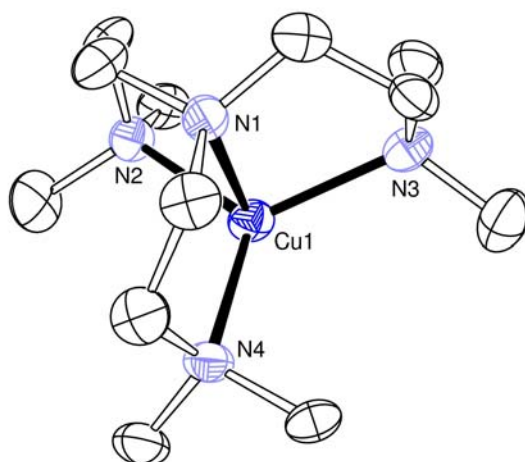


Figure 3.4.1: The molecular structure of $[\text{Cu}(\text{Me}_6\text{tren})]\text{BPh}_4$. ORTEP plot with thermal ellipsoids set at 50 % probability (hydrogen atoms and tetraphenylborate anion are not shown). Selected bond lengths [Å] and angles [°]: Cu1-N1 2.153(4), Cu1-N2 2.105(4), Cu1-N3 2.115(5), Cu1-N4 2.106(4); N1-Cu1-N2 85.96(17), N2-Cu1-N3 119.16(17), N2-Cu1-N4 119.36(17).

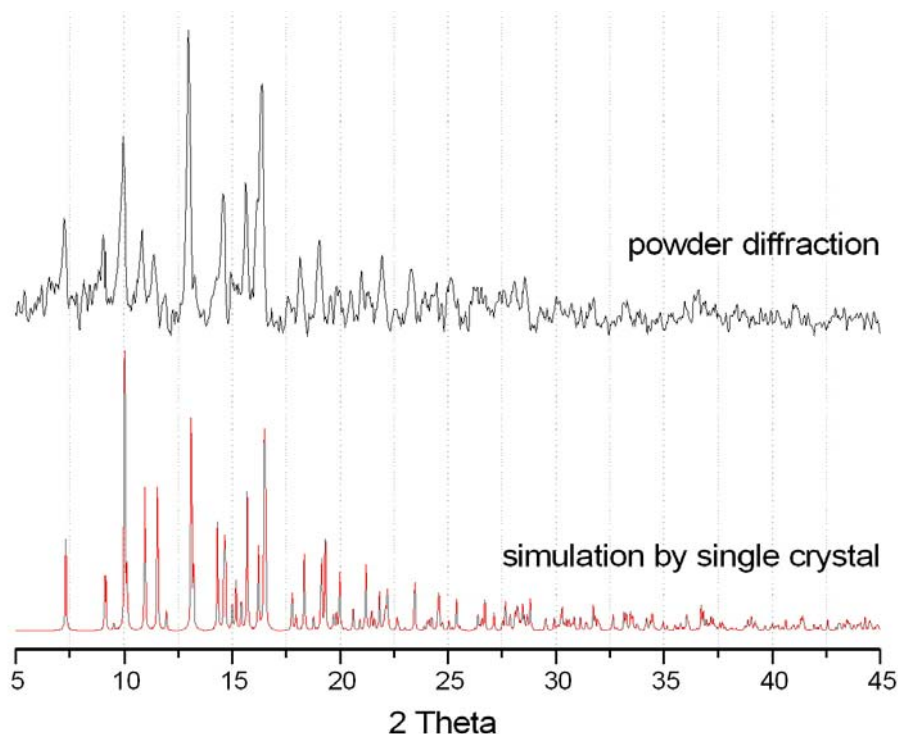


Figure 3.4.2: Powder diffraction of $[\text{Cu}(\text{Me}_6\text{tren})]\text{BPh}_4$ (black spectra). The red spectra shows the powder simulation by using single crystal data of $[\text{Cu}(\text{Me}_6\text{tren})]\text{BPh}_4$.

3.4.1 Synthesis of $[\text{Cu}_2(\text{L})_2(\text{O}_2)](\text{BPh}_4)_2$

(L = Me₆tren, Me₄apme, Me₂uns-penp and tmpa)

Under the inert atmosphere of a glove box $[\text{Cu}(\text{L})]\text{BPh}_4$ was dissolved in a very small amount of acetone, cooled to -80 °C and then oxidized with pure, dry dioxygen for 5 min. To the deep blue solution was added a large amount of precooled diethyl ether, then it was kept at the same temperature for 10 min to precipitate the according peroxo complex as a blue powder. The solution was filtered at -80 °C, the precipitate was washed with precooled diethyl ether and dried in a stream of dioxygen at approximate -40 °C. The dry product can be warmed to room temperature without any problems in regard to decomposition.

3.4.2 Synthesis of $[\text{Cu}_2(\text{L})_2(\text{O}_2)](\text{BPh}_4)_2$ in the solid state

(L = Me₆tren, Me₄apme, Me₂uns-penp and tmpa)

Under the inert atmosphere of a glove box $[\text{Cu}(\text{L})]\text{BPh}_4$ in the solid state was placed in a small vessel that was closed with a rubber septum. Outside of the glove box, the copper(I) complex was oxidized with pure dioxygen or air with a needle through the septum. Within a few seconds, the colorless or yellow copper(I) complexes formed the intensive blue peroxo complexes (Figure 3.4.3). In case of the ligands Me₂uns-penp and tmpa it is necessary to use a mortar for the oxidation reaction.

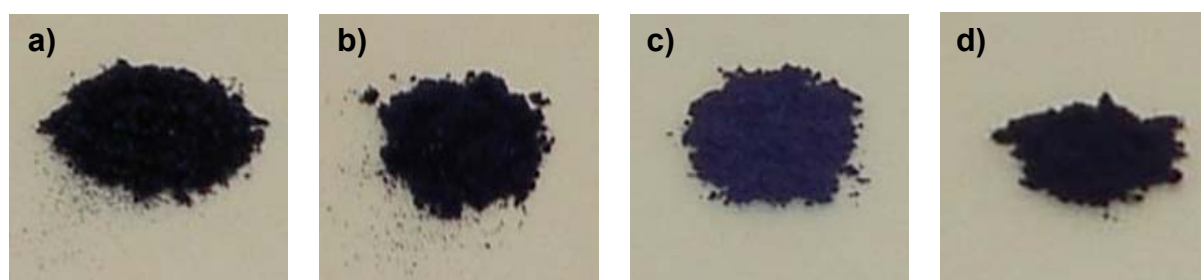


Figure 3.4.3: The photographs show the four copper(II) peroxo complexes stable at room temperature. a) $[\text{Cu}_2(\text{Me}_6\text{tren})_2(\text{O}_2)](\text{BPh}_4)_2$, b) $[\text{Cu}_2(\text{Me}_4\text{apme})_2(\text{O}_2)](\text{BPh}_4)_2$, c) $[\text{Cu}_2(\text{Me}_2\text{uns-penp})_2(\text{O}_2)](\text{BPh}_4)_2$, d) $[\text{Cu}_2(\text{tmpa})_2(\text{O}_2)](\text{BPh}_4)_2$.

3.4.3 Synthesis of $[\text{Cu}_2(\text{Me}_6\text{tren})_2(\text{O}_2)](\text{BPh}_4)_2 \cdot 3 (\text{CH}_3)_2\text{CO}$ as single crystals

Under the inert atmosphere of a glove box $[\text{Cu}(\text{Me}_6\text{tren})]\text{BPh}_4$ was dissolved in a very small amount of acetone, cooled to -80 °C and then oxidized with pure, dry dioxygen gas for 5 min. The deep blue solution obtained was kept at the same temperature for

three days leading to intensively blue colored crystals of the end-on peroxo complex $[\text{Cu}_2(\text{Me}_6\text{tren})_2(\text{O}_2)](\text{BPh}_4)_2 \cdot 3 (\text{CH}_3)_2\text{CO}$ that were found suitable for X-ray structural characterization. (Figure 3.3.1)

3.4.4 Thermal analysis of $[\text{Cu}_2(\text{L})_2(\text{O}_2)](\text{BPh}_4)_2$ in the solid state

(L = Me₆tren, Me₄apme, Me₂uns-penp and tmpa)

For determination of the pyrolysis of the peroxo complexes thermal gravimetry (TG) and differential thermal analysis (DTA) were supplied. The TG results showed for all four complexes a first mass loss between 78 °C and 118 °C, followed by some further mass losses at higher temperatures. Differential thermal analysis showed, the first mass loss is accompanied by an exothermic reaction at the decomposition temperature. This exothermic reaction must be an auto oxidation, because the measurements were performed under argon and the complexes therefore provide the oxygen.

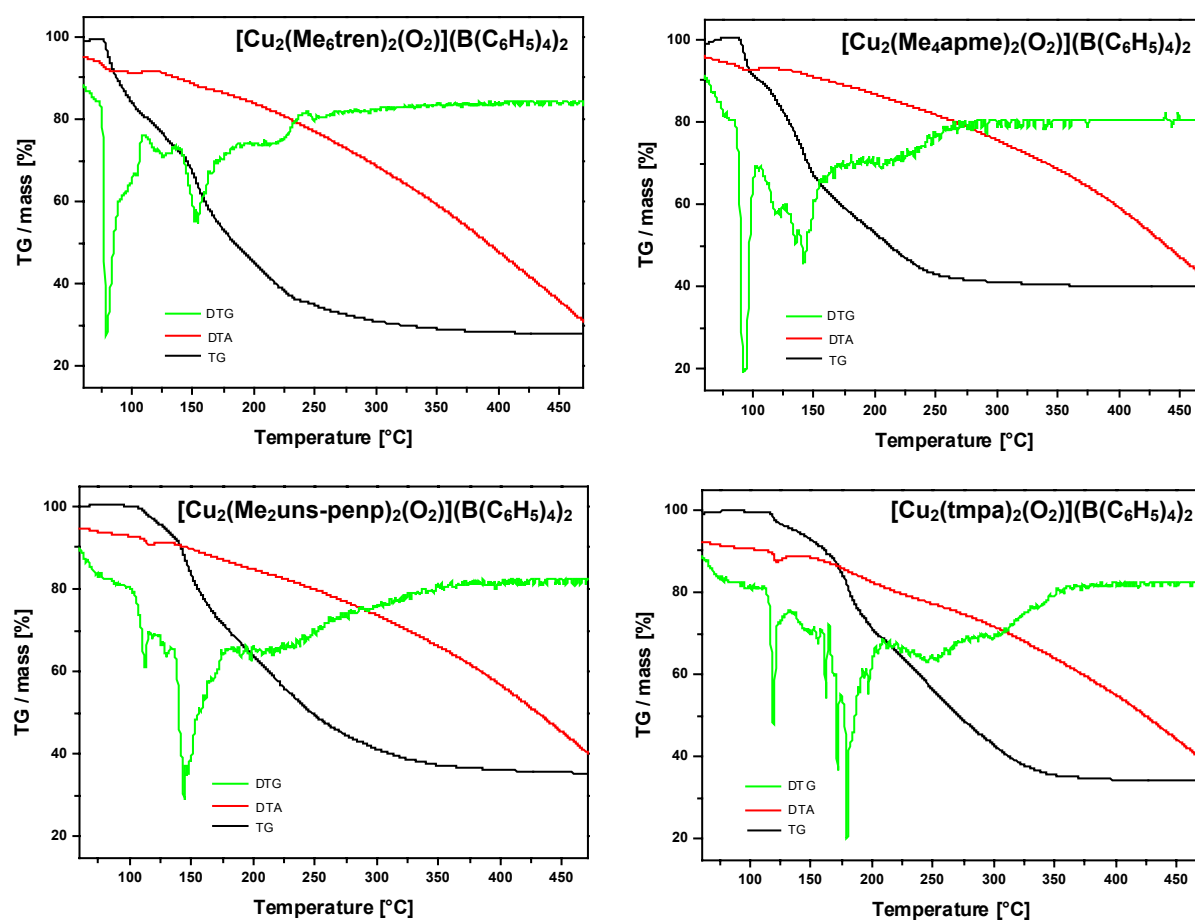


Figure 3.4.4: Thermal analysis of the four copper peroxo complexes. The diagrams include the curves for thermal gravimetry (TG), differential thermal gravimetry (DTG) and differential thermal analysis (DTA).

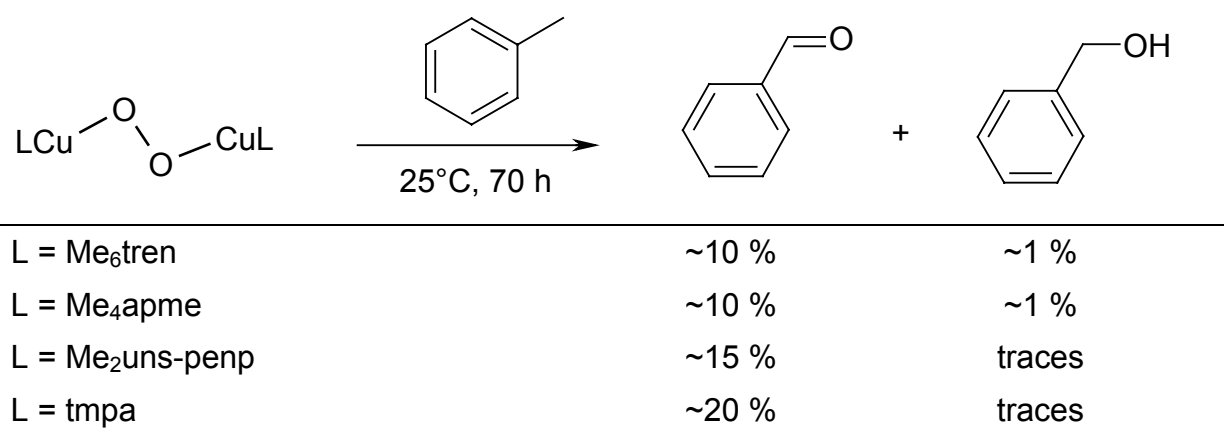
The TG, DTG and DTA experiments clearly demonstrated a ligand effect (see table 3.4.1). Tmpa, a ligand with three aromatic N-donor atoms and a decomposition temperature at 118 °C is significant more stable than Me₆tren, a pure aliphatic N-donor ligand with a decomposition temperature at 78 °C.

Table 3.4.1: Decomposition temperature of copper peroxo complexes stable at room temperature

Complex	Decomposition temperature
[Cu ₂ (Me ₆ tren) ₂ (O ₂)](BPh ₄) ₂	78 °C
[Cu ₂ (Me ₄ apme) ₂ (O ₂)](BPh ₄) ₂	91 °C
[Cu ₂ (Me ₂ uns-penp) ₂ (O ₂)](BPh ₄) ₂	110 °C
[Cu ₂ (tmpa) ₂ (O ₂)](BPh ₄) ₂	118 °C

3.4.5 Oxidation of toluene by using solid state copper peroxo complexes

The solid state character and the stability at higher temperatures open a new way for catalytic oxidation reactions using these compounds. In contrast to copper peroxo complexes used previously, these four complexes are easily prepared and handled. First reactivity studies of these complexes showed a successful oxidation of toluene at the benzylic position according to the following equation.



Different amounts of benzaldehyde and benzyl alcohol demonstrate an effect of the used ligands. Ligands with predominant aliphatic N-donor atoms (Me₆tren, Me₄apme) led to benzaldehyde as the main product, however benzyl alcohol was obtained as well. For the more aromatic N-donor atoms (Me₂uns-penp, tmpa) benzyl alcohol was

observed only in traces and the formation of benzaldehyde is preferred and was obtained in higher yields. Benzoic acid as oxidation product is possible and was expected, however could not be detected so far.

3.4.6 Reaction of $[\text{Cu}_2(\text{Me}_6\text{tren})_2(\text{O}_2)](\text{B}(\text{C}_6\text{H}_5)_4)_2$ with toluene

In a small flask, $[\text{Cu}_2(\text{Me}_6\text{tren})_2(\text{O}_2)](\text{B}(\text{C}_6\text{H}_5)_4)_2$ (20.0 mg, 0.0159 mmol) was placed and toluene (2.0 ml) was added. The cloudy mixture was stirred at room temperature. After being stirred for 70 h, the mixture was filtered and the solvent was analyzed by using GC-MS instrumentation. Yield: approximate 10 % benzaldehyde and approximate 1 % of benzyl alcohol.

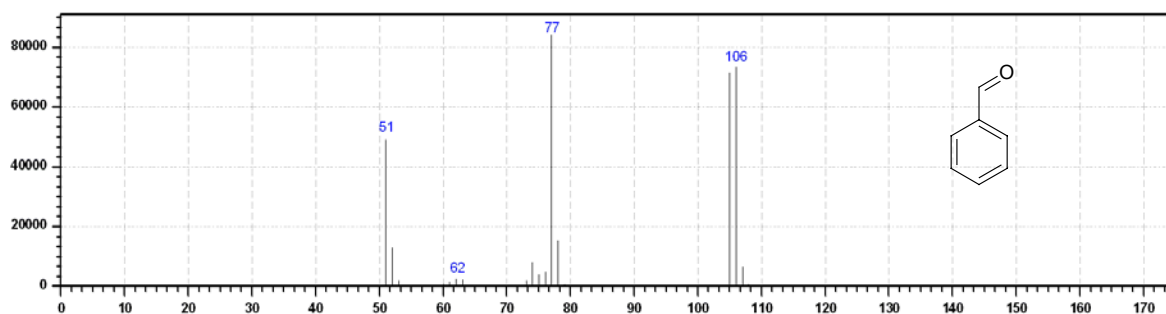


Figure 3.4.5: GC-MS spectrum of benzaldehyde ($m/z = 106$), from the reaction of $[\text{Cu}_2(\text{Me}_6\text{tren})_2(\text{O}_2)](\text{B}(\text{C}_6\text{H}_5)_4)_2$ with toluene.

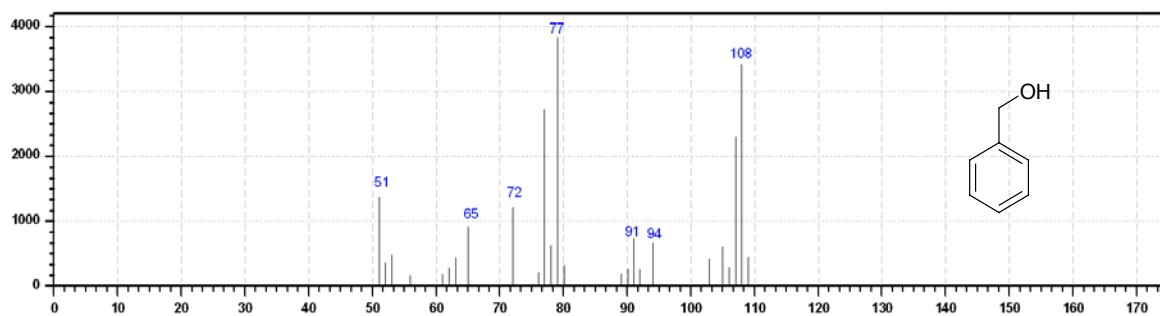


Figure 3.4.6: GC-MS spectrum of benzyl alcohol ($m/z = 108$), from the reaction of $[\text{Cu}_2(\text{Me}_6\text{tren})_2(\text{O}_2)](\text{B}(\text{C}_6\text{H}_5)_4)_2$ with toluene.

3.4.7 Reaction of $[\text{Cu}_2(\text{Me}_4\text{apme})_2(\text{O}_2)](\text{B}(\text{C}_6\text{H}_5)_4)_2$ with toluene

In a small flask, $[\text{Cu}_2(\text{Me}_4\text{apme})_2(\text{O}_2)](\text{B}(\text{C}_6\text{H}_5)_4)_2$ (20.0 mg, 0.0154 mmol) was placed and toluene (2.0 ml) was added. The cloudy mixture was stirred at room temperature. After being stirred for 70 h, the mixture was filtered and the solvent was analyzed by using GC-MS instrumentation. Yield: approximate 10 % benzaldehyde and approximate 1 % of benzyl alcohol.

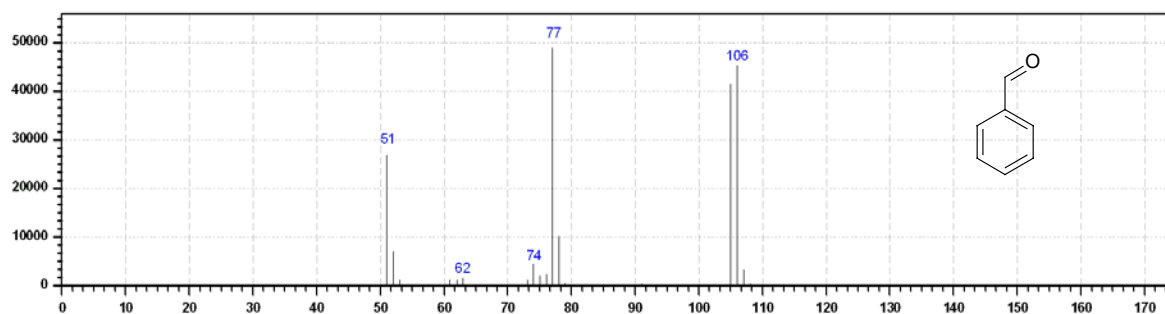


Figure 3.4.7: GC-MS spectrum of benzaldehyde (m/z = 106), from the reaction of $[\text{Cu}_2(\text{Me}_4\text{apme})_2(\text{O}_2)](\text{B}(\text{C}_6\text{H}_5)_4)_2$ with toluene.

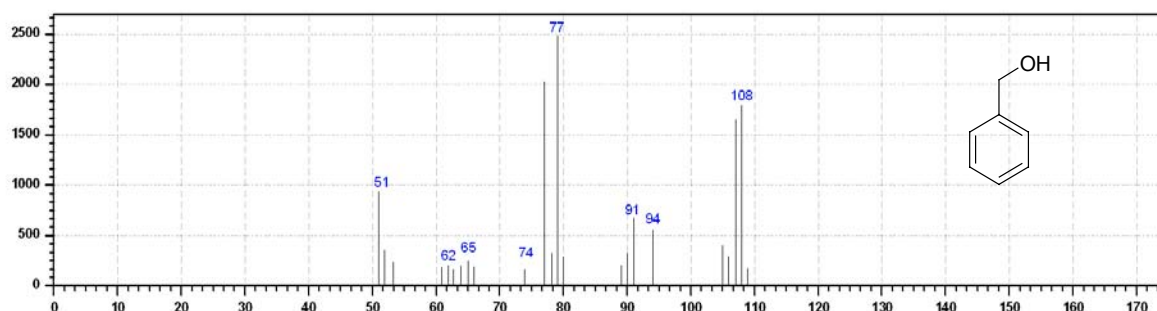


Figure 3.4.8: GC-MS spectrum of benzyl alcohol (m/z = 108), from the reaction of $[\text{Cu}_2(\text{Me}_4\text{apme})_2(\text{O}_2)](\text{B}(\text{C}_6\text{H}_5)_4)_2$ with toluene.

3.4.8 Reaction of $[\text{Cu}_2(\text{Me}_2\text{uns-penp})_2(\text{O}_2)](\text{B}(\text{C}_6\text{H}_5)_4)_2$ with toluene

In a small flask, $[\text{Cu}_2(\text{Me}_2\text{uns-penp})_2(\text{O}_2)](\text{B}(\text{C}_6\text{H}_5)_4)_2$ (20.0 mg, 0.0149 mmol) was placed and toluene (2.0 ml) was added. The cloudy mixture was stirred at room temperature. After being stirred for 70 h, the mixture was filtered and the solvent was analyzed by using GC-MS instrumentation. Yield: approximate 15 % benzaldehyde and traces of benzyl alcohol.

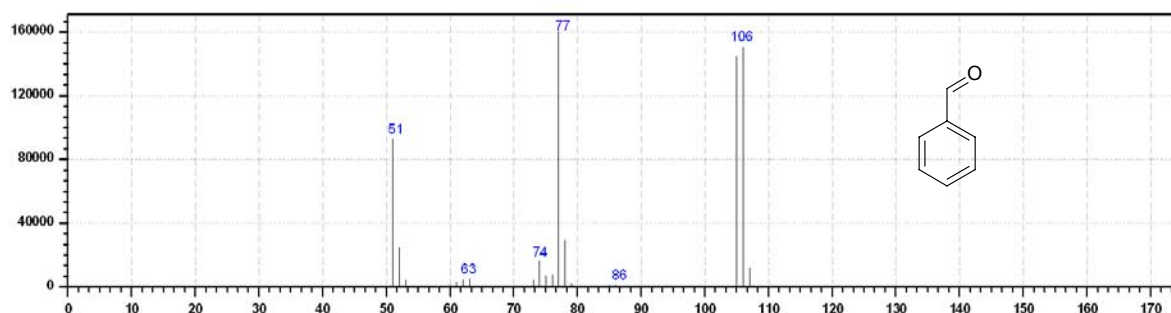


Figure 3.4.9: GC-MS spectrum of benzaldehyde (m/z = 106), from the reaction of $[\text{Cu}_2(\text{Me}_2\text{uns-penp})_2(\text{O}_2)](\text{B}(\text{C}_6\text{H}_5)_4)_2$ with toluene.

3.4.9 Reaction of $[\text{Cu}_2(\text{tmpa})_2(\text{O}_2)](\text{B}(\text{C}_6\text{H}_5)_4)_2$ with toluene

In a small flask, $[\text{Cu}_2(\text{tmpa})_2(\text{O}_2)](\text{B}(\text{C}_6\text{H}_5)_4)_2$ (20.0 mg, 0.0145 mmol) was placed and toluene (2.0 ml) was added. The cloudy mixture was stirred at room temperature. After being stirred for 70 h, the mixture was filtered and the solvent was analyzed by using GC-MS instrumentation. Yield: approximate 20 % benzaldehyde and traces of benzyl alcohol.

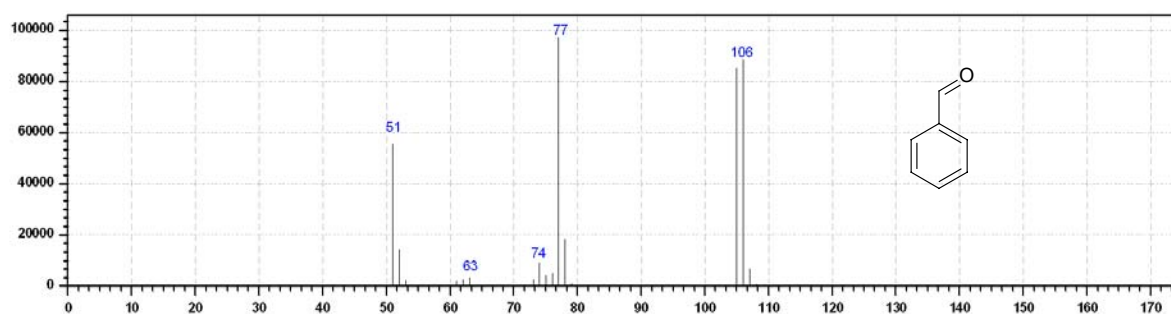


Figure 3.4.10: GC-MS spectrum of benzaldehyde ($m/z = 106$), from the reaction of $[\text{Cu}_2(\text{tmpa})_2(\text{O}_2)](\text{B}(\text{C}_6\text{H}_5)_4)_2$ with toluene.

Chapter 4 – Materials, Methods and Crystallography

4.1 Materials and Methods

4.1.1 Chemicals and solvents

All chemicals used were of p.a. quality and were purchased from either Acros, Aldrich, Fluka or Merck, if not mentioned otherwise. Solvents for air sensitive reaction were redistilled under Argon. The copper complexes $[\text{Cu}(\text{CH}_3\text{CN})_4]\text{X}$ ($\text{X} = \text{BF}_4^-$, PF_6^- , ClO_4^- , SbF_6^-) were prepared according to published procedures with slight modifications.^[116] The ligand TMG₃tren was prepared by Dr. Ekaterina Gaoutchenova, the ligand tmpa was prepared by Dipl.-Chem. Alexander Beitat.

4.1.2 Air sensitive compounds

Preparation and handling of air sensitive compounds were performed under an argon or nitrogen atmosphere. For reactions, handling and storing of these compounds either glove boxes from MBraun (equipped with water and dioxygen detectors) or standard Schlenk techniques were used.

4.1.3 Electrochemistry

All cyclic voltammetry experiments were performed at room temperature and under argon, with a Princeton BAS Model 263 instrumentation. A solution of 1.0 mmol/L Cu(I) complex and $[\text{NBu}_4]\text{BF}_4$ (0.1 mol/L) as electrolyte in acetone or acetonitrile was used. Electrodes employed were glassy carbon (working electrode), Ag/AgCl (reference electrode) and a platinum wire (auxiliary electrode). Ferrocene was used as an internal reference.

4.1.4 Elemental analysis

The elemental analyses were performed by Desert Analytics (Tucson, AZ). (The Johns Hopkins University Baltimore, USA)

4.1.5 EPR-spectroscopy

Electron paramagnetic resonance (EPR) spectra were recorded on a Bruker EMX spectrometer controlled with a Bruker ER 041 X G microwave bridge operating at X-band (~9.4 GHz). (The Johns Hopkins University Baltimore, USA).

4.1.6 ESI-MS-spectrometry

ESI mass spectra were acquired using a Finnigan LCQDeca ion-trap mass spectrometer equipped with an electrospray ionization source (Thermo Finnigan, San Jose, CA). For meta-stable species (as described below), samples were introduced from cold bath solution with a liquid-N₂ precooled plastic syringe, and quickly injected into the instrument sample port which feeds the instrument syringe pump operating at 10 µL/min via a silica capillary line. The heated capillary temperature was 250 °C and the spray voltage was 5 kV. (The Johns Hopkins University Baltimore, USA).

4.1.7 GC and GC-MS-spectrometry

The GC and the GC-MS measurements were performed using different instrumentation setups.

- All GC-MS experiments for the peroxo complexes was performed using a HP GL 6890 Chromatograph equipped with HP 5973 Mass Selective Detector. The GC-MS conditions for the product analysis were:
Injector Port Temperature: 250 °C; solvent delay: 4 min; Column Temperature: Initial Temperature: 60 °C (2 min); Gradient Rate: 13.5 °C/min (14 min); Final Temperature: 250 °C (5 min); Flow Rate: 80 ml/min.
- The GC-MS experiments for the superoxo complex were carried out and recorded using a Shimadzu GC-17A/GCMS0QP5050 Gas Chromatograph/Mass Spectrometer. The GC-MS atmosphere for the product analysis were:
Injector Port Temperature: 220 °C; Detector Temperature: 280 °C; Column Temperature: Initial Temperature: 120 °C; Initial Time: 2 min; Final Temperature: 250 °C, Final Time: 15 min, Gradient Rate: 10 °C/min; Flow Rate: 16 ml/min; Ionization voltage: 1.5 kV. (The Johns Hopkins University Baltimore, USA).

- GC experiments for the superoxo complex were carried out and recorded using a Hewlett-Packard 5890 Series II Gas Chromatograph. The GC atmosphere for the product analysis were:

Injector Port Temperature: 250 °C; Detector Temperature: 250 °C; Column Temperature: Initial Temperature: 120 °C; Initial Time: 2 min; Final Temperature: 250 °C, Final Time: 15 min, Gradient Rate: 30 °C/min; Flow Rate: 50 ml/min. (The Johns Hopkins University Baltimore, USA).

4.1.8 Low temperature IR-spectroscopy

All low temperature IR experiments were performed using a Nicolet 510 P FT-IR Spectrometer equipped with a low-temperature cell (RIEC) and CaF₂ windows (0.1 mm).

4.1.9 Low temperature Stopped-Flow studies

Rapid kinetic studies were performed using two variable-temperature stopped-flow units.

- Home-made stopped-flow unit with a 10 mm path length cell, combined with a TIDAS/NMC301-MMS/16 VIS/500-1 diode array spectrometer (J&M; 256 diodes, 300-1100 nm, 0.8 ms minimum sampling time.)
- Hi-Tech Scientific stopped-flow unit with a 2 mm path length cell, equipped with a TIDAS-16 HQ/UV-vis 512/16B diode array spectrometer (J&M, 507 diodes, 300-720 nm, 1.3 ms minimum sampling time.) (ETH Hönggerberg Zürich, Schweiz).

4.1.10 NMR-spectroscopy

The ¹H NMR spectra were recorded on a Bruker AM 400 spectrometer at 298 K in 5 mm NMR tubes. The chemical shifts (δ) were obtained in deuterated solutions by using TMS as an internal reference.

4.1.11 Resonance Raman spectroscopy

All Resonance Raman spectra were measured with a DILOR XY Raman spectrograph equipped with triple monochromator and diode array detector. A SPECTRA PHYSICS Ar/Kr mixed-gas laser was used for excitation. The spectra

were recorded with an excitation wavelength of 514.5 nm. (Christian Albrechts Universität Kiel)

4.1.12 Thermal analysis

All TG, DTG and DTA experiments were carried out and recorded using a Netzsch Luxx STA 409 PC equipped with a Netzsch Aëolos QMS 403C. 5-10 mg material was treated isothermal for 20 min at 30 °C under Argon and then heated up to 500 °C by using a gradient of 5 K/min. Al_2O_3 was used as reference for DTA measurements.

4.1.13 UV-vis spectroscopy

UV-vis spectra were recorded with different spectrophotometers.

- Agilent 8453 UV-visible Spectroscopy System equipped with a diode array detector. Low temperature measurements were performed in a four-window quartz Dewar filled with cold MeOH and a Schlenk cuvette made from quartz glass (1 cm path length).
- Cary-50 Bio spectrophotometer equipped with a fiber optic coupler (Varian) and a fiber optic dip probe (Hellma: 661.302-QX-UV-2mm-for-low-temperature). (The Johns Hopkins University Baltimore, USA).
- Hewlett-Packard Model 8453A diode array spectrophotometer equipped with a two-window quartz H.S. Martin Dewar filled with cold MeOH (25 °C to -85 °C) maintained and controlled by a Neslab VLT-95 low temp circulator is attached to the HP spectrophotometer. Spectrophotometer cells used were made by Quark Glass with column and pressure/vacuum side stopcock and 2 mm path length. (The Johns Hopkins University Baltimore, USA).

4.2 Crystallography

The powder diffractometry was performed on a STOE Stadi-P diffractometer equipped with an image plate position sensitive detector (IP-PSD) and Ge-monochromator using Cu-K α radiation ($\lambda = 1.54056 \text{ \AA}$). (Christian Albrechts Universität Kiel)

The single crystal X-ray diffraction studies were performed with the following equipment:

- A STOE IPDS-diffractometer equipped with a low temperature system (Karlsruher Glastechnisches Werk), a graphite monochromator and IP detector system. Mo-K α radiation ($\lambda = 0.71069 \text{ \AA}$) was used. The frames were integrated with the STOE software package. No absorption corrections were applied.
- A Siemens SMART CCD 1000 diffractometer equipped with a graphite monochromator and a CCD detector. Mo-K α radiation ($\lambda = 0.71073 \text{ \AA}$) was used. The collected reflections were corrected for absorption effects. (SADABS, *Siemens Area Detector Absorption Correction*, Siemens). (Forschungszentrum Karlsruhe ITC-CPV)
- A STOE IPDS 2 -diffractometer equipped with a graphite monochromator and IP detector system. Mo-K α radiation ($\lambda = 0.71069 \text{ \AA}$) was used. The frames were integrated with the STOE X software package. (Philipps-Universität Marburg)
- Oxford Diffraction Xcalibur3 system equipped with a graphite monochromator and an Enhance (Mo) X-ray Source ($\lambda = 0.71073 \text{ \AA}$) and a CCD detector. The frames were integrated with the Oxford Diffraction *CrysAlisRED* software package. (The Johns Hopkins University Baltimore, USA)

All structures were solved by Patterson or Direct Methods and refined by using full-matrix least squares in SHELXS86-97/SHELXL97^[95] or by using the SHELXTL software package.^[117]

Table 4.2.1a: Crystal data and structure refinement for [Cu(TMG₃tren)(O₂)]SbF₆

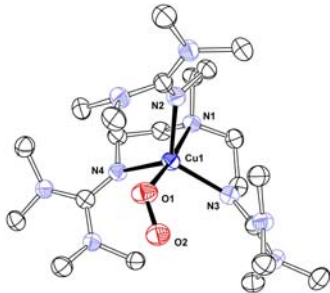
Habitus,	Plate	
Colour	Green	
Crystal size	0.25 x 0.24 x 0.05 mm ³	
Temperature	100(2) K	
Diffractometer type	STOE IPDS 2	
Wavelength	0.71073 Å	
Empirical formula	C ₃₀ H ₆₆ CuF ₆ N ₁₀ O ₅ Sb	
Formula weight	946.22 g/mol	
Crystal system, space group	Monoclinic, P2 ₁ /c	
Unit cell dimensions	a = 12.5352(7) Å b = 16.3766(6) Å c = 20.9350(12) Å	
		$\alpha = 90^\circ$ $\beta = 90.808(5)^\circ$ $\gamma = 90^\circ$
Volume	4297.2(4) Å ³	
Z, Calculated density	4, 1.463 Mg/m ³	
Absorption coefficient	1.196 mm ⁻¹	
F(000)	1960	
Theta range for data collection	1.58 to 25.00°	
Limiting indices	-14 ≤ h ≤ 14, -19 ≤ k ≤ 19, -24 ≤ l ≤ 24	
Reflections collected / unique	49201 / 7514 [R(int) = 0.0661]	
Completeness to theta = 28.45	99.2 %	
Absorption correction	Semi-empirical from equivalents	
Max. and min. transmission	0.9043 and 0.7649	
Refinement method	Full-matrix least-squares on F ²	
Data / restraints / parameters	7514 / 1 / 501	
Goodness-of-fit on F ²	0.970	
Final R indices [I > 2σ(I)]	R1 = 0.0332	
R indices (all data)	wR2 = 0.0822	
Largest diff. peak and hole	0.426 and -0.531 e. Å ⁻³	

Table 4.2.1b: Selected bond lengths [Å] and angles [°] for [Cu(TMG₃tren)(O₂)]SbF₆

Cu1-N1	2.128(2)	Cu1-N2	2.102(2)	Cu1-N3	2.080(2)
Cu1-N4	2.095(2)	Cu1-O1	1.927(2)	O1-O2	1.280(3)
N1-Cu1-N2	81.87(9)	N1-Cu1-N3	82.56(9)	N1-Cu1-N4	82.08(9)
N2-Cu1-N3	116.91(9)	N2-Cu1-N4	118.55(5)	N3-Cu1-N4	119.06(9)
N1-Cu1-O1	173.83(9)	Cu1-O1-O2	123.53(18)		

Table 4.2.2a: Crystal data and structure refinement for [Cu(TMG₃tren)(O₂)]SbF₆

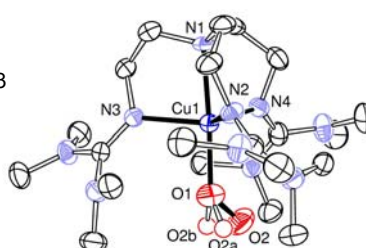
Habitus	Plate	
Colour	Green	
Crystal size	0.48 x 0.28 x 0.24 mm ³	
Temperature	193(2) K	
Diffractometer type	STOE IPDS	
Wavelength	0.71073 Å	
Empirical formula	C ₃₀ H ₆₆ CuF ₆ N ₁₀ O ₅ Sb	
Formula weight	946.22 g/mol	
Crystal system, space group	Monoclinic, P2 ₁ /c	
Unit cell dimensions	a = 12.6533(16) Å b = 16.4724(19) Å c = 21.091(3) Å	
Volume	4395.6(10) Å ³	$\alpha = 90^\circ$ $\beta = 90.818(16)^\circ$ $\gamma = 90^\circ$
Z, Calculated density	4, 1.430 Mg/m ³	
Absorption coefficient	1.170 mm ⁻¹	
F(000)	1960	
Theta range for data collection	2.24 to 26.10 °	
Limiting indices	-15 ≤ h ≤ 15, -20 ≤ k ≤ 20, -25 ≤ l ≤ 25	
Reflections collected / unique	30318 / 8401 [R(int) = 0.0576]	
Completeness to theta = 26.10	92.7 %	
Absorption correction	None	
Refinement method	Full-matrix least-squares on F ²	
Data / restraints / parameters	8401 / 6 / 511	
Goodness-of-fit on F ²	1.009	
Final R indices [I > 2σ(I)]	R1 = 0.0384	
R indices (all data)	wR2 = 0.1068	
Largest diff. peak and hole	0.733 and -0.743 e. Å ⁻³	

Table 4.2.2b: Selected bond lengths [Å] and angles [°] for [Cu(TMG₃tren)(O₂)]SbF₆

Cu1-N1 2.136(3)	Cu1-N2 2.102(3)	Cu1-N3 2.088(3)
Cu1-N4 2.096(3)	Cu1-O1 1.926(3)	O1-O2 1.184(5)
O1-O2a 1.131(9)	O1-O2b 1.109(9)	
N1-Cu1-N2 81.97(11)	N1-Cu1-N3 82.28(11)	N1-Cu1-N4 82.14(11)
N2-Cu1-N3 116.93(11)	N2-Cu1-N4 118.85(10)	N3-Cu1-N4 118.69(11)
N1-Cu1-O1 175.69(12)	Cu1-O1-O2 128.3(3)	Cu1-O1-O2a 137.9(8)
Cu1-O1-O2b 141.3(10)		

Table 4.2.3a: Crystal data and structure refinement for [Cu(TM_G3tren)]SbF₆

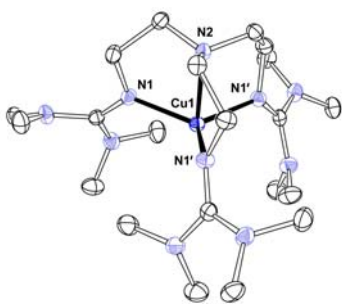
Habitus,	Block	
Colour	Colourless	
Crystal size	1.4 x 1.6 x 2.0 mm ³	
Temperature	200(2) K	
Diffractometer type	Siemens SMART CCD	
Wavelength	0.71073 Å	
Empirical formula	C ₇ H ₁₆ Cu _{0.33} F ₂ N _{3.33} Sb _{0.33}	
Formula weight	246.66	
Crystal system, space group	rhombohedral, $R\bar{3}$	
Unit cell dimensions	$a = 13.9286(16)$ Å $b = 13.9286(16)$ Å $c = 13.9286(16)$ Å	
		$\alpha = 51.2090(10)^\circ$ $\beta = 51.2090(10)^\circ$ $\gamma = 51.2090(10)^\circ$
Volume	1515.0(3) Å ³	
Z, Calculated density	6, 1.622 Mg/m ³	
Absorption coefficient	1.622 mm ⁻¹	
F(000)	756	
Theta range for data collection	2.03 to 28.28 °	
Limiting indices	-17 ≤ h ≤ 18, -18 ≤ k ≤ 18, -18 ≤ l ≤ 18	
Reflections collected / unique	17866 / 2492 [R(int) = 0.0395]	
Completeness to theta = 28.28	98.7 %	
Absorption correction	Multi-scan (SADABS)	
Refinement method	Full-matrix least-squares on F ²	
Data / restraints / parameters	2492 / 0 / 125	
Goodness-of-fit on F ²	1.278	
Final R indices [I > 2σ(I)]	R1 = 0.0362	
R indices (all data)	wR2 = 0.0848	
Largest diff. peak and hole	0.642 and -1.031 e. Å ⁻³	

Table 4.2.3b: Selected bond lengths [Å] and angles [°] for [Cu(TM_G3tren)]SbF₆

Cu1-N1	2.048(2)	Cu1-N2	2.175(4)	Cu1-N1'	2.048(2)
N2-Cu1-N1'	84.19(2)	N1-Cu1-N2	84.20(6)		
N1-Cu1-N1'	118.99(2)	N1'-Cu1-N1'	118.99(2)		

Table 4.2.4a: Crystal data and structure refinement for [Cu(TMG₃trenO)]B(C₆F₅)₄

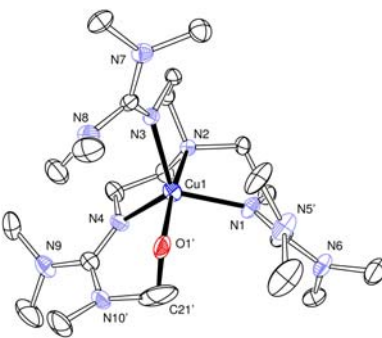
Habitus	Plate	 <p> $\alpha = 90^\circ$ $\beta = 96.8820(10)^\circ$ $\gamma = 90^\circ$ </p>
Colour	Green	
Crystal size	0.79 x 0.14 x 0.12 mm ³	
Temperature	110 K	
Diffractometer type	Oxford Diffraction CCD	
Wavelength	0.71073 Å	
Empirical formula	C ₄₅ H ₄₇ BCuF ₂₀ N ₁₀ O	
Formula weight	1198.28 g/mol	
Crystal system, space group	Monoclinic, P2 ₁ /n	
Unit cell dimensions	$a = 13.1556(2) \text{ Å}$ $b = 20.8618(3) \text{ Å}$ $c = 18.7140(3) \text{ Å}$	
Volume	5099.04(13) Å ³	
Z, Calculated density	4, 1.561 Mg/m ³	
Absorption coefficient	0.551 mm ⁻¹	
F(000)	2436	
Theta range for data collection	3.81 to 27.59 °	
Limiting indices	-17 ≤ h ≤ 17, -27 ≤ k ≤ 27, -24 ≤ l ≤ 24	
Reflections collected / unique	67755 / 11746 [R(int) = 0.0481]	
Completeness to theta = 27.59	99.4 %	
Absorption correction	Analytical	
Max. and min. transmission	0.946 and 0.764	
Refinement method	Full-matrix least-squares on F ²	
Data / restraints / parameters	11746 / 0 / 792	
Goodness-of-fit on F ²	1.082	
Final R indices [I > 2σ(I)]	R1 = 0.0493	
R indices (all data)	wR2 = 0.1111	
Largest diff. peak and hole	0.754 and -0.861 e. Å ⁻³	

Table 4.2.4b: Selected bond lengths [Å] and angles [°] for [Cu(TMG₃trenO)]B(C₆F₅)₄

Cu1-N1 2.053(2)	Cu1-N2 2.091(2)	Cu1-N3 2.117(2)
Cu1-N4 2.066(2)	Cu1-O1' 1.972(5)	O1'-C21' 1.448(12)
N1-Cu1-N2 83.23(8)	N1-Cu1-N3 116.11(9)	N1-Cu1-N4 123.95(9)
N2-Cu1-N3 82.16(8)	N2-Cu1-N4 82.67(8)	N3-Cu1-N4 115.16(8)
N2-Cu1-O1 173.1(3)	Cu1-O1'-C21' 105.1(5)	O1'-C21'-N10' 111.4(6)

Table 4.2.5a: Crystal data and structure refinement for $[\text{Cu}_2(\text{Me}_6\text{tren})_2(\text{O}_2)](\text{BPh}_4)_2$

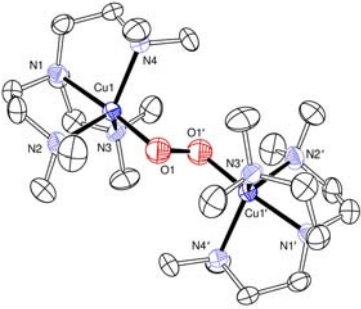
Habitus	Block	 <p> $\alpha = 90^\circ$ $\beta = 104.60(3)^\circ$ $\gamma = 90^\circ$ </p>
Colour	Dark violet	
Crystal size	0.02 x 0.02 x 0.01 mm ³	
Temperature	193(2) K	
Diffractometer type	STOE IPDS	
Wavelength	0.71073 Å	
Empirical formula	C ₈₄ H ₁₂₄ B ₂ Cu ₂ N ₈ O ₆	
Formula weight	1490.61	
Crystal system, space group	Monoclinic, P2 ₁ /n	
Unit cell dimensions	$a = 15.431(3) \text{ Å}$ $b = 13.023(3) \text{ Å}$ $c = 21.180(4) \text{ Å}$	
Volume	4118.8(14) Å ³	
Z, Calculated density	2, 1.202 Mg/m ³	
Absorption coefficient	0.571 mm ⁻¹	
F(000)	1600	
Theta range for data collection	2.15 to 26.08 °	
Limiting indices	-18 ≤ h ≤ 18, -15 ≤ k ≤ 16, -26 ≤ l ≤ 25	
Reflections collected / unique	30191 / 7725 [R(int) = 0.2082]	
Completeness to theta = 26.08	94.8 %	
Absorption correction	None	
Refinement method	Full-matrix least-squares on F ²	
Data / restraints / parameter	7725 / 0 / 470	
Goodness-of-fit on F ²	0.824	
Final R indices [I > 2σ(I)]	R1 = 0.0657	
R indices (all data)	wR2 = 0.1592	
Largest diff. peak and hole	0.645 and -0.466 e. Å ⁻³	

Table 4.2.5b: Selected bond lengths [Å] and angles [°] for $[\text{Cu}_2(\text{Me}_6\text{tren})_2(\text{O}_2)](\text{BPh}_4)_2$

Cu1-N1 2.088(6)	Cu1-N2 2.163(5)	Cu1-N3 2.141(5)
Cu1-N4 2.159(5)	Cu1-O1 1.907(5)	O1-O1' 1.368(9)
Cu1-Cu1' 4.590		
N1-Cu1-N2 83.4(2)	N1-Cu1-N3 83.3(2)	N1-Cu1-N4 83.13(19)
N2-Cu1-N3 118.18(19)	N2-Cu1-N4 120.2(2)	N3-Cu1-N4 117.50(19)
Cu1-O1-O1' 116.5(5).		

Table 4.2.6a: Crystal data and structure refinement for [Cu(Me₆tren)]BPh₄

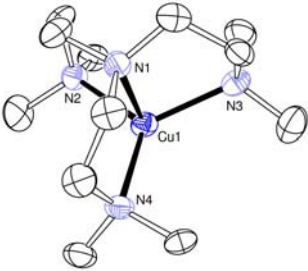
Habitus	Plate	
Colour	Colourless	
Crystal size	0.35 x 0.30 x 0.01 mm ³	
Temperature	193(2) K	
Diffractometer type	Siemens SMART CCD	
Wavelength	0.71073 Å	
Empirical formula	C ₃₆ H ₅₀ BCuN ₄	
Formula weight	613.15	
Crystal system, space group	Triclinic, P $\bar{1}$	
Unit cell dimensions	$a = 10.064(2)$ Å $b = 12.566(3)$ Å $c = 13.541(3)$ Å	
		$\alpha = 92.844(4)^\circ$ $\beta = 92.213(4)^\circ$ $\gamma = 105.851(4)^\circ$
Volume	1642.9(6) Å ³	
Z, Calculated density	2, 1.239 Mg/m ³	
Absorption coefficient	0.695 mm ⁻¹	
F(000)	656	
Theta range for data collection	1.51 to 28.45 °	
Limiting indices	-13 ≤ h ≤ 13, -16 ≤ k ≤ 16, -18 ≤ l ≤ 17	
Reflections collected / unique	20326 / 7969 [R(int) = 0.1719]	
Completeness to theta = 28.45	96.1 %	
Absorption correction	Multi-scan (SADABS)	
Max. and min. transmission	0.9931 and 0.7929	
Refinement method	Full-matrix least-squares on F ²	
Data / restraints / parameters	7969 / 0 / 385	
Goodness-of-fit on F ²	0.911	
Final R indices [I > 2σ(I)]	R1 = 0.0740	
R indices (all data)	wR2 = 0.1829	
Largest diff. peak and hole	0.449 and -0.774 e. Å ⁻³	

Table 4.2.6b: Selected bond lengths [Å] and angles [°] for [Cu(Me₆tren)]BPh₄

Cu1-N1	2.153(4)	Cu1-N2	2.105(4)	Cu1-N3	2.115(5)
Cu1-N4	2.106(4)				
N1-Cu1-N2	85.96(17)	N1-Cu1-N3	85.96(17)	N1-Cu1-N4	86.18(17)
N2-Cu1-N3	119.16(17)	N2-Cu1-N4	119.36(17)	N3-Cu1-N4	120.06(17)

Table 4.2.7a: Crystal data and structure refinement for [Cu(Me₆tren)Cl]BPh₄

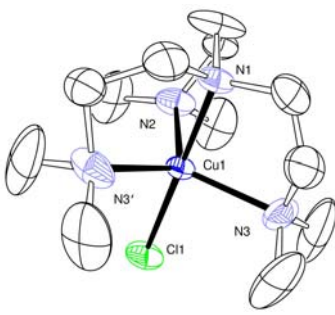
Habitus	Plate	
Colour	Green	
Crystal size	0.36 x 0.32 x 0.16 mm ³	
Temperature	193(2) K	
Diffractometer type	STOE IPDS	
Wavelength	0.71073 Å	
Empirical formula	C ₃₆ H ₅₀ BClCuN ₄	
Formula weight	648.60	
Crystal system, space group	Orthorhombic, Pmna	
Unit cell dimensions	a = 22.206(4) Å b = 12.906(3) Å c = 11.892(2) Å	
		α = 90 ° β = 90 ° γ = 90 °
Volume	3408.1(12) Å ³	
Z, Calculated density	4, 1.264 Mg/m ³	
Absorption coefficient	0.750 mm ⁻¹	
F(000)	1380	
Theta range for data collection	1.83 to 24.12 °	
Limiting indices	-25 ≤ h ≤ 25, -14 ≤ k ≤ 14, -13 ≤ l ≤ 11	
Reflections collected / unique	12304 / 2828 [R(int) = 0.0379]	
Completeness to theta = 24.12	99.1 %	
Absorption correction	None	
Refinement method	Full-matrix least-squares on F ²	
Data / restraints / parameters	2828 / 0 / 233	
Goodness-of-fit on F ²	1.033	
Final R indices [I > 2σ(I)]	R1 = 0.0382	
R indices (all data)	wR2 = 0.1018	
Largest diff. peak and hole	0.321 and -0.310 e. Å ⁻³	

Table 4.2.7b: Selected bond lengths [Å] and angles [°] for [Cu(Me₆tren)Cl]BPh₄

Cu1-N1 2.025(3)	Cu1-N2 2.170(3)	Cu1-N3 2.152(3)
Cu1-N3' 2.152(3)	Cu1-Cl1 2.2081(11)	
N1-Cu1-N2 84.49(13)	N1-Cu1-N3 85.03(9)	N1-Cu1-N3' 85.03(9)
N2-Cu1-N3 119.17(10)	N2-Cu1-N3' 119.17(10)	N3-Cu1-N3' 119.26(19)
N1-Cu1-Cl1 179.20(10)		

Table 4.2.8a: Crystal data and structure refinement for [Cu(Me₄apme)]BPh₄

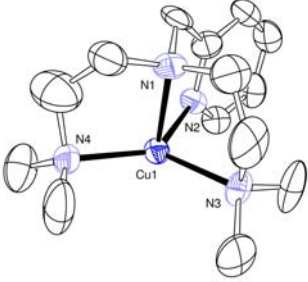
Habitus	Plate	
Colour	Yellow	
Crystal size	0.28 x 0.16 x 0.04 mm ³	
Temperature	193(2) K	
Diffractometer type	STOE IPDS	
Wavelength	0.71073 Å	
Empirical formula	C ₃₈ H ₄₆ BCuN ₄	
Formula weight	633.14	
Crystal system, space group	Triclinic, $P\bar{1}$	
Unit cell dimensions	$a = 10.983(2) \text{ Å}$ $b = 12.233(2) \text{ Å}$ $c = 25.791(5) \text{ Å}$	
		$\alpha = 85.38(3)^\circ$ $\beta = 79.32(3)^\circ$ $\gamma = 80.56(3)^\circ$
Volume	3354.6(12) Å ³	
Z, Calculated density	4, 1.254 Mg/m ³	
Absorption coefficient	0.683 mm ⁻¹	
F(000)	1344	
Theta range for data collection	1.91 to 24.14 °	
Limiting indices	-10 ≤ h ≤ 12, -14 ≤ k ≤ 14, -29 ≤ l ≤ 20	
Reflections collected / unique	10914 / 8012 [R(int) = 0.0780]	
Completeness to theta = 24.14	74.8 %	
Absorption correction	None	
Refinement method	Full-matrix least-squares on F ²	
Data / restraints / parameters	8012 / 0 / 802	
Goodness-of-fit on F ²	0.831	
Final R indices [I > 2σ(I)]	R1 = 0.0643	
R indices (all data)	wR2 = 0.1487	
Largest diff. peak and hole	0.562 and -0.341 e. Å ⁻³	

Table 4.2.8b: Selected bond lengths [Å] and angles [°] for [Cu(Me₄apme)Cl]BPh₄

Cu1-N1 2.156(7)	Cu1-N2 2.004(6)	Cu1-N3 2.132(7)
Cu1-N4 2.048(9)		
N1-Cu1-N2 84.0(3)	N1-Cu1-N3 84.9(3)	N1-Cu1-N4 87.5(3)
N2-Cu1-N3 103.0(3)	N2-Cu1-N4 135.2(3)	N3-Cu1-N4 120.0(3)

Table 4.2.9a: Crystal data and structure refinement for [Cu(Me₄apme)Cl]BPh₄

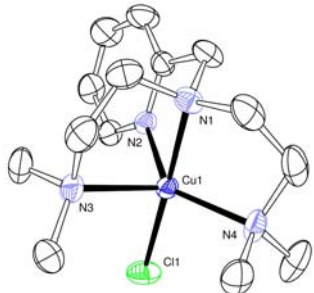
Habitus	Plate	
Colour	Green	
Crystal size	0.44 x 0.24 x 0.16 mm ³	
Temperature	193(2) K	
Diffractometer type	STOE IPDS	
Wavelength	0.71073 Å	
Empirical formula	C ₃₈ H ₄₆ BClCuN ₄	
Formula weight	668.59	
Crystal system, space group	Orthorhombic, Pbca	
Unit cell dimensions	a = 16.1764(16) Å b = 16.6426(11) Å c = 25.2678(17) Å	
		$\alpha = 90^\circ$ $\beta = 90^\circ$ $\gamma = 90^\circ$
Volume	6802.5(9) Å ³	
Z, Calculated density	8, 1.306 Mg/m ³	
Absorption coefficient	0.754 mm ⁻¹	
F(000)	2824	
Theta range for data collection	2.87 to 24.14 °	
Limiting indices	-18 ≤ h ≤ 18, -18 ≤ k ≤ 17, -28 ≤ l ≤ 26	
Reflections collected / unique	38823 / 5317 [R(int) = 0.0407]	
Completeness to theta = 24.14	98.0 %	
Absorption correction	None	
Refinement method	Full-matrix least-squares on F ²	
Data / restraints / parameters	5317 / 0 / 410	
Goodness-of-fit on F ²	1.067	
Final R indices [I > 2σ(I)]	R1 = 0.0349	
R indices (all data)	wR2 = 0.0986	
Largest diff. peak and hole	0.487 and -0.300 e. Å ⁻³	

Table 4.2.9b: Selected bond lengths [Å] and angles [°] for [Cu(Me₄apme)Cl]BPh₄

Cu1-N1	2.0400(17)	Cu1-N2	2.0607(16)	Cu1-N3	2.2247(18)
Cu1-N4	2.0715(18)	Cu1-Cl1	2.2387(6)		
N1-Cu1-N2	81.40(7)	N1-Cu1-N3	83.49(7)	N1-Cu1-N4	85.15(8)
N2-Cu1-N3	102.02(7)	N2-Cu1-N4	136.45(7)	N3-Cu1-N4	117.37(7)
N1-Cu1-Cl1	177.93(5)				

Table 4.2.10a: Crystal data and structure refinement for [Cu(Me₂uns-penp)]BPh₄

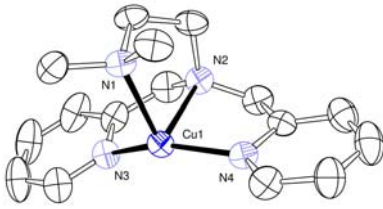
Habitus	Block	
Colour	Yellow	
Crystal size	0.34 x 0.20 x 0.16 mm ³	
Temperature	193(2) K	
Diffractometer type	STOE IPDS	
Wavelength	0.71073 Å	
Empirical formula	C ₄₀ H ₄₂ BCuN ₄	
Formula weight	653.13	
Crystal system, space group	Monoclinic, P2 ₁ /n	
Unit cell dimensions	$a = 12.5591(17) \text{ Å}$ $b = 11.3571(11) \text{ Å}$ $c = 23.968(3) \text{ Å}$	
		$\alpha = 90^\circ$ $\beta = 96.635(16)^\circ$ $\gamma = 90^\circ$
Volume	3395.7(7) Å ³	
Z, Calculated density	4, 1.278 Mg/m ³	
Absorption coefficient	0.677 mm ⁻¹	
F(000)	1376	
Theta range for data collection	1.93 to 24.14 °	
Limiting indices	-14 ≤ h ≤ 14, -12 ≤ k ≤ 12, -27 ≤ l ≤ 27	
Reflections collected / unique	19575 / 5363 [R(int) = 0.1192]	
Completeness to theta = 24.14	98.8 %	
Absorption correction	None	
Refinement method	Full-matrix least-squares on F ²	
Data / restraints / parameters	5363 / 0 / 421	
Goodness-of-fit on F ²	0.919	
Final R indices [I > 2σ(I)]	R1 = 0.0561	
R indices (all data)	wR2 = 0.1461	
Largest diff. peak and hole	0.757 and -1.561 e. Å ⁻³	

Table 4.2.10b: Selected bond lengths [Å] and angles [°] for [Cu(Me₂uns-penp)]BPh₄

Cu1-N1 2.188(3)	Cu1-N2 2.189(3)	Cu1-N3 1.956(3)
Cu1-N4 1.944(4)		
N1-Cu1-N2 85.04(13)	N1-Cu1-N3 100.47(14)	N1-Cu1-N4 107.72(13)
N2-Cu1-N3 84.63(14)	N2-Cu1-N4 84.81(14)	N3-Cu1-N4 148.83(15)

Table 4.2.11a: Crystal data and structure refinement for [Cu(Me₂uns-penp)Cl]BPh₄

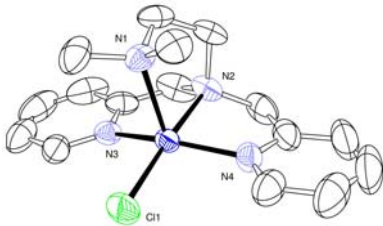
Habitus	Block	
Colour	Green	
Crystal size	0.52 x 0.40 x 0.36 mm ³	
Temperature	298(2) K	
Diffractometer type	STOE IPDS	
Wavelength	0.71073 Å	
Empirical formula	C ₄₀ H ₄₂ BClCuN ₄	
Formula weight	688.58	
Crystal system, space group	Triclinic, $P\bar{1}$	
Unit cell dimensions	$a = 14.227(3) \text{ Å}$ $b = 15.209(3) \text{ Å}$ $c = 17.637(4) \text{ Å}$	$\alpha = 102.41(3)^\circ$ $\beta = 94.83(3)^\circ$ $\gamma = 108.14(3)^\circ$
Volume	3494.6(12) Å ³	
Z, Calculated density	4, 1.309 Mg/m ³	
Absorption coefficient	0.736 mm ⁻¹	
F(000)	1444	
Theta range for data collection	2.62 to 28.28 °	
Limiting indices	-18 ≤ h ≤ 18, -20 ≤ k ≤ 18, -23 ≤ l ≤ 22	
Reflections collected / unique	31654 / 15461 [R(int) = 0.0344]	
Completeness to theta = 28.28	89.1 %	
Absorption correction	None	
Refinement method	Full-matrix least-squares on F ²	
Data / restraints / parameters	15461 / 0 / 851	
Goodness-of-fit on F ²	0.887	
Final R indices [I > 2σ(I)]	R1 = 0.0382	
R indices (all data)	wR2 = 0.0999	
Largest diff. peak and hole	0.450 and -0.366 e. Å ⁻³	

Table 4.2.11b: Selected bond lengths [Å] and angles [°] for [Cu(Me₂uns-penp)Cl]BPh₄

Cu1-N1 2.2463(19)	Cu1-N2 2.051(2)	Cu1-N3 2.016(2),
Cu1-N4 2.014(2)	Cu1-Cl1 2.2342(9))	
N1-Cu1-N2 85.07(8),	N1-Cu1-N3 92.97(8)	N1-Cu1-N4 105.56(8)
N2-Cu1-N3 83.11(9)	N2-Cu1-N4 81.68(10)	N3-Cu1-N4 154.82(9)
N2-Cu1-Cl1 176.02(6))		

Table 4.2.12a: Crystal data and structure refinement for [Cu(Me₂uns-penp)Cl]BPh₄

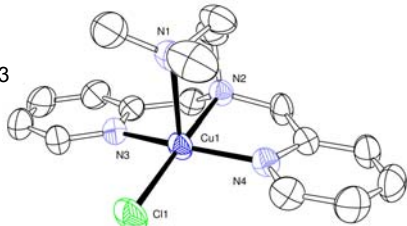
Habitus	Block	
Colour	Blue	
Crystal size	0.32 x 0.24 x 0.16 mm ³	
Temperature	293(2) K	
Diffractometer type	STOE IPDS	
Wavelength	0.71073 Å	
Empirical formula	C ₄₀ H ₄₂ BClCuN ₄	
Formula weight	688.58	
Crystal system, space group	Monoclinic, C2/c	
Unit cell dimensions	a = 22.962(5) Å b = 15.200(3) Å c = 21.604(4) Å	
Volume	7174(2) Å ³	$\alpha = 90^\circ$ $\beta = 107.93(3)^\circ$ $\gamma = 90^\circ$
Z, Calculated density	8, 1.275 Mg/m ³	
Absorption coefficient	0.717 mm ⁻¹	
F(000)	2888	
Theta range for data collection	2.34 to 25.93 °	
Limiting indices	-28 ≤ h ≤ 28, -18 ≤ k ≤ 18, -26 ≤ l ≤ 26	
Reflections collected / unique	25479 / 6784 [R(int) = 0.0516]	
Completeness to theta = 25.93	96.9 %	
Absorption correction	None	
Refinement method	Full-matrix least-squares on F ²	
Data / restraints / parameters	6784 / 0 / 426	
Goodness-of-fit on F ²	0.827	
Final R indices [I > 2σ(I)]	R1 = 0.0333	
R indices (all data)	wR2 = 0.0748	
Largest diff. peak and hole	0.304 and -0.250 e. Å ⁻³	

Table 4.2.12b: Selected bond lengths [Å] and angles [°] for [Cu(Me₂uns-penp)Cl]BPh₄

Cu1-N1 2.329(2)	Cu1-N2 2.0541(17)	Cu1-N3 2.004(2)
Cu1-N4 1.998(2)	Cu1-Cl1 2.2381(7)	
N1-Cu1-N2 84.77(8)	N1-Cu1-N3 99.34(9)	N1-Cu1-N4 91.78(9)
N2-Cu1-N3 81.62(8)	N2-Cu1-N4 82.86(7)	N3-Cu1-N4 159.95(8)
N2-Cu1-Cl1 175.65(6)		

Table 4.2.13a: Crystal data and structure refinement for [Cu(tmpa)]BPh₄

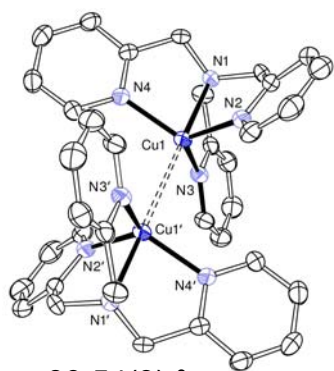
Habitus	Block	 <p> $\alpha = 89.54(3)^\circ$ $\beta = 81.36(3)^\circ$ $\gamma = 79.89(3)^\circ$ </p>
Colour	Yellow	
Crystal size	0.36 x 0.36 x 0.32 mm ³	
Temperature	193(2) K	
Diffractometer type	STOE IPDS	
Wavelength	0.71073 Å	
Empirical formula	C ₄₂ H ₃₈ BCuN ₄	
Formula weight	673.11	
Crystal system, space group	Triclinic, $P\bar{1}$	
Unit cell dimensions	$a = 11.523(2) \text{ Å}$ $b = 13.805(3) \text{ Å}$ $c = 21.577(4) \text{ Å}$	
Volume	3340.1(12) Å ³	
Z, Calculated density	4, 1.339 Mg/m ³	
Absorption coefficient	0.691 mm ⁻¹	
F(000)	1408	
Theta range for data collection	2.24 to 25.94 °	
Limiting indices	-14 ≤ h ≤ 14, -16 ≤ k ≤ 16, -26 ≤ l ≤ 26	
Reflections collected / unique	24381 / 12007 [R(int) = 0.0645]	
Completeness to theta = 25.94	92.2 %	
Absorption correction	None	
Refinement method	Full-matrix least-squares on F ²	
Data / restraints / parameters	12007 / 0 / 865	
Goodness-of-fit on F ²	1.060	
Final R indices [I > 2σ(I)]	R1 = 0.0438	
R indices (all data)	wR2 = 0.1335	
Largest diff. peak and hole	0.579 and -0.963 e. Å ⁻³	

Table 4.2.13b: Selected bond lengths [Å] and angles [°] for [Cu(tmpa)]BPh₄

Cu1-N1 2.199(2)	Cu1-N2 2.037(2)	Cu1-N3 2.034(2)
Cu1-N4 2.072(3)	Cu1-Cu1' 2.8341(9)	
N1-Cu1-N2 81.64(8)	N1-Cu1-N3 81.90(9)	N1-Cu1-N4 81.20(9)
N2-Cu1-N3 121.24(9)	N2-Cu1-N4 116.47(9)	N3-Cu1-N4 115.97(9)
N1-Cu1-Cu1' 177.65(7)		

Table 4.2.14a: Crystal data and structure refinement for [Cu(tmpa)Cl]BPh₄

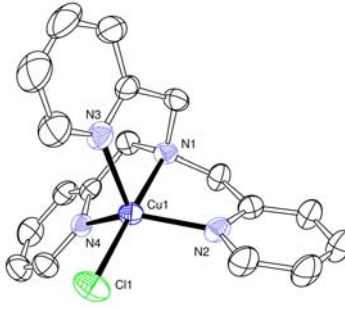
Habitus	Plate	
Colour	Green	
Crystal size	0.68 x 0.16 x 0.08 mm ³	
Temperature	193(2) K	
Diffractometer type	STOE IPDS	
Wavelength	0.71073 Å	
Empirical formula	C ₄₅ H ₄₄ BClCuN ₄ O	
Formula weight	766.64	
Crystal system, space group	Monoclinic, P2 ₁ /c	
Unit cell dimensions	a = 14.092(3) Å b = 18.489(4) Å c = 15.115(3) Å	
Volume	3851.2(13) Å ³	α = 90 °
Z, Calculated density	4, 1.322 Mg/m ³	β = 102.06(3) °
Absorption coefficient	0.677 mm ⁻¹	γ = 90 °
F(000)	1604	
Theta range for data collection	2.48 to 26.06 °	
Limiting indices	-16 ≤ h ≤ 15, -22 ≤ k ≤ 21, -18 ≤ l ≤ 18	
Reflections collected / unique	28163 / 7108 [R(int) = 0.0837]	
Completeness to theta = 26.06	93.2 %	
Absorption correction	None	
Refinement method	Full-matrix least-squares on F ²	
Data / restraints / parameters	7108 / 0 / 480	
Goodness-of-fit on F ²	0.911	
Final R indices [I > 2σ(I)]	R1 = 0.0520	
R indices (all data)	wR2 = 0.1349	
Largest diff. peak and hole	0.565 and -0.368 e. Å ⁻³	

Table 4.2.14b: Selected bond lengths [Å] and angles [°] for [Cu(tmpa)Cl]BPh₄

Cu1-N1	2.046(3)	Cu1-N2	2.032(7)	Cu1-N3	2.114(3)
Cu1-N4	2.034(3)	Cu1-Cl1	2.2321(12)		
N1-Cu1-N2	81.31(12)	N1-Cu1-N3	80.17(13)	N1-Cu1-N4	82.93(12)
N2-Cu1-N3	111.47(13)	N2-Cu1-N4	134.24(12)	N3-Cu1-N4	107.67(12)
N1-Cu1-Cl1	178.51(10)				

Chapter 5 – Summary / Zusammenfassung

5.1 Summary

The synthesis and characterization of new synthetic copper “dioxygen adduct complexes” had gained a lot of interest during the last years. The reason for the increased interest is based on the fact that these compounds can be regarded as model complexes for the reactivity of redox active copper enzymes. These enzymes had demonstrated that selective oxidations of organic substrates with air under ambient conditions are possible. These reactions are of high interest in the laboratory and in industry and therefore special attention has been focused upon the synthesis, characterization and the reactivity of copper dioxygen adduct complexes. This is also the topic of the research described herein and the results of the different projects have been separated in two parts: copper superoxo and peroxy complexes.

Copper superoxo complexes described herein are intensively green colored compounds in which the copper ions are tetracoordinated through a tripodal amine and an additional superoxo ligand (O_2^-) in the axial position of a trigonal bipyramid coordination polyeder.

In the intensively blue colored peroxy complexes two copper ions are again tetracoordinated through tripodal amine ligands. Additionally they contain a peroxy-group (O_2^{2-}) that bridges the two copper ions. Figure 5.1.1 shows the interaction of superoxo complexes and peroxy complexes in the reaction of copper(I) compounds with dioxygen.

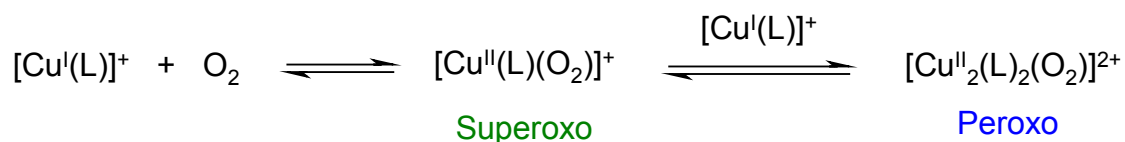


Figure 5.1.1: Reaction of copper(I) complexes with dioxygen.

5.1.1 Superoxo complexes

The amine TMG₃tren has been synthesized previously as an optimized ligand system for the preparation of end-on coordinated copper superoxo complexes. TMG₃tren consists of an aliphatic tren backbone that shows sterical crowding due to the guanidine groups and additionally has electronic properties of N-donor atoms between imine and amine groups. Especially the sterically demanding guanidine groups are responsible for the stabilization of end-on superoxo complexes because due to them dimerisation reactions are avoided. Tripodal ligands with an aliphatic tren backbone support end-on coordination of dioxygen in the copper complex, because the copper ion is already coordinated by four N-donor atoms and therefore only one coordination site is left for binding of dioxygen. However, it has not been possible to completely characterize such a species in the past. After a large number of experiments, it was finally possible, in the course of this work, to obtain the reactive intermediate [Cu(TMGG₃tren)O₂]⁺ in form of single crystals at -80 °C. Therefore, the structural characterization of this compound is the first X-ray proof for a synthetic copper superoxo complex with an end-on coordination.

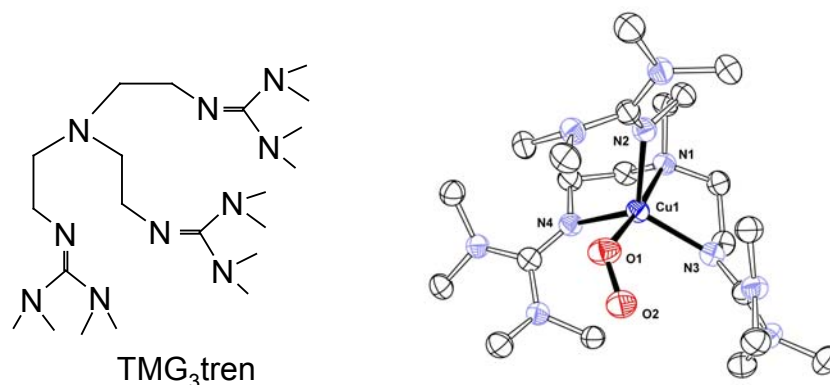


Figure 5.1.2: The ligand TMG₃tren and the molecular structure of the superoxo complex [Cu(TMGG₃tren)O₂]⁺.

Studies of the reactivity showed ligand hydroxylation analogous to the copper enzyme PHM. This type of ligand hydroxylation (Figure 5.1.3) was observed for the first time for synthetic model compounds. During the reactions of the superoxo complex with a number of mono- and diphenolic substrates the corresponding oxygenated and oxidized products were formed.

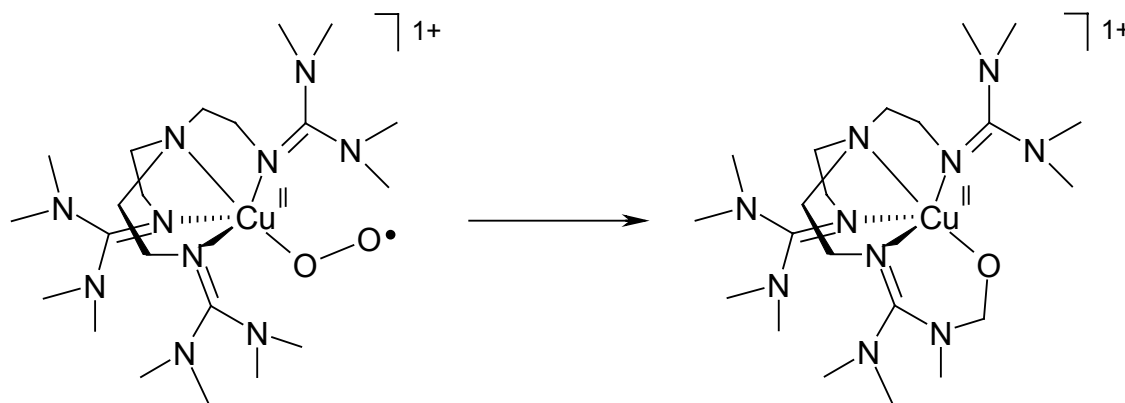


Figure 5.1.3: Ligand hydroxylation in the complex $[\text{Cu}(\text{TMG}_3\text{tren})\text{O}_2]^+$.

That the initial step of the hydroxylation reaction seems to be the abstraction of a hydrogen atom from a phenol could be demonstrated using the hydrogen atom donor TEMPO-H that does not cause secondary reactions.

5.1.2 Peroxo-complexes

For the synthesis of end-on coordinated peroxo complexes tripodal amine ligands (based on substituted tren) have been successfully used in the past. Figure 5.1.4 shows a series of ligands with different types of N-donor atoms. If the aliphatic N-donor atoms of Me_6tren are substituted in a systematic way by introducing pyridine N-donor atoms finally the ligand tmpa is obtained.

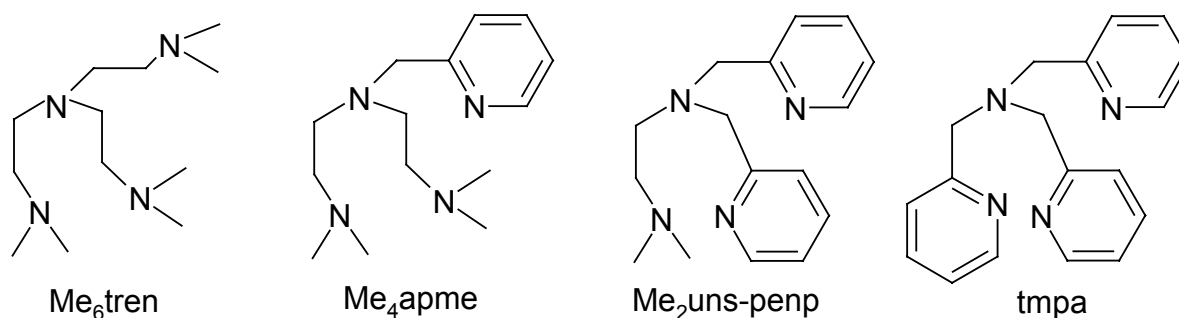


Figure 5.1.4: Series of ligands based on the tren backbone.

Based on these four ligands, the influence of the N-donor atoms on the reactivity of dioxygen binding of the according copper(I) complexes was investigated using stopped-flow techniques. For these studies, the corresponding copper(I)-complexes

were synthesized and reacted with dioxygen at low temperatures in propionitrile as solvent. The systematic kinetic investigations showed that the stability of end-on copper superoxo complexes is clearly increased if more aliphatic N-donor atoms are present. This systematic increase or decrease of stabilities is not observed for the according peroxo complexes; here the complex of the ligand Me₂uns-penp was the most stable compound, followed by the Me₄apme and tmpa complexes. The peroxo complex with the pure aliphatic ligand Me₆tren showed the lowest stability in this series. A reasonable explanation is indicated by the crystal structures of the copper(II)-chloride complexes with these four ligands. The chloride complexes can be prepared easily and, as demonstrated previously, can provide information on the peroxo complexes if it is not possible to obtain their molecular structures. Here it was observed that the copper(II)-chloride complex of the ligand Me₂uns-penp has a square pyramidal geometry, in contrast to the trigonal bipyramidal environment of the other three complexes. Most likely this geometry is retained in solution as well. From our results we assume that the coordination of the peroxide ligand in the equatorial position leads to the observed higher stability of the peroxo complex.

However, the influence of the used solvent is extremely important. Studies using the non-coordinating solvent acetone showed the expected systematic increase of stabilities from the peroxo complexes of the ligand Me₆tren to the peroxo complexes of the ligand tmpa, using the anion tetraphenylborate.

Isolation of the four peroxo complexes in the solid state without using solvents led for the first time to room temperature stable compounds. This is quite remarkable, because in the past these complexes have only been known as extremely sensitive complexes which only persist at low temperatures. Using tetraphenylborate as anion, we could increase the decomposition temperature to more than 70 °C. The influence of the ligands was demonstrated in the different decomposition temperatures. In contrast to the stopped-flow measurements in propionitrile, a systematic increase of stabilities was observed, analogous to the studies with the solvent acetone. The complex with tmpa has a decomposition temperature above 110 °C and therefore is significantly more stable than the according Me₆tren complex with a decomposition temperature around 70 °C.

Furthermore, the complex [Cu₂(Me₆tren)(O₂)](BPh₄)₂ could be structurally characterized. This is only the third example of such a species that could be

characterized by X-ray crystallography. Previously molecular structures of this type of peroxo complexes have been reported 1988 by Karlin and 2004 by Suzuki and coworkers.

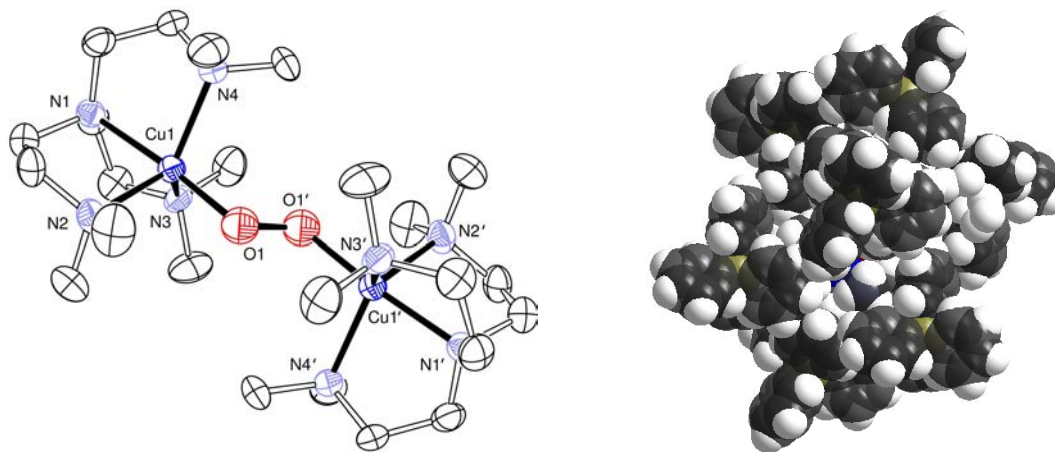


Figure 5.1.5: Molecular structure of the peroxo complex $[\text{Cu}_2(\text{Me}_6\text{tren})_2(\text{O}_2)]^{2+}$ and the anion shielding.

Responsible for the high temperature stability is the crystal packing of the anions. The peroxo complex is completely shielded by eight tetraphenylborate anions and this encapsulation completely suppresses any further reactions. Application of other anions like PF_6^- , BF_4^- or $\text{B}(\text{C}_6\text{F}_5)_4^-$ did not show this stabilization effect. In Figure 5.1.5 the peroxo complex and its encapsulation by eight tetraphenylborate anions is presented.

Preliminary reactivity studies of these complexes in the solid state showed successful oxidations of organic compounds. For example, the oxidation of toluene at room temperature to benzaldehyde and benzyl alcohol was performed. Different yields of benzaldehyde and benzyl alcohol obtained demonstrated an effect of the used ligands. Complexes with more aromatic nitrogen donor atoms present, so far, showed better results. Such oxidations are possible because in a way, the investigated peroxo complexes are rather similar to hydrogen peroxide. In the complexes investigated the hydrogen atoms of the hydrogen peroxide molecule can be regarded as being substituted by copper complexes.

5.2 Zusammenfassung

Die Synthese und Charakterisierung neuer synthetischer Kupfer „Sauerstoff-Addukt-Komplexe“ ist nach wie vor von großem Interesse, da durch die Verwendung solcher niedermolekularer Modellverbindungen für Kupferproteine eine Brücke zwischen natürlich ablaufenden Prozessen und der großtechnischen Anwendung in der chemischen Industrie geschlagen werden kann. In dieser Arbeit wurden speziell „end-on“ koordinierte „Kupfer-Sauerstoff-Addukt-Komplexe“ synthetisiert, charakterisiert und auf ihre Reaktivität hin untersucht. Hierbei wurden diese "end-on" Verbindungen in Superoxokomplexe und Peroxokomplexe unterteilt.

Bei Superoxokomplexen handelt es sich um intensiv grün gefärbte Verbindungen, die ein zentrales Kupferion enthalten, welches zum einen durch einen tripodalen Aminliganden komplexiert ist und zum anderen an eine Superoxo-Gruppe (O_2^-) gebunden ist.

Die intensiv blau gefärbten Peroxokomplexe hingegen bestehen aus zwei, durch tripodale Aminliganden koordinierte Kupferkomplexe, welche durch eine Peroxo-Gruppe (O_2^{2-}) verbrückt sind. In Abb. 5.2.1 ist der Zusammenhang zwischen Superoxokomplexen und Peroxokomplexen bei der Reaktion von Kupfer(I)-Komplexen mit elementarem Sauerstoff dargestellt.

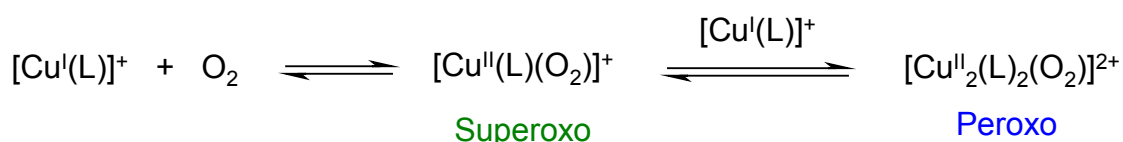


Abb. 5.2.1: Reaktionsverlauf der Reaktion von Kupfer(I)-Komplexen mit Sauerstoff.

5.2.1 Superoxokomplexe

In der Vergangenheit wurde mit dem Liganden TMG_3tren ein System entwickelt, welches speziell für die Darstellung eines „end-on“ koordinierten Kupfer-superoxokomplexes prädestiniert ist. Dieser Ligand verbindet sämtliche Vorteile zur Ausbildung eines solchen Komplexes, da er zum einen sterisch anspruchsvoll ist und zum anderen ein aliphatisches tren-Gerüst besitzt. Auch die elektronischen Eigenschaften der Stickstoffdonoratome, die von ihren Donoreigenschaften zwischen

Iminen und Aminen liegen, dürften eine wichtige Rolle spielen. Der sterisch höhere Anspruch wird durch das Einbringen von Guanidin-Gruppen am tren-Gerüst verursacht. Hierdurch wird in einem Kupferkomplex die Superoxo-Spezies stabilisiert, da der sterische Anspruch die Bindung eines weiteren Kupfer(I)-Komplexes unter Ausbildung eines dimeren Peroxokomplexes verhindert. Zum anderen begünstigt der tripodale Ligand mit seinem aliphatischen tren-Gerüst die Ausbildung einer end-on-Koordination, da das zentrale Kupferion bereits vierfach koordiniert vorliegt und so nur noch eine Koordinationsstelle dem Sauerstoff zur Verfügung stellt. Nach einer Vielzahl von Experimenten ist es letztendlich im Rahmen dieser Arbeit gelungen, das reaktive Intermediat $[\text{Cu}(\text{TMG}_3\text{tren})(\text{O}_2)]^+$ als kristallinen Feststoff bei $-80\text{ }^\circ\text{C}$ zu erhalten. Mittels Einkristallstrukturanalyse konnte nun erstmals der kristallographische Beweis eines solchen „end-on“ gebundenen Kupfer-Superoxokomplexes in einer niedermolekularen Modellverbindung erbracht werden.

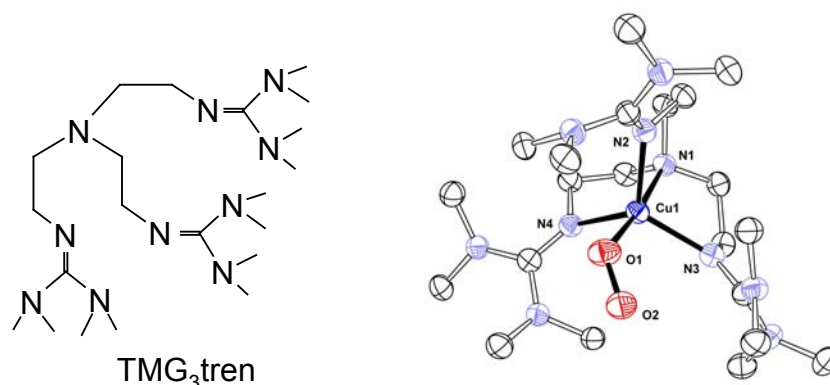


Abb. 5.2.2: Der Ligand TMG_3tren und die Molekülstruktur des Superoxokomplexes $[\text{Cu}(\text{TMG}_3\text{tren})(\text{O}_2)]^+$.

Reaktivitätsuntersuchungen an diesem System zeigten eine Ligand-Hydroxylierung, wie sie auch im Kupferenzym PHM beobachtet wird. Diese, erstmals für eine Modellverbindung nachgewiesene analoge Ligand-Hydroxylierung, (Abb. 5.2.2) wurde bei der Reaktion mit einer Reihe von Mono- und Diphenolsubstraten beobachtet, wobei die entsprechenden oxygenierten oder dioxxygenierten Produkte entstanden.

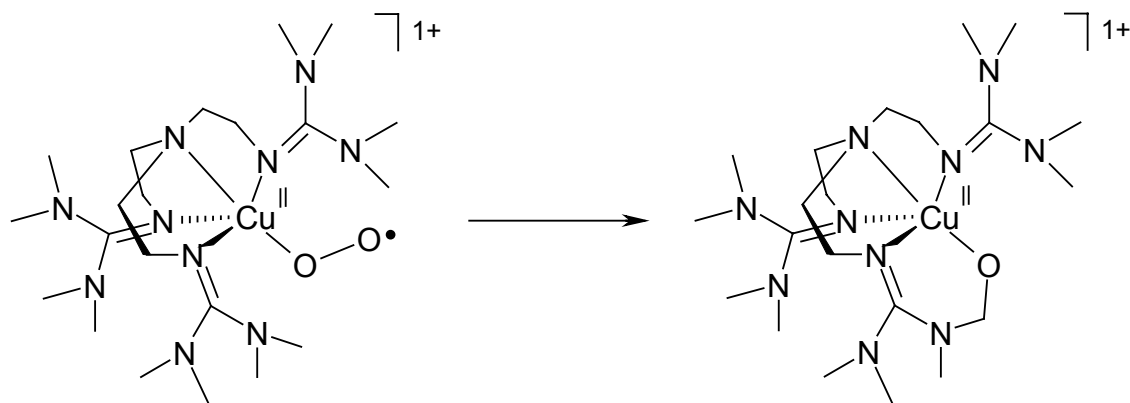


Abb. 5.2.3: Ligand-Hydroxylierung des Komplexes $[\text{Cu}(\text{TMG}_3\text{tren})(\text{O}_2)]^+$.

Die als Anfangsschritt postulierte H-Abstraktion von einem Phenol konnte durch die Verwendung des H-Atom-Donators TEMPO-H, welcher keine Folgereaktion zulässt, bestätigt werden.

5.2.2 Peroxokomplexe

Zur Darstellung von „end-on“ koordinierten Peroxokomplexen eignen sich am besten tripodale Aminliganden auf der Basis von substituiertem tren. Die in Abb. 5.2.4 dargestellten Liganden besitzen alle ein tren-Gerüst, unterscheiden sich allerdings in der Beschaffenheit der N-Donor-Atome. Vom Me_6tren zum tmpa hin werden sukzessive die aliphatischen N-Donoratome durch aromatische Pyridin-N-Donoratome ersetzt.

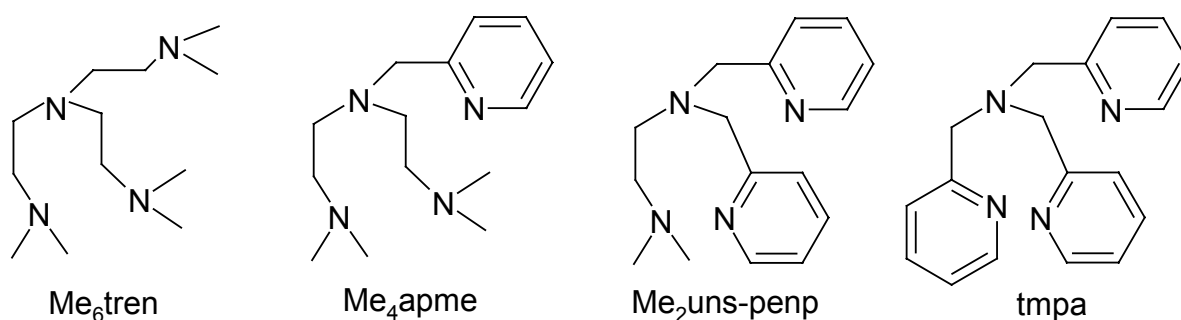


Abb. 5.2.4: Tripodale Liganden mit tren-Gerüst.

Auf Grundlage dieser vier Liganden wurde mit Hilfe der „Stopped-Flow“-Technik der Einfluss des aromatischen Anteils im Ligandengerüst untersucht. Hierzu wurden die entsprechenden Kupfer(I)-Komplexe synthetisiert und bei tiefen Temperaturen in

Propionitril mit Sauerstoff zur Reaktion gebracht. Es konnte gezeigt werden, dass die primär gebildeten Superoxo-Intermediate mit Zunahme des aromatischen Charakters des Liganden an Stabilität verlieren. Im Fall der Peroxokomplexe zeigte der Komplex mit dem Ligand Me₂uns-penp überraschenderweise die höchste Stabilität, gefolgt von den Peroxokomplexen der Liganden Me₄apme und tmpa. Der rein aliphatische Ligand Me₆tren zeigte die geringste Stabilität als Peroxokomplex. Der Vergleich der Kupfer(II)-chlorid-Komplexe dieser vier Liganden liefert eine Erklärung für die hohe Stabilität des Kupfer-Me₂uns-penp-Peroxo-Komplexes, da im Gegensatz zu den Peroxokomplexen die Chloridkomplexe kristallographisch leicht zugänglich sind. Die Molekülstruktur des Chloridkomplexes mit dem Liganden Me₂uns-penp weist im Gegensatz zu den anderen Verbindungen eine quadratisch pyramidale Struktur auf, während die anderen in einer trigonal bipyramidalen Geometrie kristallisieren. Diese unterschiedlichen Geometrien werden vermutlich auch in Lösung vorliegen.

Neben der besonderen Geometrie des Me₂uns-penp-Komplexes spielt auch die Koordinationsfähigkeit des Lösungsmittels bei der Stabilität der Peroxokomplexe eine Rolle, da in dem nichtkoordinierenden Lösungsmittel Aceton dieser Effekt nicht beobachtet wurde. Hier wurde ein klarer (erwarteter) Trend in der Stabilität beobachtet. Unter Verwendung von Tetraphenylborat als Anion zeigt der Peroxokomplex des Liganden Me₆tren die geringste Stabilität, welche zum tmpa-Komplex hin stetig ansteigt.

Isoliert man die Peroxokomplexe als trockenen Feststoff, zeigen die sonst doch sehr empfindlichen Verbindungen eine hohe Temperaturstabilität. Dies ist in soweit bemerkenswert, da bislang davon ausgegangen wurde, dass solche Peroxokomplexe nur bei tiefen Temperaturen stabil sind. Durch die Verwendung von Tetraphenylborat als Anion ist es allerdings im Rahmen dieser Arbeit gelungen, die Temperaturstabilität auf über 70 °C zu steigern. Hierbei spiegelte sich auch der Einfluss des aromatischen Anteils des Ligandengerüsts wieder. Allerdings zeigte sich hier ein Unterschied zu den in Propionitril durchgeführten „Stopped-Flow“-Untersuchungen, welcher schon unter Verwendung von Aceton als Lösungsmittel beobachtet wurde. Während die Peroxokomplexe im koordinierenden Lösungsmittel Propionitril keinen Trend in der Stabilität zeigten, ergab sich für die Feststoffe jedoch die erwartete Reihung. Der Peroxokomplex des rein aliphatischen Ligand Me₆tren ist

nur bis knapp über 70 °C beständig, während sich die Stabilität hin zum tmpa auf über 110 °C steigert.

Darüber hinaus ist es gelungen, einen solchen Peroxokomplex auch kristallographisch zu charakterisieren. Der Komplex $[\text{Cu}_2(\text{Me}_6\text{tren})_2(\text{O}_2)]^{2+}$ ist, nachdem Karlin 1988 und Suzuki 2004 eine solche Peroxoverbindung beschrieben haben, der dritte kristallographische Nachweis einer solchen Spezies.

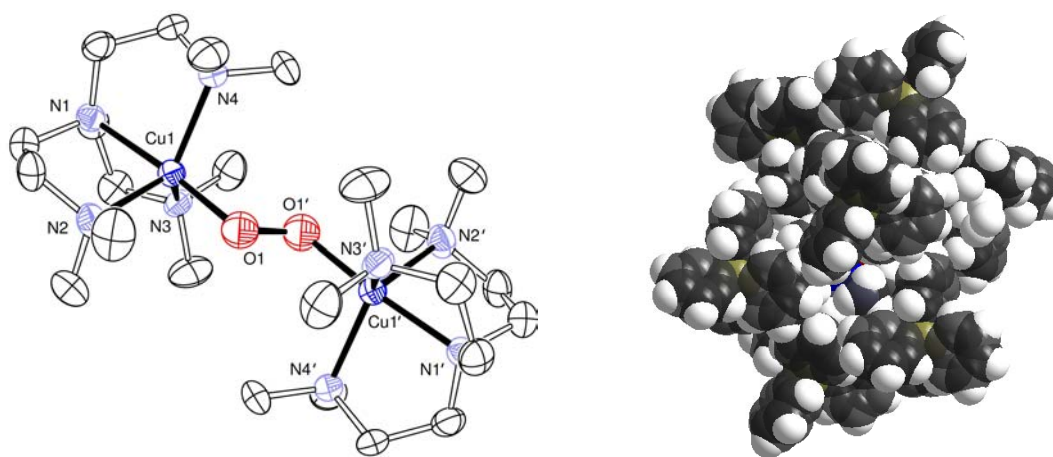


Abb. 5.2.5: Molekülstruktur des Peroxokomplexes $[\text{Cu}_2(\text{Me}_6\text{tren})_2(\text{O}_2)]^{2+}$ und Anionenpackung.

Die hohe Temperaturstabilität ist in der kristallographischen Anordnung der Anionen begründet, da der Peroxokomplex durch acht Tetraphenylboratanionen vollständig eingekapselt wird und so vor der Zersetzung geschützt wird. Die Verwendung anderer Anionen wie PF_6^- , BF_4^- oder $\text{B}(\text{C}_6\text{F}_5)_4^-$ zeigten diese Stabilität nicht. In Abb. 5.2.5 ist die Molekülstruktur des reinen Peroxokomplexes als auch die kristallographische Packung der acht Tetraphenylboratanionen gezeigt.

Erste Untersuchungen zur Reaktivität dieser Verbindungen zeigten, dass diese Feststoffe in der Lage sind, entsprechend dem ähnlich aufgebautem Wasserstoffperoxid, organische Verbindungen zu oxidieren. So ist es z. B. gelungen, bei Raumtemperatur Toluol zu Benzylalkohol und Benzaldehyd zu oxidieren. Auch hier zeigten die überwiegend aromatisch komplexierten Verbindungen einen Vorteil gegenüber den aliphatisch koordinierten Komplexen.

Publications

Full Papers

- Crystallographic Characterization of a Synthetic 1:1 End-On Copper Dioxygen Adduct Complex

C. Würtele, E. Gaoutchenova, K. Harms, M. C. Holthausen, J. Sundermeyer, S. Schindler, *Angew. Chem.*, **2006**, 118, 3951 [*Angew. Chem. Int.*, Ed. **2006**, 45, 3867]

- Syntheses, Characterization and Reactivity of Iron(II), Nickel(II), Copper(II) and Zinc(II) Complexes of the Ligand N,N,N',N'-Tetrakis(2-pyridylmethyl)-benzene-1,3-diamine (1,3-tpbd) and Its Phenol Derivative 2,6-Bis[bis(2-pyridylmethyl)amino]-p-cresol (2,6-tpcd)

S. Foxon, J.-Y. Xu, S. Turba, M. Leibold, F. Hampel, F. W. Heinemann, O. Walter, C. Würtele, M. Holthausen, S. Schindler, *Eur. J. Inorg. Chem.*, **2007**, 429

- Transformation of Nitrile to Cyanide and Aldehyde Using a Cobalt(II) Complex and Dioxygen

J. Müller, C. Würtele, O. Walter, S. Schindler, *Angew. Chem.*, **2007**, 119, 7922 [*Angew. Chem. Int. Ed.*, **2007**, 46, 7775]

- Reactions of a Copper(II) Superoxo Complex Lead to CH and OH Substrate Oxygenation: Modeling Copper-Monooxygenase CH Hydroxylation

D. Maiti, D.-H. Lee, K. Gaoutchenova, C. Würtele, M. C. Holthausen, A. A. Narducci Sarjeant, J. Sundermeyer, S. Schindler, K. D. Karlin, *Angew. Chem.*, **2007**, 120, 88 [*Angew. Chem. Int. Ed.*, **2007**, 47, 82]

- Aromatic Hydroxylation in a Copper Bis(imine) Complex Mediated by a μ - η^2 - η^2 Peroxo Dicopper Core: A Mechanistic Scenario
O. Sander, A. Henß, C. Näther, C. Würtele, M. C. Holthausen, S. Schindler, F. Tuczek, *Chem. Eur. J.*, **in press**
- Desymmetrization of Diols as a Key Step for the Selective Synthesis of Unsymmetric Disubstituted Diamondoids (Nanodiamonds)
H. Schwertfeger, C. Würtele, M. Serafin, H. Hausmann, R. M. K. Carlson, J. E. P. Dahl, P. R. Schreiner, *J. Org. Chem.*, **accepted**
- Reversible Binding of Dioxygen by Copper(I) Complexes with Tripodal Tetraamine Ligands
C. Würtele, I. Kerezsi, A. Beitat, S. Foxon, P. K. Wick and S. Schindler
Ready for submission to *Inorg. Chem.*
- Extreme Stabilization of Copper Peroxo Complexes in the Solid State by Anion Encapsulation
C. Würtele, O. Sander, F. Tuczek and S. Schindler
Ready for submission to *Chem. Comm.*

Oral Presentations

- Stabilisierung von „Kupfer-Sauerstoffkomplexen“
3. Koordinationschemie-Treffen, 18.-20. Februar 2007 (Berlin)
- „Kupfer-Sauerstoff-Adduktkomplexe“ in Biologie und Chemie
Fachbereichstag der Biologie und Chemie, 5. Juni 2006 (Giessen)
- Reaktion von tripodalen Cu(I)-Komplexen mit Sauerstoff
2. Koordinationschemie-Treffen, 19.-21. Februar 2006 (Göttingen)

Poster Presentations

- Characterization of an End-on Copper Superoxo Complex
Christian Würtele and Siegfried Schindler
1st European Chemistry Congress, 27. - 31. August 2006 (Budapest)
- Characterization of a Synthetic 1:1 End-On Copper Dioxygen Adduct Complex
Christian Würtele and Siegfried Schindler
Kolloquium des DFG Schwerpunktprogramms 1118, 07. - 09. Mai 2006
(Schleiden)

Curriculum Vitae

Christian Erhard Würtele

Geburtsdatum : 18.11.1975 in Hanau

Familienstand: ledig

Staatsangehörigkeit: deutsch

Ausbildung

1992-1995	Ludwig-Geissler-Schule, Hanau Abschluss: Allgemeine Hochschulreife
1995-1998	Berufsausbildung: Chemetall GmbH, Frankfurt Abschluss: Chemielaborant
1998-2004	Studium der Chemie an der Justus-Liebig-Universität, Gießen.
Sep. 2000	Diplomvorprüfung
Juni 2004	Diplomhauptprüfung
April 2004 - Jan. 2005	Praktische Durchführung der Diplomarbeit am Institut für Anorganische und Analytische Chemie der Justus-Liebig-Universität Gießen, Thema: „Untersuchungen zur Aktivierung von Sauerstoff an tripodalen ein- und mehrkernigen Kupfer(I)-Komplexen“, Betreuer: Prof. Dr. Siegfried Schindler
Seit Feb. 2005	Promotion am Institut für Anorganische und Analytische Chemie der Justus-Liebig-Universität Gießen, Thema: End-on „Copper Dioxygen Adduct Complexes“, Betreuer: Prof. Dr. Siegfried Schindler
Aug. - Nov. 2007	Dreimonatiger Forschungsaufenthalt in der Arbeitsgruppe von Prof. Rybak-Akimova an der TUFTS-University Medford (USA)

Berufliche Tätigkeiten

1998	Dreimonatige Tätigkeit als Chemielaborant; Chemetall GmbH, Frankfurt
1999	Zweimonatige Tätigkeit als Werksstudent; Clariant GmbH, Frankfurt
2002 - 2005	Wissenschaftliche Hilfskraft zur Betreuung von Nebenfachstudenten; Justus-Liebig-Universität, Gießen
seit 2005	Wissenschaftlicher Mitarbeiter zur Betreuung von Hauptfachstudenten; Justus-Liebig-Universität, Gießen

Weiterbildung

2005	Sechswöchige Intensivschulung zur Kristallstrukturanalyse am Forschungszentrum Karlsruhe
2006	Einwöchige Sommerschule: „Grundlagen der Einkristallstrukturbestimmung“ des GDCh- Arbeitskreises Chemische Kristallographie

Auszeichnungen

1998	Aufnahme in das Begabtenförderungsprogramm der IHK Frankfurt am Main
2006	Vorstellung meiner Diplomarbeit als Kurzvortrag am Fachbereichstag Biologie und Chemie der Justus- Liebig-Universität, Gießen, als eine herausragende Arbeit
2007	Doktorandenstipendium finanziert über den DAAD für einen Forschungsaufenthalt in der Arbeits- gruppe von Prof. Rybak-Akimova an der TUFTS- University Medford, in den USA

References

- [1] A. F. Holleman, E. Wiberg, *Lehrbuch der Anorganischen Chemie*, 101st ed., Walter de Gruyter, Berlin; New York, **1995**.
- [2] M. Pascaly, I. Jolk, B. Krebs, *Chemie in unserer Zeit* **1999**, 33, 334.
- [3] S. Schindler, *Eur. J. Inorg. Chem.* **2000**, 2311.
- [4] S. J. Lippard, J. M. Berg, *Bioanorganische Chemie*, Spektrum, Heidelberg, Berlin, Oxford, **1995**.
- [5] W. Kaim, B. Schwederski, *Bioanorganische Chemie*, B. G. Teubner, Stuttgart, **1991**.
- [6] L. M. Mirica, X. Ottenwaelder, T. D. P. Stack, *Chem. Rev.* **2004**, 104, 1013.
- [7] E. A. Lewis, W. B. Tolman, *Chem. Rev.* **2004**, 104, 1047.
- [8] C. Würtele, Diploma thesis, Justus-Liebig-Universität Gießen (Germany), **2005**.
- [9] W. Kaim, J. Rall, *Angew. Chem.* **1996**, 108, 47; *Angew. Chem. Int. Ed.* **1996**, 35, 43.
- [10] *Star Trek, The Original Series*, Journey to Babel, Season 2, Episode 10 **1967**.
- [11] C. Würtele, E. Gaoutchenova, K. Harms, M. C. Holthausen, J. Sundermeyer, S. Schindler, *Angew. Chem.* **2006**, 118, 3951; *Angew. Chem. Int. Ed.* **2006**, 45, 3867.
- [12] R. R. Jacobson, Z. Tyeklar, A. Farooq, K. D. Karlin, S. Liu, J. Zubieta, *J. Am. Chem. Soc.* **1988**, 110, 3690.
- [13] N. Kitajima, K. Fujisawa, Y. Moro-oka, K. Toriumi, *J. Am. Chem. Soc.* **1989**, 111, 8975.
- [14] K. Fujisawa, M. Tanaka, Y. Moro-oka, N. Kitajima, *J. Am. Chem. Soc.* **1994**, 116, 12079.
- [15] A. Wada, M. Harata, K. Hasegawa, K. Jitsukawa, H. Masuda, M. Mukai, T. Kitagawa, H. Einaga, *Angew. Chem.* **1998**, 110, 874; *Angew. Chem. Int. Ed.* **1998**, 37, 798.
- [16] J. Reim, B. Krebs, *Angew. Chem.* **1994**, 106, 2040; *Angew. Chem. Int. Ed.* **1994**, 33, 1969.
- [17] N. W. Aboelella, E. A. Lewis, A. M. Reynolds, W. W. Brennessel, C. J. Cramer, W. B. Tolman, *J. Am. Chem. Soc.* **2002**, 124, 10660.

- [18] S. Mahapatra, J. A. Halfen, E. C. Wilkinson, G. Pan, X. Wang, V. G. Young Jr., C. J. Cramer, J. Que, L., W. B. Tolman, *J. Am. Chem. Soc.* **1996**, *118*, 11555.
- [19] K. D. Karlin, N. Wei, B. Jung, S. Kaderli, P. Niklaus, A. D. Zuberbühler, *J. Am. Chem. Soc.* **1993**, *115*, 9506.
- [20] M. Schatz, M. Becker, F. Thaler, F. Hampel, S. Schindler, R. R. Jacobson, Z. Tyeklar, N. N. Murthy, P. Ghosh, Q. Chen, J. Zubieta, K. D. Karlin, *Inorg. Chem.* **2001**, *40*, 2312.
- [21] K. Komiyama, H. Furutachi, S. Nagatomo, A. Hashimoto, H. Hayashi, S. Fujinami, M. Suzuki, T. Kitagawa, *Bull. Chem. Soc. Jpn.* **2004**, *77*, 59.
- [22] M. Schatz, M. Becker, O. Walter, G. Liehr, S. Schindler, *Inorg. Chim. Acta* **2001**, 324.
- [23] C. Janiak, T. M. Klapötke, H.-J. Meyer, *Moderne Anorganische Chemie*, Walter de Gruyter, Berlin, New York, **1999**.
- [24] A. G. Blackman, *Eur. J. Inorg. Chem.* **2008**, 2633.
- [25] M. Becker, F. W. Heinemann, S. Schindler, *Chem. Eur. J.* **1999**, *5*, 3124.
- [26] M. Weitzer, M. Schatz, F. Hampel, F. W. Heinemann, S. Schindler, *Dalton Trans.* **2002**, *5*, 686.
- [27] C. Würtele, *3. Koordinationschemie-Treffen*, Berlin, **2007**.
- [28] V. Raab, J. Kipke, O. Burghaus, J. Sundermeyer, *Inorg. Chem.* **2001**, *40*, 6964.
- [29] M. Schatz, V. Raab, S. P. Foxon, G. Brehm, S. Schneider, M. Reiher, M. C. Holthausen, J. Sundermeyer, S. Schindler, *Angew. Chem.* **2004**, *116*, 4460; *Angew. Chem. Int. Ed.* **2004**, *43*, 4360.
- [30] L. Q. Hatcher, K. D. Karlin, *J. Biol. Inorg. Chem.* **2004**, *9*, 669.
- [31] S. V. Kryatov, E. V. Rybak-Akimova, S. Schindler, *Chem. Rev.* **2005**, *105*, 2175.
- [32] L. J. Que Jr., W. B. Tolman, *Angew. Chem.* **2002**, *114*, 1160; *Angew. Chem. Int. Ed.* **2002**, *41*, 1114.
- [33] E. I. Solomon, P. Chen, M. Metz, S.-K. Lee, A. E. Palmer, *Angew. Chem.* **2001**, *113*, 4702; *Angew. Chem. Int. Ed.* **2002**, *40*, 4570.
- [34] D. J. E. Spencer, N. W. Aboelella, A. M. Reynolds, P. L. Holland, W. B. Tolman, *J. Am. Chem. Soc.* **2002**, *124*, 2108.
- [35] P. Chen, D. E. Root, C. Campochiaro, K. Fujisawa, E. I. Solomon, *J. Am. Chem. Soc.* **2003**, *125*, 466.

- [36] N. W. Aboeella, S. V. Kryatov, B. F. Gherman, W. W. Brennessel, J. Young, V. G., R. Sarangi, E. V. Rybak-Akimova, K. O. Hodgson, B. Hedman, E. I. Solomon, C. J. Cramer, W. B. Tolman, *J. Am. Chem. Soc.* **2004**, *126*, 16896.
- [37] A. M. Reynolds, B. F. Gherman, C. J. Cramer, W. B. Tolman, *Inorg. Chem.* **2005**, *44*, 6989.
- [38] S. T. Prigge, B. A. Eipper, R. E. Mains, L. M. Amzel, *Science* **2004**, *304*, 864.
- [39] M. Weitzer, S. Schindler, G. Brehm, S. Schneider, E. Hörmann, B. Jung, S. Kaderli, A. D. Zuberbühler, *Inorg. Chem.* **2003**, *42*, 1800.
- [40] C. X. Zhang, S. Kaderli, M. Costas, E.-I. Kim, Y.-M. Neuhold, K. D. Karlin, A. D. Zuberbühler, *Inorg. Chem.* **2003**, *42*, 1807.
- [41] The term superbasic refers to neutral guanidine ligands, that have a $\text{pK}(\text{BH}^+)$ value more than six orders of magnitude higher than that of the most basic tertiary amines. Typically they are used as ligands for protons ("proton sponges"); see: V. Raab, J. Kipke, R. M. Gschwind, J. Sundermeyer, *Chem. Eur. J.* **2002**, *8*, 1682.
- [42] B. A. Jazdzewski, A. M. Reynolds, P. L. Holland, V. G. Young, S. Kaderli, A. D. Zuberbühler, W. B. Tolman, *J. Biol. Inorg. Chem.* **2003**, *8*, 381.
- [43] Please note that in earlier study^[29] we erroneously reported an angle $\alpha(\text{Cu-O-O})$ of 132.2° in Figure 3 -the correct value, however, is $\alpha(\text{Cu-O-O}) = 121.4$.
- [44] J. P. Klinman, *Chem. Rev.* **1996**, *96*, 2541.
- [45] M. A. McGuirl, D. D. K., *Encyclopedia of Inorganic Chemistry*, Vol. 2, **2005**, pp. 1201.
- [46] J. P. Klinman, *J. Biol. Chem.* **2006**, *281*, 3013.
- [47] P. Chen, E. I. Solomon, *Proc. Natl. Acad. Sci. USA* **2004**, *101*, 13105.
- [48] S. Itoh, *Curr. Opin. Chem. Biol.* **2006**, *10*, 115.
- [49] K. Yoshizawa, N. Kihara, T. Kamachi, Y. Shiota, *Inorg. Chem.* **2006**, *45*, 3034.
- [50] A. Crespo, M. A. Martí, A. E. Roitberg, L. M. Amzel, D. A. Estrin, *J. Am. Chem. Soc.* **2006**, *128*, 12817.
- [51] D. Maiti, H. C. Fry, J. S. Woertink, M. A. Vance, E. I. Solomon, K. D. Karlin, *J. Am. Chem. Soc.* **2007**, *129*, 264.
- [52] D. Maiti, H. R. Lucas, A. A. Narducci Sarjeant, K. D. Karlin, *J. Am. Chem. Soc.* **2007**, *129*, 6998.
- [53] D. Maiti, A. A. Narducci Sarjeant, K. D. Karlin, *J. Am. Chem. Soc.* **2007**, *129*, 6720.

- [54] M. Mizuno, K. Honda, J. Cho, H. Furutachi, T. Tosha, T. Matsumoto, S. Fujinami, S. Kitagawa, M. Suzuki, *Angew. Chem.* **2006**, *118*, 7065; *Angew. Chem. Int. Ed.* **2006**, *45*, 6911.
- [55] T. Fujii, S. Yamaguchi, Y. Funahashi, T. Ozawa, T. Tosha, T. Kitagawa, H. Masuda, *Chem. Commun.* **2006**, 4428.
- [56] S. Yamaguchi, H. Masuda, *Sci. Technol. Adv. Mater.* **2005**, *6*, 34.
- [57] T. Fujii, A. Naito, S. Yamaguchi, A. Wada, Y. Funahashi, K. Jitsukawa, S. Nagatomo, T. Kitagawa, H. Masuda, *Chem. Commun.* **2003**, 2700.
- [58] A. Decker, E. I. Solomon, *Curr. Opin. Chem. Biol.* **2005**, *9*, 152.
- [59] D. Schröder, M. C. Holthausen, J. Schwarz, *J. Phys. Chem.* **2004**, *108*, 14407.
- [60] Y. Nakao, K. Hirao, T. Taketsugu, *J. Chem. Phys.* **2001**, *114*, 7935.
- [61] J. P. Evans, K. Ahn, J. P. Klinman, *J. Biol. Chem.* **2003**, *278*, 49691.
- [62] A. T. Bauman, E. T. Yukl, K. Alkevich, A. L. McCormack, N. J. Blackburn, *J. Biol. Chem.* **2006**, *281*, 4190.
- [63] P. Chen, K. Fujisawa, E. I. Solomon, *J. Am. Chem. Soc.* **2000**, *122*, 10177.
- [64] B. Gherman, D. E. Heppner, W. B. Tolman, C. J. Cramer, *J. Biol. Inorg. Chem.* **2006**, *11*, 197.
- [65] J. Cramer, W. B. Tolman, *Acc. Chem. Res.* **2007**, *40*, 601.
- [66] See Supporting Information.
- [67] Experimental details of the structure determination can be found in the Supporting Information. CCDC-661204 (**3**) contains the supplementary crystallographic data for this paper. These data can be obtained free of charge from The Cambridge Crystalligraphic Data Center via www.ccdc.cam.ac.uk/data_request/cif.
- [68] Henkel and co-workers have also recently reported an example of O₂ activation and methyl-group hydroxylation in binuclear copper complexes with bis(guanidine) ligands; see: S. Herres, A. J. Heuwing, U. Flörke, J. Schneider, G. Henkel, *Inorg. Chim. Acta* **2005**, *358*, 1089.
- [69] S. Herres-Pawlis, U. Flörke, G. Henkel, *Eur. J. Inorg. Chem.* **2005**, 3815.
- [70] J. L. McLain, J. Lee, J. T. Groves, *Biomimetic Oxid. Catal. Trans. Met. Compl.* **2000**, 91.
- [71] L. Que Jr., *Acc. Chem. Res.* **2007**, *40*, 493.

- [72] W. J. Song, M. S. Seo, S. DeBeer George, T. Ohta, R. Song, M. J. Kang, T. Tosha, T. Kitagawa, E. I. Solomon, W. Nam, *J. Am. Chem. Soc.* **2007**, *129*, 1268.
- [73] K. Qin, C. D. Incarvito, A. L. Rheingold, K. H. Theopold, *J. Am. Chem. Soc.* **2002**, *124*, 14008.
- [74] E. V. Gauchenova, PhD thesis, Philipps-Universität Marburg (Germany), **2006**.
- [75] D. P. Goldberg, *Acc. Chem. Res.* **2007**, *40*, 626.
- [76] L. Li, A. A. Narducci Sarjeant, M. A. Vance, L. N. Zakharov, A. L. Rheingold, E. I. Solomon, K. D. Karlin, *J. Am. Chem. Soc.* **2005**, *127*, 15360.
- [77] K. Itoh, H. Hayashi, H. Furutachi, T. Matsumoto, S. Nagatomo, T. Tosha, S. Terada, S. Fujinami, M. Suzuki, T. Kitagawa, *J. Am. Chem. Soc.* **2005**, *127*, 5212.
- [78] H.-C. Liang, E. Kim, C. D. Incarvito, A. L. Rheingold, K. D. Karlin, *Inorg. Chem.* **2002**, *41*, 2209.
- [79] D. A. Modarelli, F. C. Rossitto, P. M. Lahti, *Tet. Lett.* **1989**, *30*, 4473.
- [80] H. Henry-Riyad, T. T. Tidwell, *Phys. Org. Chem.* **2003**, *16*, 559.
- [81] S. Itoh, S. Fukuzumi, *Acc. Chem. Res.* **2007**, *40*, 592.
- [82] E. I. Solomon, R. Sarangi, J. S. Woertink, A. J. Augustine, J. Yoon, S. Ghosh, *Acc. Chem. Res.* **2007**, *40*, 581.
- [83] K. D. Karlin, Z. Tyeklar, *Bioinorganic Chemistry of Copper*, Chapman & Hall, New York, **1993**.
- [84] E. E. Chufán, S. C. Puiu, K. D. Karlin, *Acc. Chem. Res.* **2007**, *40*, 563.
- [85] J. Reedijk, E. Bouwman, *Bioinorganic Catal.*, 2nd ed., Marcel Dekker, New York, **1999**.
- [86] L. I. Simandi, *Advances in Catalytic Activation of Dioxygen by Metal Complexes*, Vol. 26, Kluwer Academic Publisher, Dordrecht, Boston, London, **2003**.
- [87] K. D. Karlin, S. Kaderli, A. D. Zuberbühler, *Acc. Chem. Res.* **1997**, *30*, 139.
- [88] S. Itoh, Y. Tachi, *Dalton Trans.* **2006**, 4531.
- [89] Z. Tyeklar, R. R. Jacobson, N. Wei, N. N. Murthy, J. Zubieta, K. D. Karlin, *J. Am. Chem. Soc.* **1993**, *115*, 2677.
- [90] H. Hayashi, S. Fujinami, S. Nagatomo, S. Ogo, M. Suzuki, A. Uehara, Y. Watanabe, T. Kitagawa, *J. Am. Chem. Soc.* **2000**, *122*, 2124.
- [91] S. P. Foxon, O. Walter, S. Schindler, *Eur. J. Inorg. Chem.* **2002**, 111.

- [92] G. J. P. Britovsek, J. England, A. J. P. White, *Inorg. Chem.* **2005**, *44*, 8125 .
- [93] K. D. Karlin, J. C. Hayes, J. P. Hutchinson, J. R. Hyde, J. Zubieta, *Inorg. Chim. Acta* **1982**, *64*, 219.
- [94] H. Gampp, M. Maeder, C. J. Meyer, A. D. Zuberbühler, *Talanta* **1985**, *32*, 95.
- [95] SHELX-97:, G. M. Sheldrick, Universität Göttingen, **1997**.
- [96] B. S. Lim, R. H. Holm, *Inorg. Chem.* **1998**, *37*, 4898 .
- [97] F. A. Cotton, X. Feng, M. Matusz, R. Poli, *J. Am. Chem. Soc.* **1988**, *110*, 7077.
- [98] C. He, J. L. DuBois, B. Hedman, K. O. Hodgson, S. J. Lippard, *Angew. Chem.* **2002**, *113*, 1532; *Angew. Chem. Int. Ed.* **2001**, *40*, 1484.
- [99] M. Hutin, C. A. Schalley, G. Bernardinelli, J. R. Nitschke, *Chem. Eur. J.* **2006**, *12*, 4069.
- [100] M. G. B. Drew, A. Lavery, V. McKee, S. M. Nelson, *Dalton Trans.* **1985**, 1771.
- [101] C. Mealli, C. S. Arcus, J. L. Wilkinson, T. J. Marks, J. A. Ibers, *J. Am. Chem. Soc.* **1976**, *98*, 711.
- [102] M. Gargano, N. Ravasio, M. Rossi, A. Tiripicchio, M. Tiripicchio Camellini, *Dalton Trans.* **1989**, 921.
- [103] C. Piguet, G. Bernardinelli, A. F. Williams, *Inorg. Chem.* **1989**, *28*, 2920.
- [104] A. Al-Obaidi, G. Baranovi, J. Coyle, C. G. Coates, J. J. McGarvey, V. McKee, J. Nelson, *Inorg. Chem.* **1998**, *37*, 3567.
- [105] K. T. Potts, M. Keshavarz-K, F. S. Tham, H. D. Abruna, C. Arana, *Inorg. Chem.* **1993**, *32*, 4450.
- [106] K. D. Karlin, J. C. Hayes, S. Juen, J. P. Hutchinson, J. Zubieta, *Inorg. Chem.* **1982**, *21*, 4106.
- [107] A. W. Addison, T. N. Rao, J. Reedijk, J. van Rijn, G. C. Verschoor, *Dalton Trans.* **1984**, 1349.
- [108] M. J. Baldwin, P. K. Ross, J. P. Pate, Z. Tyeklar, K. D. Karlin, E. I. Solomon, *J. Am. Chem. Soc.* **1991**, *113*, 8671.
- [109] D. Maiti, D.-H. Lee, K. Gaoutchenova, C. Würtele, M. C. Holthausen, A. A. Narducci Sarjeant, J. Sundermeyer, S. Schindler, K. D. Karlin, *Angew. Chem.* **2007**, *120*, 88; *Angew. Chem. Int. Ed.* **2007**, *47*, 82.
- [110] J. E. Bol, W. L. Driessen, R. Y. N. Ho, B. Maase, L. Que, J. Reedijk, *Angew. Chem.* **1997**, *109*, 1022; *Angew. Chem. Int. Ed.* **1997**, *36*, 998.
- [111] H. Börzel, P. Comba, C. Katsichtis, W. Kiefer, A. Lienke, V. Nagel, H. Pritzkow, *Chem. Eur. J.* **1999**, *5*, 1716.

- [112] M. Koder, K. Katayama, Y. Tachi, K. Kano, S. Hirota, S. Fujinami, M. Suzuki, *J. Am. Chem. Soc.* **1999**, *121*, 11006.
- [113] P. Comba, P. Hilfenhaus, K. D. Karlin, *Inorg. Chem.* **1997**, *36*, 2309.
- [114] K. D. Karlin, D.-H. Lee, S. Kaderli, A. D. Zuberbühler, *Chem. Comm.* **1997**, 475.
- [115] E. Asato, S. Hashimoto, N. Matsumoto, S. Kida, *Dalton Trans.* **1990**, 1741.
- [116] G. J. Kubas, in *Inorg. Synth.*, Vol. 19, **1979**, pp. 90.
- [117] SHELXTL 6.10, Bruker AXS, Madison WI, USA, **2000**.